LONDON'S GLOBAL UNIVERSITY

UCL

Nitrogen Migration during Coal Splitting and Staging Process and Assisted Combustion: A Reactive Molecular Dynamics Study

Zhongze Bai

A thesis submitted for the degree of

Doctor of Philosophy

of

University College London

Department of Mechanical Engineering

University College London

2023

Declaration

I, Zhongze Bai, confirm that the work presented in this thesis is my own. Where information has been derived from other sources, I confirm that this has been indicated in the thesis.

Signature: _____ Date: _____

Abstract

Coal splitting and staging is a potential approach for reducing nitrogen oxide (NOx) emissions during coal oxidation, which converts NOx into harmless gas (N_2) using coal pyrolysis gas. The NOx removal behaviours in this process are determined by the nitrogenous species in pyrolysis gas. In the current work, reactive force field (ReaxFF) molecular dynamics (MD) is used to examine the pyrolysis process of nitrogenous compounds in coal and the NOx reduction by nitrogenous species from coal pyrolysis gas. The effects of water (an important component of coal) on pyridine (a main nitrogen-containing compound in coal) pyrolysis were studied. At different water-content circumstances, common and uncommon intermediates were found and identified. Water influenced both the amount of nitrogen atoms in the polycondensation product and the consuming rates of pyridine molecules. The modifications in reaction pathways brought on by the presence of water were illustrated as well. The efficiency of NO abatement with nitrogenous species in pyrolysis gas (HCN and NH_3) was also studied in relation to temperature, oxygen content, nitrogen-containing species content, and nitrogen-free species (CH_4, CO, and H_2). The atomic-level reaction pathways for NO abatement and N_2 generation were identified under varying conditions. Besides, the behaviours of NO abatement by HCN and NH_3 under various circumstances were compared and control methods for the pyrolysis and reburning processes were suggested.

Assisted combustion, where electric field (EF) and ozone are applied during coal combustion, is an effective method for NOx control. The influence of EF and ozone on fuel-NOx generation from pyridine (the main nitrogenous chemical in coal) oxidation were studied via ReaxFF MD simulations. The number of key products (CO, CO_2, NO, NO_2 and N_2) were quantified for the pyridine oxidation under varying external electric field conditions and in the presence of ozone, respectively. The mechanisms of pyridine combustion with electric fields and ozone addition were revealed at atomic scales.

In summary, this study provides new insights into the nitrogen migration during coal splitting and staging as well as assisted combustion. The new findings lay theoretical foundations for strategizing effective NOx control ways in practice.

Impact Statement

This thesis provides microscopic insights into nitrogen migration during coal splitting and staging process as well as assisted combustion by electric field and ozone. The new findings add knowledge to the fundamental mechanisms of NOx regulating and inspire the control strategies of pollutant emissions.

Specifically, Chapter 3 reveals the impacts of H_2O molecules on pyridine pyrolysis, demonstrating a possibility to control coal pyrolysis reactions by altering the water content of coal. The essential mechanisms during NO abatement by nitrogenous species in coal pyrolysis gas (HCN and NH_3) are examined in Chapter 4 in relation to temperature, oxygen content, nitrogenous species (HCN and NH_3) concentration, and nitrogen-free species (CH_4, CO, and H_2). Results suggest that the increase of temperature and the proportion of NH_3 of nitrogen-containing species is an effective way to enhance the NO reduction performance. Besides, appropriately reducing O_2 concentrations and increasing the number of nitrogen-containing species can improve the NO reduction performance by coal pyrolysis gas. Finally, CH_4 and CO decrease the NO reduction performance, and CH_4 shows more inhibitory effects than CO. But the NO removal behaviours are slightly enhanced by H_2 molecules. Chapter 5 studies the emissions performance of pyridine combustion under varying electric field imposition and ozone concentrations, respectively. The pyridine oxidation is shown to produce less CO and NO emissions when there is an electric field present. Additionally, the atomic level study of the pyridine oxidation reaction processes under various electric fields explains variations in the primary products under different electric field characteristics. Ozone speeds up the combustion of pyridine and makes it easier for CO to become CO_2 and insoluble NO to become soluble NO_2 in water. Active particles including OH, HO_2, HO_3, and H_2O_2 are produced as a result of ozone's participation in reactions with intermediates.

The present thesis proves the reactive force field (ReaxFF) molecular dynamics (MD) is a valuable approach for studying the fundamental mechanisms of chemical processes. It also establishes the scientific foundation for enhancing NOx control behaviours during coal combustion. Specifically, a deeper understanding of NOx generation and reduction at the atomic level can facilitate the optimisation of operation conditions and combination of current technologies to reduce NOx emissions more efficiently in practice. In addition, it will also

facilitate the development of new technologies for NOx control, such as catalyst design and new mechanisms for NOx emission reduction.

Acknowledgements

First and foremost, I would like to express my sincerely gratitude to my supervisors, Prof. Kai Luo and Prof. Stavroula Balabani, for their continued assistance and guidance during my PhD research at University College London. My special thanks are to Prof. Xizhuo Jiang from Northeastern University (China) for her invaluable suggestions and support to my research. I also appreciate the understanding and encouragement from my friends, parents and colleagues.

Finally, this thesis was supported by the UK Engineering and Physical Sciences Research Council under the project “UK Consortium on Mesoscale Engineering Sciences (UKCOMES)” (Grant No. EP/R029598/1). CoSeC, the Computational Science Centre for Research Communities, provided computational resources through UKCOMES for this project.

UCL Research Paper Declaration Form: referencing the doctoral candidate's own published work(s)

Please use this form to declare if parts of your thesis are already available in another format, e.g. if data, text, or figures:

- have been uploaded to a preprint server;
- are in submission to a peer-reviewed publication;
- have been published in a peer-reviewed publication, e.g. journal, textbook.

This form should be completed as many times as necessary. For instance, if you have seven thesis chapters, two of which containing material that has already been published, you would complete this form twice.

1. For a research manuscript that has already been published (if not yet published, please skip to section 2)**:**		
a) Where was the work published? (e.g. journal name)	Energy	
b) Who published the work? (e.g. Elsevier/Oxford University Press):	Elsevier	
c) When was the work published?	12/08/2021	
d) Was the work subject to academic peer review?	Yes	
e) Have you retained the copyright for the work?	No	
[If no, please seek permission from the relevant publisher and check the box next to the below statement]: ☐ *I acknowledge permission of the publisher named under 1b to include in this thesis portions of the publication named as included in 1a.*		
2. For a research manuscript prepared for publication but that has not yet been published (if already published, please skip to section 3)**:**		
a) Has the manuscript been uploaded to a preprint server? (e.g. medRxiv):	Please select.	**If yes, which server?** Click or tap here to enter text.
b) Where is the work intended to be published? (e.g. names of journals that you are planning to submit to)	Click or tap here to enter text.	
c) List the manuscript's authors in the intended authorship order:	Click or tap here to enter text.	
d) Stage of publication	Please select.	
3. For multi-authored work, please give a statement of contribution covering all authors (if single-author, please skip to section 4**):**		
Zhongze Bai performed the research, analysed data and wrote the manuscript draft. Xi Zhuo Jiang co-supervised the research and revised the manuscript. KHL supervised the project and finalised the manuscript.		

4. In which chapter(s) of your thesis can this material be found?			
Chapter 3			
5. e-Signatures confirming that the information above is accurate (this form should be co-signed by the supervisor/ senior author unless this is not appropriate, e.g. if the paper was a single-author work):			
Candidate:	Zhongze Bai	**Date:**	30/03/2023
Supervisor/ Senior Author (where appropriate)**:**	Kai H. Luo	**Date:**	30/03/2023

UCL Research Paper Declaration Form: referencing the doctoral candidate's own published work(s)

Please use this form to declare if parts of your thesis are already available in another format, e.g. if data, text, or figures:

- have been uploaded to a preprint server;
- are in submission to a peer-reviewed publication;
- have been published in a peer-reviewed publication, e.g. journal, textbook.

This form should be completed as many times as necessary. For instance, if you have seven thesis chapters, two of which containing material that has already been published, you would complete this form twice.

6. For a research manuscript that has already been published (if not yet published, please skip to section 2)**:**		
f) Where was the work published? (e.g. journal name)	Proceedings of the Combustion Institute	
g) Who published the work? (e.g. Elsevier/Oxford University Press):	Elsevier	
h) When was the work published?	15/07/2022	
i) Was the work subject to academic peer review?	Yes	
j) Have you retained the copyright for the work?	Yes	
[If no, please seek permission from the relevant publisher and check the box next to the below statement]: ☐ *I acknowledge permission of the publisher named under 1b to include in this thesis portions of the publication named as included in 1a.*		
7. For a research manuscript prepared for publication but that has not yet been published (if already published, please skip to section 3)**:**		
e) Has the manuscript been uploaded to a preprint server? (e.g. medRxiv):	Please select.	**If yes, which server?** Click or tap here to enter text.
f) Where is the work intended to be published? (e.g. names of journals that you are planning to submit to)	Click or tap here to enter text.	
g) List the manuscript's authors in the intended authorship order:	Click or tap here to enter text.	
h) Stage of publication	Please select.	
8. For multi-authored work, please give a statement of contribution covering all authors (if single-author, please skip to section 4**):**		
Zhongze Bai performed the research, analysed data and wrote the manuscript draft. Xi Zhuo Jiang co-supervised the research and revised the manuscript. KHL supervised the project and finalised the manuscript.		

9. In which chapter(s) of your thesis can this material be found?			
Chapter 4.1			
10. e-Signatures confirming that the information above is accurate (this form should be co-signed by the supervisor/ senior author unless this is not appropriate, e.g. if the paper was a single-author work):			
Candidate:	Zhongze Bai	**Date:**	30/03/2023
Supervisor/ Senior Author (where appropriate)**:**	Kai H. Luo	**Date:**	30/03/2023

UCL Research Paper Declaration Form: referencing the doctoral candidate's own published work(s)

Please use this form to declare if parts of your thesis are already available in another format, e.g. if data, text, or figures:

- have been uploaded to a preprint server;
- are in submission to a peer-reviewed publication;
- have been published in a peer-reviewed publication, e.g. journal, textbook.

This form should be completed as many times as necessary. For instance, if you have seven thesis chapters, two of which containing material that has already been published, you would complete this form twice.

11. For a research manuscript that has already been published (if not yet published, please skip to section 2)**:**		
k) Where was the work published? (e.g. journal name)	Process Safety and Environmental Protection	
l) Who published the work? (e.g. Elsevier/Oxford University Press):	Elsevier	
m) When was the work published?	04/03/2023	
n) Was the work subject to academic peer review?	Yes	
o) Have you retained the copyright for the work?	Yes	
[If no, please seek permission from the relevant publisher and check the box next to the below statement]: ☐ *I acknowledge permission of the publisher named under 1b to include in this thesis portions of the publication named as included in 1a.*		
12. For a research manuscript prepared for publication but that has not yet been published (if already published, please skip to section 3)**:**		
i) Has the manuscript been uploaded to a preprint server? (e.g. medRxiv):		**If yes, which server?** Click or tap here to enter text.
j) Where is the work intended to be published? (e.g. names of journals that you are planning to submit to)		
k) List the manuscript's authors in the intended authorship order:	Click or tap here to enter text.	
l) Stage of publication		
13. For multi-authored work, please give a statement of contribution covering all authors (if single-author, please skip to section 4**):**		
Zhongze Bai performed the research, analysed data and wrote the manuscript draft. Xi Zhuo Jiang co-supervised the research and revised the manuscript. KHL supervised the project and finalised the manuscript.		

14. In which chapter(s) of your thesis can this material be found?			
Section 4.2			
15. e-Signatures confirming that the information above is accurate (this form should be co-signed by the supervisor/ senior author unless this is not appropriate, e.g. if the paper was a single-author work):			
Candidate:	Zhongze Bai	**Date:**	30/03/2023
Supervisor/ Senior Author (where appropriate)**:**	Kai H. Luo	**Date:**	30/03/2023

UCL Research Paper Declaration Form: referencing the doctoral candidate's own published work(s)

Please use this form to declare if parts of your thesis are already available in another format, e.g. if data, text, or figures:

- have been uploaded to a preprint server;
- are in submission to a peer-reviewed publication;
- have been published in a peer-reviewed publication, e.g. journal, textbook.

This form should be completed as many times as necessary. For instance, if you have seven thesis chapters, two of which containing material that has already been published, you would complete this form twice.

16. For a research manuscript that has already been published (if not yet published, please skip to section 2)**:**		
p) Where was the work published? (e.g. journal name)	Journal of the Energy Institute	
q) Who published the work? (e.g. Elsevier/Oxford University Press):	Elsevier	
r) When was the work published?	03/01/2023	
s) Was the work subject to academic peer review?	Yes	
t) Have you retained the copyright for the work?	Yes	
[If no, please seek permission from the relevant publisher and check the box next to the below statement]: ☐ *I acknowledge permission of the publisher named under 1b to include in this thesis portions of the publication named as included in 1a.*		
17. For a research manuscript prepared for publication but that has not yet been published (if already published, please skip to section 3)**:**		
m) Has the manuscript been uploaded to a preprint server? (e.g. medRxiv):		**If yes, which server?** Click or tap here to enter text.
n) Where is the work intended to be published? (e.g. names of journals that you are planning to submit to)		
o) List the manuscript's authors in the intended authorship order:	Click or tap here to enter text.	
p) Stage of publication		
18. For multi-authored work, please give a statement of contribution covering all authors (if single-author, please skip to section 4**):**		
Zhongze Bai performed the research, analysed data and wrote the manuscript draft. Xi Zhuo Jiang co-supervised the research and revised the manuscript. KHL supervised the project and finalised the manuscript.		

19. In which chapter(s) of your thesis can this material be found?			
Chapter 4.3			
20. e-Signatures confirming that the information above is accurate (this form should be co-signed by the supervisor/ senior author unless this is not appropriate, e.g. if the paper was a single-author work):			
Candidate:	Zhongze Bai	**Date:**	30/03/2023
Supervisor/ Senior Author (where appropriate)**:**	Kai H. Luo	**Date:**	30/03/2023

UCL Research Paper Declaration Form: referencing the doctoral candidate's own published work(s)

Please use this form to declare if parts of your thesis are already available in another format, e.g. if data, text, or figures:

- have been uploaded to a preprint server;
- are in submission to a peer-reviewed publication;
- have been published in a peer-reviewed publication, e.g. journal, textbook.

This form should be completed as many times as necessary. For instance, if you have seven thesis chapters, two of which containing material that has already been published, you would complete this form twice.

21. For a research manuscript that has already been published (if not yet published, please skip to section 2)**:**		
u) Where was the work published? (e.g. journal name)	Fuel	
v) Who published the work? (e.g. Elsevier/Oxford University Press):	Elsevier	
w) When was the work published?	19/10/2022	
x) Was the work subject to academic peer review?	Yes	
y) Have you retained the copyright for the work?	Yes	
[If no, please seek permission from the relevant publisher and check the box next to the below statement]: ☐ *I acknowledge permission of the publisher named under 1b to include in this thesis portions of the publication named as included in 1a.*		
22. For a research manuscript prepared for publication but that has not yet been published (if already published, please skip to section 3)**:**		
q) Has the manuscript been uploaded to a preprint server? (e.g. medRxiv):	Please select.	**If yes, which server?** Click or tap here to enter text.
r) Where is the work intended to be published? (e.g. names of journals that you are planning to submit to)	Click or tap here to enter text.	
s) List the manuscript's authors in the intended authorship order:	Click or tap here to enter text.	
t) Stage of publication	Please select.	
23. For multi-authored work, please give a statement of contribution covering all authors (if single-author, please skip to section 4**):**		
Zhongze Bai performed the research, analysed data and wrote the manuscript draft. Xi Zhuo Jiang co-supervised the research and revised the manuscript. KHL supervised the project and finalised the manuscript.		

24. In which chapter(s) of your thesis can this material be found?			
Chapter 5.1			
25. e-Signatures confirming that the information above is accurate (this form should be co-signed by the supervisor/ senior author unless this is not appropriate, e.g. if the paper was a single-author work):			
Candidate:	Zhongze Bai	**Date:**	30/03/2023
Supervisor/ Senior Author (where appropriate)**:**	Kai H. Luo	**Date:**	30/03/2023

UCL Research Paper Declaration Form: referencing the doctoral candidate's own published work(s)

Please use this form to declare if parts of your thesis are already available in another format, e.g. if data, text, or figures:

- have been uploaded to a preprint server;
- are in submission to a peer-reviewed publication;
- have been published in a peer-reviewed publication, e.g. journal, textbook.

This form should be completed as many times as necessary. For instance, if you have seven thesis chapters, two of which containing material that has already been published, you would complete this form twice.

26. For a research manuscript that has already been published (if not yet published, please skip to section 2)**:**		
z) Where was the work published? (e.g. journal name)	Chemical Engineering Science	
aa) Who published the work? (e.g. Elsevier/Oxford University Press):	Elsevier	
bb) When was the work published?	06/11/2022	
cc) Was the work subject to academic peer review?	Yes	
dd) Have you retained the copyright for the work?	Yes	
[If no, please seek permission from the relevant publisher and check the box next to the below statement]: ☐ *I acknowledge permission of the publisher named under 1b to include in this thesis portions of the publication named as included in 1a.*		
27. For a research manuscript prepared for publication but that has not yet been published (if already published, please skip to section 3)**:**		
u) Has the manuscript been uploaded to a preprint server? (e.g. medRxiv):	Please select.	**If yes, which server?** Click or tap here to enter text.
v) Where is the work intended to be published? (e.g. names of journals that you are planning to submit to)	Click or tap here to enter text.	
w) List the manuscript's authors in the intended authorship order:	Click or tap here to enter text.	
x) Stage of publication	Please select.	
28. For multi-authored work, please give a statement of contribution covering all authors (if single-author, please skip to section 4**):**		
Zhongze Bai performed the research, analysed data and wrote the manuscript draft. Xi Zhuo Jiang co-supervised the research and revised the manuscript. KHL supervised the project and finalised the manuscript.		

29. In which chapter(s) of your thesis can this material be found?			
Chapter 5.2			
30. e-Signatures confirming that the information above is accurate (this form should be co-signed by the supervisor/ senior author unless this is not appropriate, e.g. if the paper was a single-author work):			
Candidate:	Zhongze Bai	**Date:**	30/03/2023
Supervisor/ Senior Author (where appropriate)**:**	Kai H. Luo	**Date:**	30/03/2023

Content

List of Figures

List of Tables

Nomenclature

Acronyms / Abbreviations

AAEM	alkali and alkaline earth metallic
AMBER	assisted model building with energy minimization
APH	air preheater
ChemTrayzer	Chemical Trajectory Analyzer
CFD	computational fluid dynamics
CFF	consistent force field
CHARMM	chemistry at Harvard macromolecular mechanics
CVFF	consistent valence force field
DFT	density functional theory
EF	electric field
ESR	electron spin resonance
IDTs	ignition delay times
LAMMPS	large-scale atomic/molecular massively parallel simulation
LNB	low NOx burner
MD	molecular dynamics
MMFF	Merck molecular force field
MP2	second-order Moller–Plesset perturbation theory
NF	net flux
NNE	microcanonical ensemble
NVT	canonical ensemble
OFA	over fire air
PANS	peroxylacyl nitrates
PFBC	pressurized fluidized bed combustion
PM	particulate matters
QEq	charge equilibration methods
QM	quantum mechanics
ReaxFF	reactive force field
SCR	selective catalytic reduction
SE	standard error
SNCR	selective non-catalytic reduction

Solid-Py/SVUV-PIMS	solid pyrolysis/synchrotron vacuum ultraviolet photoionization mass spectrometry
TGA	thermo-gravimetric analysis
UBC	unburned carbon
VMD	visual molecular dynamics
VOCs	volatile organic compounds

Symbols

BO	bond order
#	number
cm	centimetre
E	electric field strength
E_{bond}	energy of the bonds between atoms
E_{Colomb}	coulomb interaction between atoms
E_{conj}	conjugation energy for aromatic structures
E_{over}	energy penalty for the bond energy of over-coordinated atoms
E_{pen}	energy penalty for atoms forming two double bonds with surrounding atoms
E_{system}	total potential energy of the system
E_{tors}	dihedral angle energy related to the four-body interaction energy
E_{under}	energy penalty for the bond energy of under-coordinated atoms
E_{val}	bond angle energy related to the three-body interaction energy
$E_{vdWaals}$	non-bonded interactions between molecules
fs	femtosecond
g	gram
K	kelvin
n	number
NHi	umbrella term of NH_3, NH_2 and NH.
nm	nanometer
o	circle
P_{bo}	empirical parameters

ps	picoseconds
q	the atomic charge
R	ratio of the molecule number of HCN or NH_3
r	distance
T	temperature
t	time
v	velocity
V	volt
J	electrostatic potential between atoms
$J0$	atom self-Coulomb interaction

Greek Letters

Å	angstrom
Δ	difference
±	ratio of the numbers of water to pyridine
λ	excess air coefficient
β	ratio of the numbers of ozone to pyridine
σ	single bond
π	double bond
ππ	triple bond
χ	electronegativity

Subscripts

ac	active centre
f	free site
i & j	atom number

Chapter 1 Introduction

1.1 Background and Motivation

Coal has been the principal fuel of the global energy system since the industrial revolution because of its relative abundance and low cost [1, 2]. Figure 1.1 shows the world's coal consumption by region during 2000-2021. Overall, the coal consumption increased significantly over those years in developing economies. Though the advanced economies decrease the coal utilization slightly, the world's coal consumption still remains at a high level in recent years. The coal utilization will highly show the increase trend because of the growing populations and modernization especially in developing countries [3]. However, nitrogen oxides (NOx) from coal burning result in significant environmental issues such as acid rain and photochemical smog [4]. Diverse methods for lowering NOx emissions have been developed in order to safeguard the environment from pollution and comply with the ever-stricter NOx emission rules.

Coal splitting and staging is an effective approach to control NOx emissions using coal pyrolysis gas with excellent NOx reduction performance as well as relatively low operating cost compared with other reburn fuels like gas, oil and coal [5].

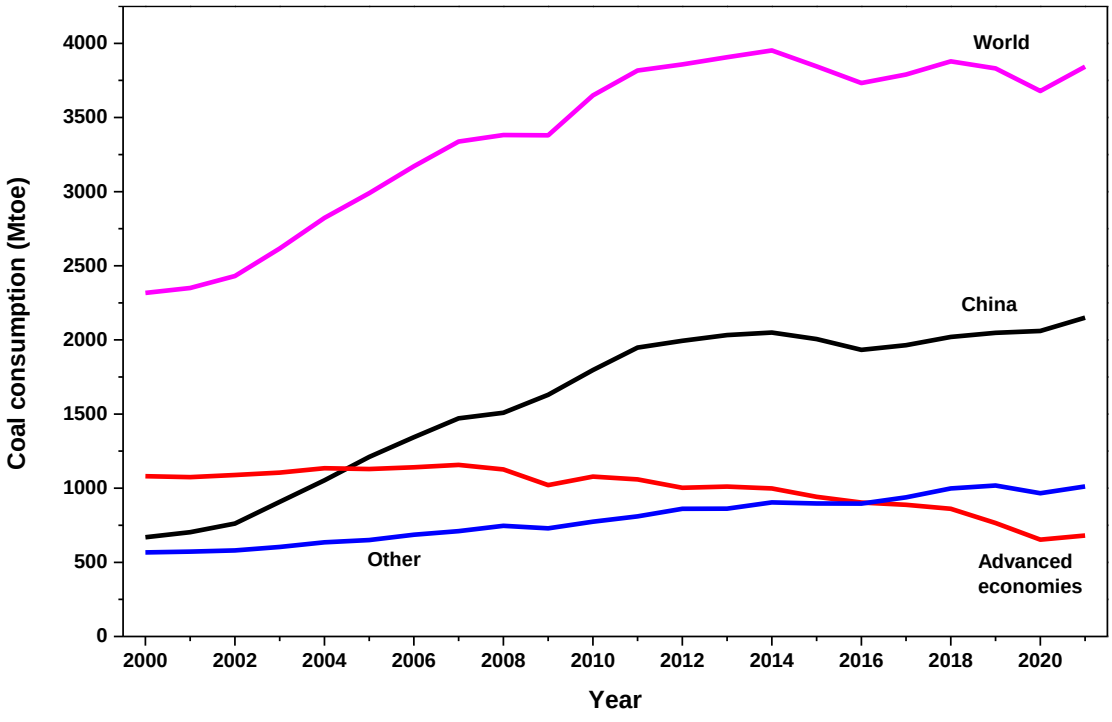

Figure 1.1 Coal consumption by region during 2000-2021 [6].

During this process, the combustion process is divided into three zones in series as shown in Figure 1.2. Coal undergoes pyrolysis process forming pyrolysis gas and solid char first. In the main zone, the char is oxidized to release heat and NOx is formed. In the reburn zone, pyrolysis gas is injected to convert NOx from main zone to clean N_2 under fuel-rich conditions. Excess air is provided to oxide remaining species and ensure complete combustion in the burnout zone. The reburn fuel (coal pyrolysis gas) plays vital role in the NOx reduction behaviours of this technology. The nitrogen-containing species in pyrolysis gas have been found to be crucial for NOx removal behaviours in coal splitting and staging process in earlier research [5, 7]. Thus, understanding the underlying mechanisms of nitrogen migration during the pyrolysis and reduction processes is critical as it can assist in optimising operational parameters that reduce NOx emissions from coal oxidation.

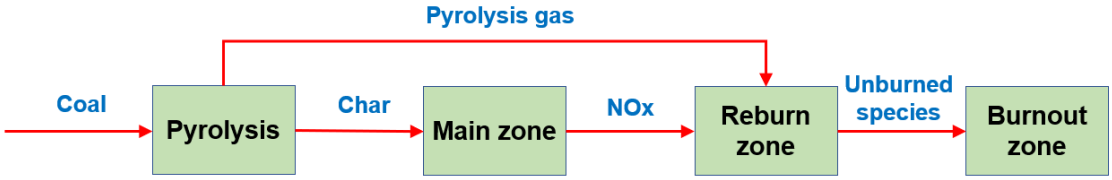

Figure 1.2 Schematic diagram of coal splitting and staging process.

In addition, assisted combustion is a widely used method to reduce NOx emissions by controlling the oxidation process. In particular, electric field (EF) assisted combustion, which modifies reaction processes by applying changing EF strengths during fuel combustion, is an efficient approach to reduce NOx emissions [8-10]. Additionally, the majority of the NOx pollutants during coal combustion are nitric oxide (NO), with lower levels of nitrogen dioxide (NO_2) [11]. Due to the high solubility of NO_2 in water, it may be quickly eliminated by water [12]. In contrast, NO in exhaust gases must be eliminated using selective catalytic reduction (SCR), which has a high operating cost [12]. This is because NO is poorly soluble in water. One of the most potent oxidizers, ozone (O_3), can alter proportion of NO and NO_2 in NOx emissions and enhance combustion performance (including ignition, flame propagation, and flame stability) [13]. As a result, the addition of ozone can be used as a practical and promising technique to decrease NOx pollutants from coal utilization.

1.2 Literature Review

1.2.1 Nitrogen Oxides (NOx)

NOx is a generic term for nitrogen oxides, including N_2O, NO, N_2O_2, N_2O_3, NO_2, N_2O_4 and N_2O_5. The properties of those compounds are summarized in Table 1.1. Among them, NO, NO_2 and N_2O are the most abundant nitrogen oxides in the air, and N_2O_2 and N_2O_4 are dimers of NO and NO_2, respectively [14]. N_2O_3 and N_2O_5 exist in extremely low concentrations, and their influence are often negligible. NO is a colourless gas can cause the failure to absorb O_2 to blood like carbon oxide (CO). Also, NO is unstable and reacts with oxygen-containing species in air such as HO_2, O_2 and O_3 to generate NO_2 formation, which may drive bronchoconstriction, inflammation and reduced immune response even at low concentrations [15]. N_2O is a kind of greenhouse gas with a long lifetime, which has 298 times the atmospheric heat-trapping ability of carbon dioxide (CO_2) [16].

Table 1.1 Composition of nitrogen oxides (NOx) [14].

Formula	Name	Nitrogen Valence	Properties
N_2O	nitrous oxide	1	colourless gas water soluble
NO N_2O_2	nitric oxide dinitrogen dioxide	2	colourless gas slightly water soluble
N_2O_3	dinitrogen trioxide	3	black solid water soluble decomposes in water
NO_2 N_2O_4	nitrogen dioxide dinitrogen tetroxide	4	red-brown gas very water soluble decomposes in water
N_2O_5	dinitrogen pentoxide	5	white solid very water soluble decomposes in water

The interaction of NOx and water forms nitrous acid (HNO_2) or nitric acid (HNO_3), contributing to acid rain deposition, as Figure 1.3 shows. Acid rain has adverse impacts on forests [17-19], soils [20-22], surface waters and aquatic animals [23]. It can also cause paint to peel, corrosion of steel structures and weathering of stone buildings and statues [24, 25].

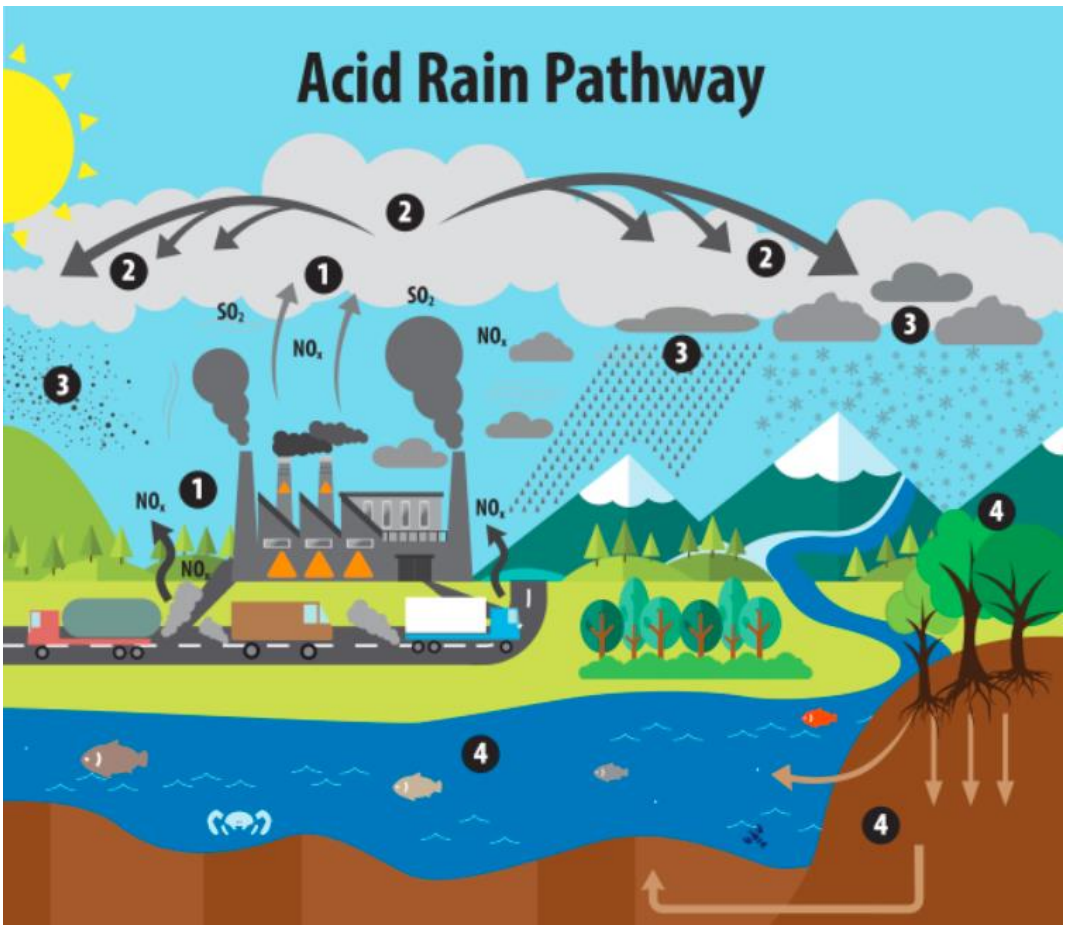

Figure 1.3 Acid rain pathway [26].

As shown in Figure 1.4, photochemical smog is another main environmental problem caused by NOx, where NOx reacts with volatile organic compounds (VOCs) in the atmosphere under light conditions generating peroxylacyl nitrates (PANs), tropospheric ozone, and aldehydes [27]. Those products are usually toxic to humans and can cause severe sickness, a shortened life span and premature death [27].

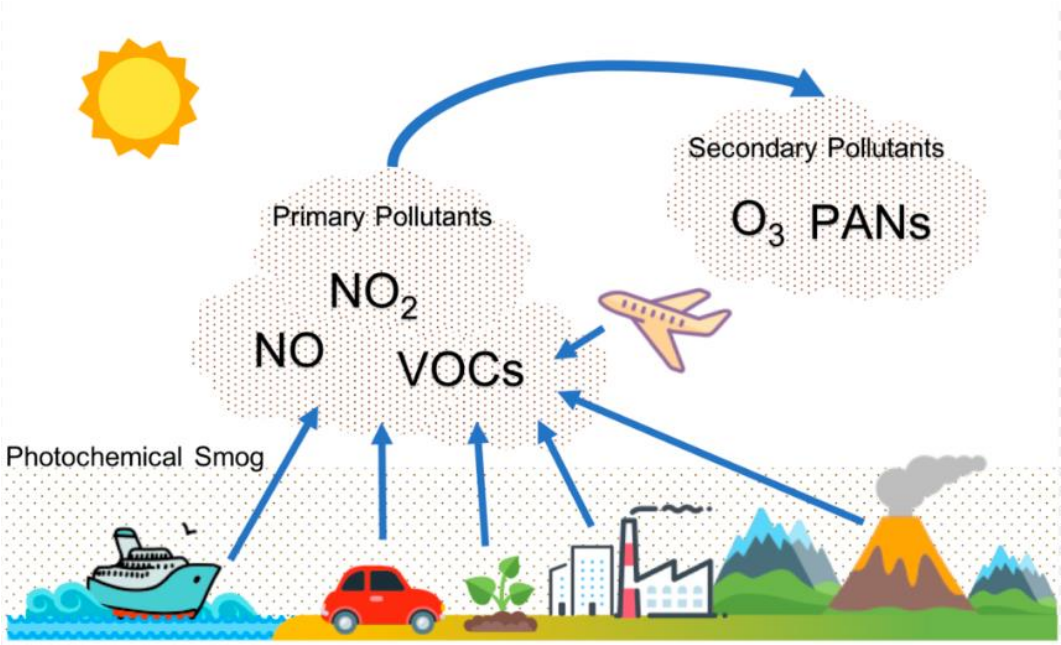

Figure 1.4 Diagram of photochemical smog formation [27].

1.2.2 NOx Control Technologies

NOx control methods include two categories: primary control technologies and secondary control methods, which will be further characterized in Section 1.2.2.1 – 1.2.2.3.

1.2.2.1 Primary Control Technologies

Primary control technologies decrease NOx formation from combustion by the alteration of operational conditions. The main methods include low NOx burner (LNB), over fire air (OFA) and coal assisted combustion.

1.2.2.1.1 Low NOx Burners (LNBs)

LNBs limit NOx formation by controlling the stoichiometric and temperature profiles of the combustion process [28, 29]. As Figure 1.5 shows, the input air is separated into two parts, primary air and secondary air, thereby causing the following atmospheres: (1) the reduced oxygen concentrations inhibit the generation of both fuel and thermal NOx in primary zone; and (2) the reduced flame temperature due to insufficient combustion further reduces the formation of thermal NOx. LNBs can reduce NOx emissions by 50% or more compared with common combustion process [30].

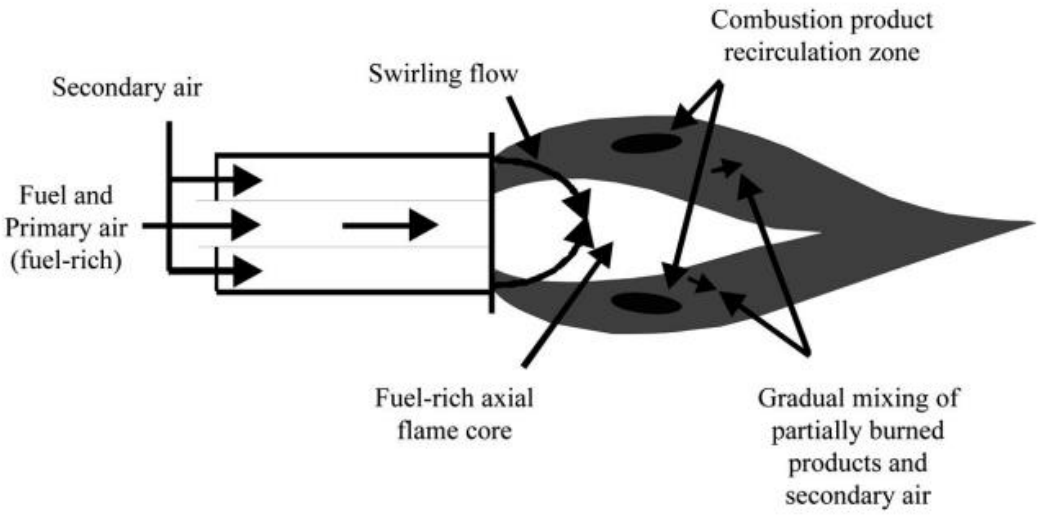

Figure 1.5 Schematic of a low-NOx burner [30].

1.2.2.1.2 Over Fire Air (OFA)

OFA is another popular method of air staging, where 5–20% of the total combustion air is injected into ports above the normal combustion zone [14, 31, 32]. In general, OFA is used in combination with LNBs, which may increase the NOx reductions by an additional 10 to 25% [29].

However, the use of LNBs and OFA can cause the increase of unburned carbon (UBC) and carbon oxide (CO) concentrates in exhaust gases, which reduces combustion efficiency and increases pollutants of particulate matter (PM) and CO. This problem can be minimized by the careful control of combustion parameters and appropriately designed LNBs and OFA systems.

1.2.2.1.3 Assisted Combustion

Ozone and EF both have the power to restrict the yields of pollutants and control flame properties including ignition, combustion temperature, flame shape, etc [13, 33]. The EF impact on NOx production from fuel oxidation has been widely investigated before. For example, Zake and co-workers studied the impact of the EF on NO output during the oxidation of natural gas through experiments [34]. Results suggested that EF had the abilities to reduce the thermal NOx generation during natural gas burning by 30% to 80% [34]. Barmina and co-workers carried out an experimental investigation on the impact of EF on the combustion of biomass in gasifiers [35]. Results showed that applying external EF lowered CO and NOx emissions. EF was discovered to be able to regulate

NOx emissions during airborne methane burning by Most and colleagues [36]. It has also been shown in earlier research through tests and computational fluid dynamics (CFD) simulations that EF can lower NO_x emissions during propane oxidation [37-39]. The aforementioned studies illustrated the overall impacts of EF on NOx pollutants from fuel oxidation, however there are still some details that are unknown. For instance, might the EF regulate the formation of fuel-NOx with the exception of thermal NOx? How the EF strength quantitatively impacts the NOx emissions? More thorough research utilising time- and space-resolved approaches is needed to answer such problems. In addition, previous studies mainly focused on the gaseous fuels without considering complex solid fuels.

Numerous investigations on ozone assisted combustion have concentrated on the impact of O_3 on ignition [40, 41], flame propagation [42, 43] and flame stabilization [44, 45] during fuel oxidation. Tachibana and co-workers conducted a series of experiments to investigate how ozone affected compression ignition engine combustion [46]. The findings show that ozone can reduce CO, C_nH_m, and soot emissions while increasing NOx emissions. When examining the impact of ozone on the oxidation parameters of internal combustion engines, Nasser and co-workers also came to the same conclusion [47]. Previous research has shown that the addition of ozone may significantly alter the exhaust emissions produced during fuel combustion. Less research has been done, meanwhile, on how adding O_3 affects emissions of pollutants from burning fuel. There are certain fundamental issues that remain unanswered. For instance, it is still unknown what the underlying processes are that cause ozone to impact NOx generation during combustion. Additionally, the previous research did not examine the component of NOx pollutants under various ozone concentrations, which might have an impact on the operating costs of the NOx removal process. Thus, the impacts of EF and ozone on NOx generation during coal oxidation must be revealed in order to better manage NOx emissions during coal combustion.

1.2.3 Secondary Control Technologies

By employing only primary control technologies, it may be difficult to comply with current or future NOx standards for coal combustion; thus, secondary control technologies are needed to further minimise NOx emissions. Selective NOx reduction and fuel staging are examples of secondary controls that lower NOx

emissions from fuel combustion in the primary zone.

1.2.3.1 Selective Reduction

Selective noncatalytic reduction (SNCR) and selective catalytic reduction (SCR) are two types of selective reduction technologies, where nitrogenous chemicals (such as ammonia and urea) are used to reduce NOx to N_2 selectively in the presence of oxygen.

In SNCR, nitrogen-containing reagent is injected into the boiler's upper furnace region as shown in Figure 1.6, where the NOx reduction can achieve 30%-75% [30, 48]. The overall reactions of NO reduction by ammonia and urea are as follows:

$$2(NH_2)_2CO + 4NO + O_2 \rightarrow 4H_2O + 2CO_2 + 4N_2 \quad \text{(R1.1)}$$

$$4NH_3 + 4NO + O_2 \rightarrow 4N_2 + 6H_2O \quad \text{(R1.2)}$$

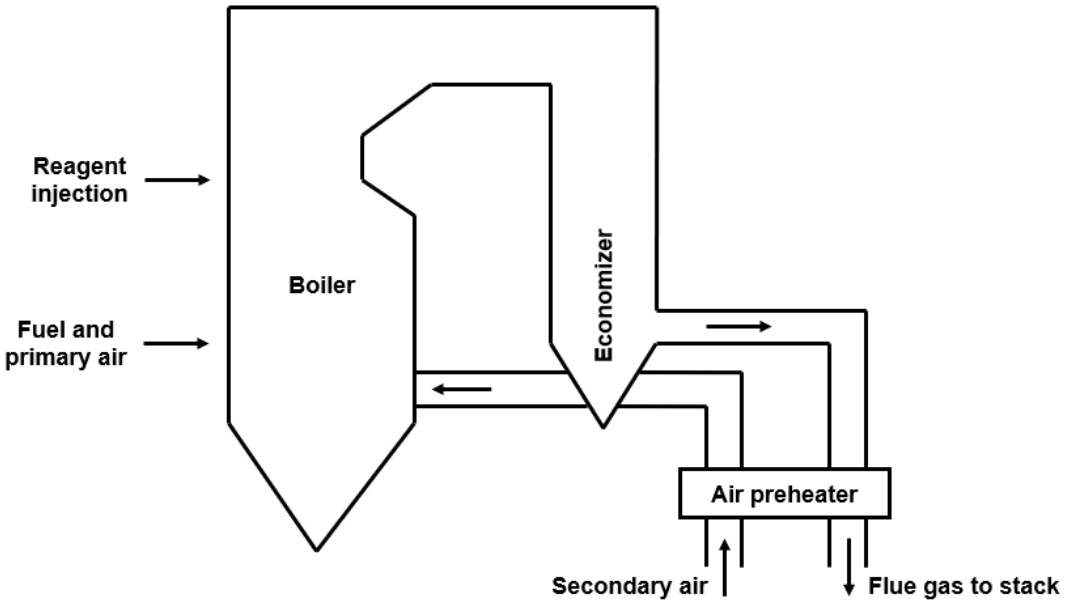

Figure 1.6 Schematic of SNCR process [30].

In general, there are three pathways for the reaction between reagent and NO: (1) NOx is converted to N_2 by reagent, (2) NOx generation from the oxidation of reagent by O_2 in flue gas, and (3) reagent remains unreacted and pass through causing "NH_3 slip". The reaction temperature has huge influence on the SNCR performance, which normally ranges from 900°C to 1150°C. The relatively low temperature (less than 900°C) decreases the reduction reactions, resulting in the increase of remaining NOx and reagent. For relatively high temperature (higher

than 1150°C), the oxidation of reagents domains compared to the reduction reactions of NOx, and thereby inhibits the NOx reduction performance of SNCR.

For SCR process, the overall reaction is similar to that of SNCR, but catalysts are required and the reaction temperature (350°C – 400°C) is typically lower than that of SNCR [30, 49]. The NOx reduction efficiency of SCR is significantly higher than that of SNCR, and is capable of achieving up to 90% [50]. As observed in Figure 1.7, the SCR reactor is typically situated upstream of the air preheater and after the boiler economizer (APH). The economizer bypass is used to ensure optimal flue gas temperature under low load situations [51].

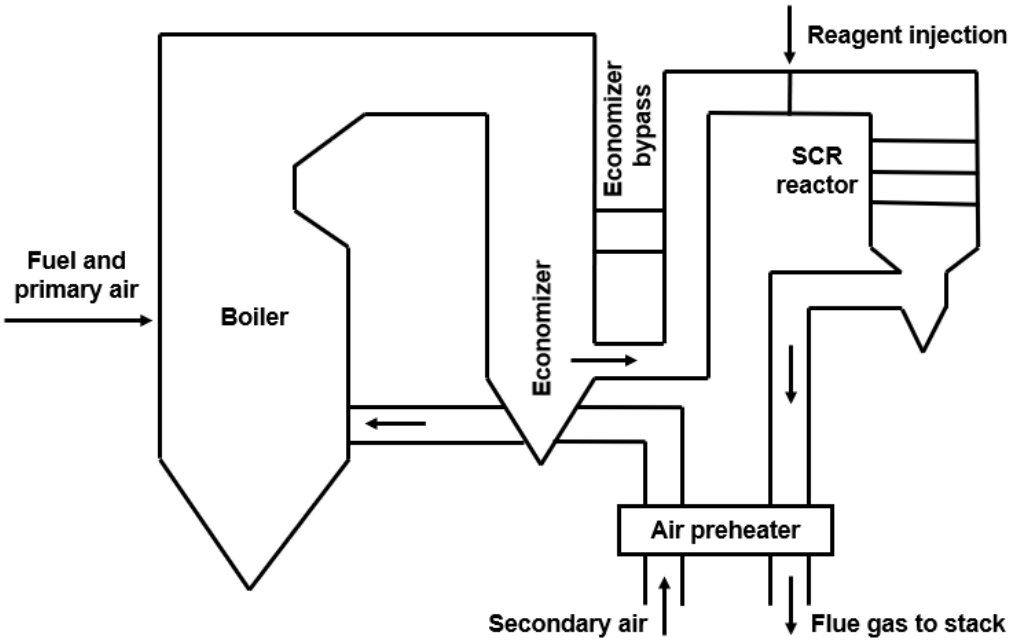

Figure 1.7 Schematic of SCR process [30].

The type of catalyst is important for the NO reduction behaviours in SCR. Basically, catalysts are classified into three types: (1) the supported noble metal catalysts (like Pt/Al_2O_3), (2) the base metal oxide catalysts (like MnOx and CuOx) and (3) metal ion exchanged zeolites-crystalline silicate (such as Cu-ZSM-5) [52]. "NH_3 slip" phenomenon also occurs in SCR process with the same reason with SNCR process. Another concern for SCR is the catalyst deactivation, which is caused by impurities in the flue gas poisoning catalysts. Thus, periodic maintenance and replacement are needed for catalysts, and correspondingly, the operating costs of SCR system are higher than those of SNCR system.

1.2.3.2 Fuel Staging

Figure 1.8 schematically presents the fuel staging process, where 10%-30% of total heat input is provided by the injection of auxiliary fuel (main fuel or another fuel) in reburn zone and a slightly fuel rich conditions are created to reduce NOx to N_2 ultimately [53]. With this technology, NOx emissions may be reduced by 50%-60% [52]. Finally, burnout air is provided after reburn zone to ensure complete combustion of fuels. Compared with selective reduction, fuel staging has a lower NOx reduction efficiency, but the capital costs and operating costs of fuel staging are significantly lower than those of SCR. To meet future more stringent NOx emissions regulations, a relatively economical choice is the combination of fuel staging and selective reduction technologies. In this process, the fuel reburning technology is used to reduce the NOx concentration at the furnace outlet as much as possible, which reduces the load on the SNCR/SCR system. Thus, the size of the SNCR/SCR system equipment, reagent consumption and catalyst dosage can be reduced. By this way, lower NOx emissions can be achieved with minimizing the investment and operating costs of the SNCR/SCR equipment.

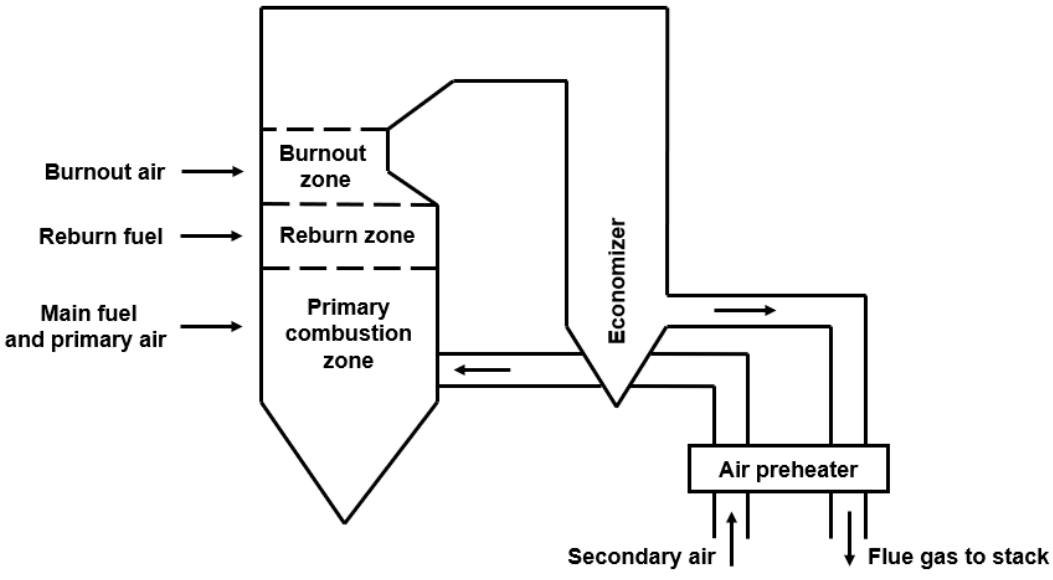

Figure 1.8 Schematic of fuel staging process [30].

Reburn fuels play dominant roles in the NOx removal performance of fuel staging, and the choice of reburn fuel is determined largely by fuel availability, a balance of operating costs versus capital costs, and the specifics of the boiler

[30]. Coal is usually used as reburn fuel with easy accessibility and low costs during coal combustion. However, coal reburning requires a relatively longer residence time and a large upper furnace because of its poor burnout, which also decreases the NOx reduction performance [30]. Natural gas may be an alternative reburn fuel with good burnout and NOx removal performance. Whereas its limited accessibility and relatively high costs constrain the spread of natural gas reburning. Besides, the NOx removal abilities of natural gas are lower than those of nitrogen-containing reagents like NH_3. Therefore, coal splitting and staging technology is developed to overcome those issues, which is introduced subsequently.

1.2.3.3 Coal Splitting and Staging Process

Coal pyrolysis gas is a promising reburn fuel for NOx reduction, which is derived from coal pyrolysis process and easy to obtain, and contains nitrogenous species such as HCN and NH_3. Thus, coal pyrolysis gas reburning (coal splitting and staging) has higher NOx removal behaviours, and it is relatively easy to spread this technology. The schematic of coal splitting and staging can refer to Figure 2.2. A further advantage is the possibility of adjusting pyrolysis conditions to the specific coal properties and thus producing an optimum reburn fuel with maximum NOx reduction efficiency [5]. Of course, that also brings challenges to control the coal pyrolysis and NOx reduction processes by coal pyrolysis gas, and thus the study of coal splitting and staging is necessary and important.

In 1996, Greul and co-workers carried out experimental studies on the coal splitting and staging process for the first time [5]. They pointed out that the optimum air/fuel ratio was around 0.9, and the nitrogenous species in coal pyrolysis gas determined the NOx removal behaviours. Also, the nitrogen-free species (CH_4) showed negative influence on the NO reduction process by coal pyrolysis gas [7]. The same conclusion was also corroborated by Rüdiger and co-wokrers' work, where they found that the increase of nitrogenous species content in coal pyrolysis gas could improve the NOx removal performance [7].

The above studies have demonstrated that the composition of pyrolysis gas (especially for nitrogenous species) and the operating parameters (like temperatures and oxygen content) in the reburn zone are important for NOx removal. However, the underlying mechanisms of nitrogenous species

generation from coal pyrolysis and NOx reduction by nitrogen-containing species still lack study. Therefore, there are huge potentials to improve NOx reduction performance by controlling the operating conditions of the coal splitting and staging process, which highlights the importance of studying the nitrogen migration during coal pyrolysis and NOx abatement by nitrogenous species in coal pyrolysis gas under varying operating conditions. The reviews are shown in Section 1.2.4 and Section 1.2.6, respectively.

1.2.4 Nitrogen Migration during Pyrolysis Process

1.2.4.1 Coal Pyrolysis

Pyrolysis is the first stage of coal splitting and staging process, profoundly affecting the generation of pyrolysis gas and char. Thus, understanding the coal pyrolysis process is vital for efficient and clean utilization of coal. Figure 1.9 shows a schematic for coal pyrolysis, and the pyrolysis process consists of two sets of reactions: primary devolatilization reactions and subsequent secondary gas phase reactions [54]. The former includes the thermal breakage of weak aliphatic bonds to generate many free radicals, which may react with each other to produce volatile products and may also undergo condensation reactions to produce semi-coke. The later includes the decomposition reactions of volatile generating smaller hydrocarbons and gases and the condensation reactions of semi-coke forming coke.

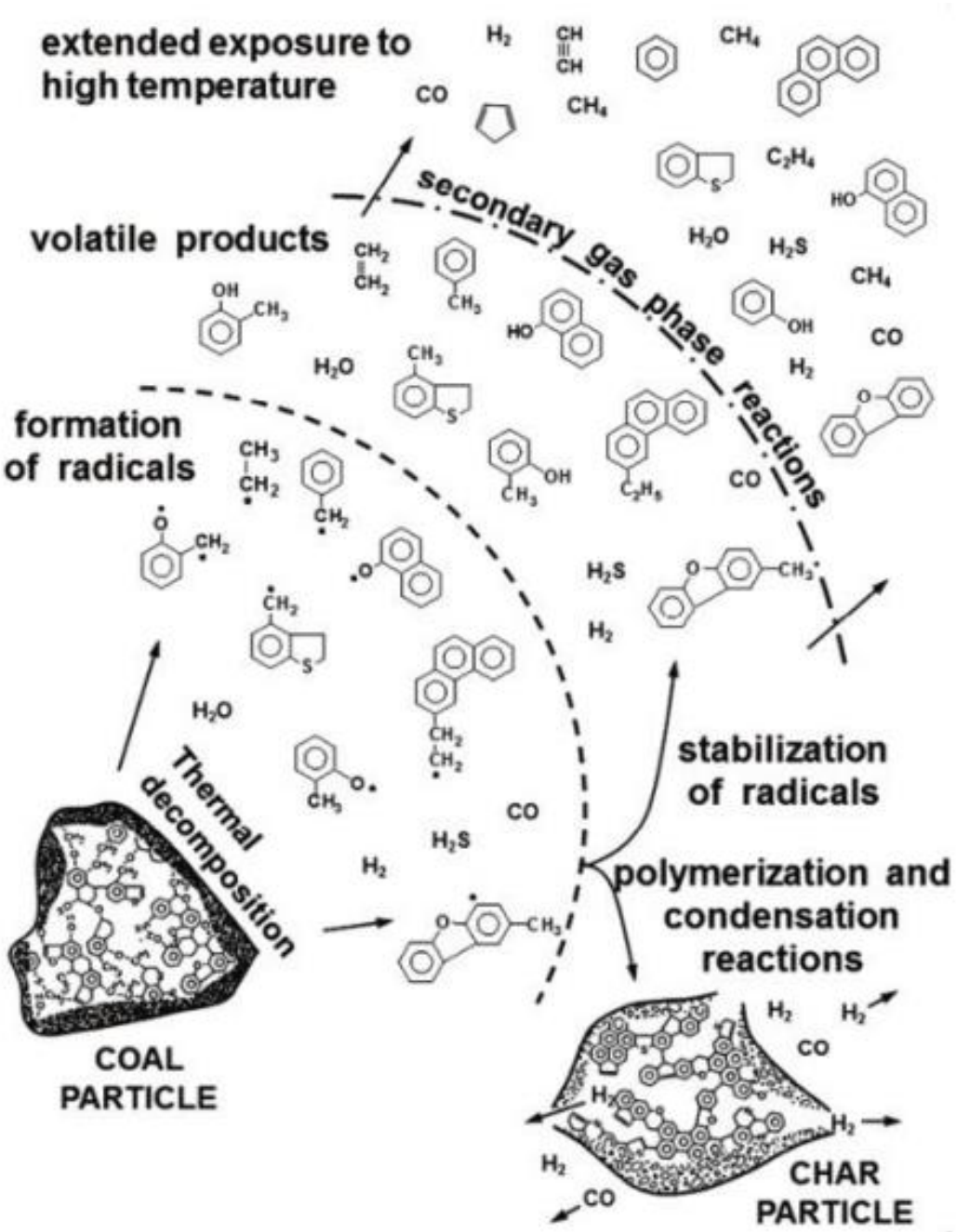

Figure 1.9 Reactions and processes of coal pyrolysis [54].

Coal pyrolysis is affected by many factors, including coal type, particle size, pyrolysis temperature, pyrolysis pressure, pyrolysis atmosphere, heating rate, etc [55-58]. In-depth understanding of the influence of these factors on the coal pyrolysis process is of significance for regulating the coal pyrolysis process. This thesis mainly focuses on the generation process of nitrogenous species in pyrolysis gas under varying conditions.

In 1978, Solomon and Colket studied the distribution of nitrogen in products during coal pyrolysis [59]. It was indicated that the initial nitrogen released by coal

was in tar, and it could secondary release nitrogen in non-tar volatiles at high temperatures. The composition of nitrogen-containing compounds during coal pyrolysis was investigated by Nelson and co-workers [60]. They found that the primary nitrogen-containing products were HCN and NH_3 and high temperatures were beneficial to the formation of HCN. Then, Rüdiger and co-workers carried out experiments to describe product distribution during coal pyrolysis at various temperatures [7]. The main products were char, tar, HCN+NH_3 and gas. It was found that due to the promotion effects of high temperature on the thermal decomposition of NH_3 and HCN, the amount of NH_3 and HCN increased first and then declined with the temperature rising.

Recently, ReaxFF MD has been widely applied in coal pyrolysis to detect intermediates more accurately in the pyrolysis process [61-65]. However, in the literature [61-64], their works mainly focus on the research of pyrolysis products (char, tar and gas) at different temperatures. The pyrolysis properties of nitrogen in coal were not included in their studies. Zheng and co-workers studied the distribution of nitrogen element in coal pyrolysis products such as char, tar and gas [65]. It is found from coal pyrolysis simulations that more than 65% N still remains in C_{40}+ fragments, about 25% N migrates into C_5–C_{40} fragments, and only 10% N transfers into small radicals and gases [65].

The above studies illustrate the nitrogen migration during coal pyrolysis and the influence of operating parameters (like temperature, heating rate, etc) on coal pyrolysis process. Moreover, some key components in coal such as moisture, alkali metals (such as Ca, Na, K, etc) have significant effects on the pyrolysis process [66-68]. One of them, water, an inherent coal component, has the ability to speed up coal pyrolysis and significantly change the product distributions in pyrolysis gas. In addition, compared to changes in the quantity of alkali metals, it is simpler to vary the water content of coal by intentionally adding or subtracting water. Studying how water affects nitrogen-containing compounds during coal pyrolysis is therefore very interesting since it may be a useful method for controlling the pyrolysis process.

Chen and co-workers investigated the influence of H_2O and CO_2 during char gasification and found H_2O and CO_2 had an obvious influence on char gasification through experiments [69]. Research was conducted by Ouyang and co-workers on the effects of water during the pyrolysis of char [70]. They pointed out that H_2O increased char reaction rate, decreased char yield and enhanced char structure.

Hu and co-workers carried out experiments to study the influence of H_2O on the coal pyrolysis process [71]. Results indicated the production of tar and light tar reduced during coal pyrolysis as the water content rose. Gou and colleagues investigated how water vapour affected the coal pyrolysis products [66]. They discovered that the production of HCN, NH_3, H_2, and CO, which can prevent NOx generation during coal pyrolysis, was facilitated by water [66].

Although numerous studies have been done on coal pyrolysis, the underlying mechanisms of nitrogen transfer pathways are lack of study. It is extremely difficult to directly use coal to study the conversion mechanisms of nitrogen during coal combustion because of the complicated and uncertain chemical structure of coal, the low nitrogen concentration, and the impact of other radicals or functional groups [72]. To know more about nitrogen transformations during pyrolysis, an alternative method is to study the pyrolysis of main nitrogen-containing compounds in coal.

1.2.4.2 Nitrogen-containing Compounds in Coal

As Figure 1.10 shows, the main nitrogen-containing compounds are pyrrolic and pyridinic structures [11]. Pyridinic structures include pyridine [59, 60, 73], picoline [74, 75], pyridol [76], quinoline [77-79], acridine [76] and pyrazine/pyrimidine/pyridazine [80-83]; pyrrolic compounds include pyrrole [84, 85], methylpyrrole [86], indole [78, 87] and carbazole [78, 87]. Though those nitrogen-containing compounds have different structures and pyrolysis behaviours (for example: pyridines are more stable than pyrroles [78, 79, 88], HCN is easier formed from components with two N-atoms in the ring [74]), the main pyrolysis and oxidation pathways are similar. All of them undergo ring-open reactions forming chain intermediates first, and release HCN subsequently [11]. In this thesis, pyridine is chosen as the representative to explore the nitrogen migration during coal pyrolysis. Pyridine is a six-membered nitrogenous heterocyclic aromatic with the chemical formula C_5H_5N [89]. All atoms in pyridine are in a plane and the structure of pyridine is shown in Figure 1.10. Detailed bond parameters can be found in previous work [90].

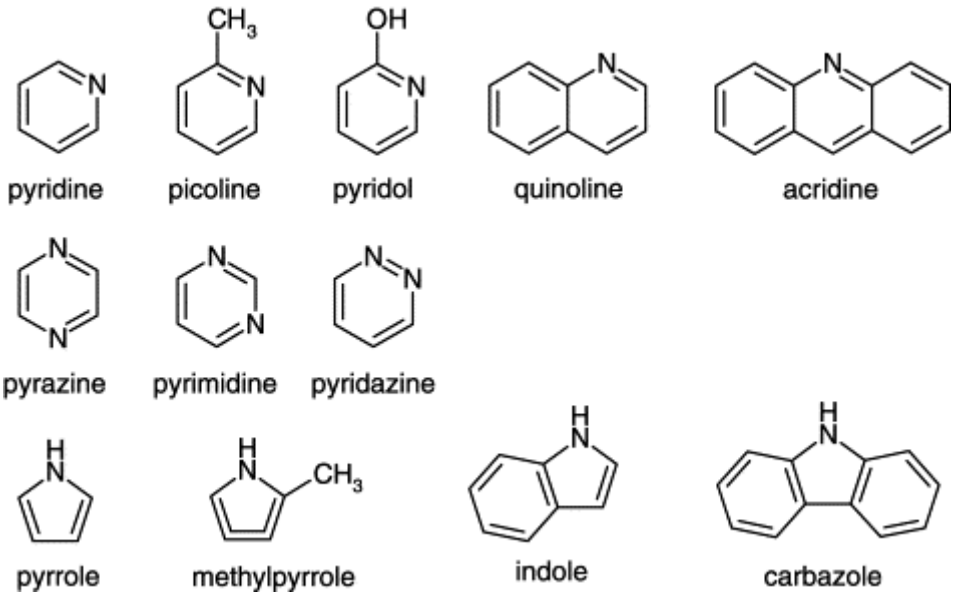

Figure 1.10 Nitrogen containing cyclic compounds in coal [11].

1.2.4.3 Pyridine Pyrolysis

There have been intensive studies on pyridine pyrolysis and the influence of H_2O molecules on coal pyrolysis by simulations and experiments. Houser and co-workers found that C_2H_2 and HCN were the main intermediates of pyridine pyrolysis [73]. The kinetics of pyrolysis of pyridine was investigated by Mackie and co-workers and they pointed out that the principal initiation reaction of pyridine pyrolysis is o-C_5H_5N → 2-,3-,4-C_5H_4N + H and six possible open-chain species of C_5H_4N [91], which is also confirmed by the literature [92, 93]. Besides, they also proposed reactions that were pyridine reacted with H atom to form o-C_5H_6N, then o-C_5H_6N generated methyl pyrrolyl radical [91]. Hore and Russell suggested pyridne pyrolysis scheme with major and minor reactions by calculations at semi-empirical and ab initio levels [92]. In 2000, Memon and co-workers did further stuck tube study on the mechanisms and decomposition rates of pyridine [93]. Reaction pathways during pyridine pyrolysis were investigated by Ninomiya and co-workers using semi-empirical PM3 molecular orbital calculations [90]. The reactions were obtained by the calculations of activation energy. Recently, Liu and Guo studied pyridine pyrolysis using reactive force field (ReaxFF) molecular dynamics (MD) simulations. Their work researched the effects of temperature, density and heating rates on pyridine pyrolysis products distributions [94]. Liu and co-workers investigated nitrogen transformations during coal pyrolysis with water through density functional theory (DFT) calculations [95]. They concluded that H_2O molecules enhanced the production

of NH_3, while inhibiting the generation of HCN.

To sum up, the underlying mechanisms of pyridine pyrolysis and the influence of pyrolysis parameters (like temperature, heating rates and density) are well studied before. However, the underlying mechanisms of pyridine pyrolysis with water addition are still unclear in the above studies, which is necessary to be further explored.

1.2.5 NOx Emissions from Char Oxidation

NO is considered the main component of NOx emissions from combustion [11, 96]. There are three principal sources of NOx formation in combustion process: thermal NOx, prompt NOx and fuel NOx [97].

1.2.5.1 Thermal NOx

Thermal NOx is generated via the reactions between O_2 and N_2 under high temperatures. The three main reactions forming NOx are [98]:

$$O + N_2 \rightarrow NO + N \quad \text{(R1.3)}$$

$$N + O_2 \rightarrow NO + O \quad \text{(R1.4)}$$

$$N + OH \rightarrow NO + H \quad \text{(R1.5)}$$

R1.3 and R1.4 are proposed by Zeldovich in 1946 for the first time [98]. After that, Lavoie and co-workers proposed the importance of R1.5 on the formation of thermal NOx [99]. The generation of thermal NOx is highly determined by the reaction temperature. Specifically, the generation of thermal NOx is slow and unimportant below 1800K, however, thermal NOx increases significantly with temperature over 1800K [100].

1.2.5.2 Prompt NOx

Prompt NOx is generated by the reactions between N_2 and radicals (such as C, CH, and CH_2 derived from fuel) at the beginning of combustion [101]. That results in the generation of nitrogen-containing intermediates (like HCN, CN, NH, etc), which can be oxidized to NO eventually. The main reactions are as follows [101]:

$$CH + N_2 \rightarrow HCN + N \quad \text{(R1.6)}$$

$$CH_2 + N_2 \rightarrow HCN + NH \quad \text{(R1.7)}$$

$$CH_3 + N_2 \rightarrow HCN + NH_2 \quad \text{(R1.8)}$$

$C_2+N_2 \rightarrow 2CN$ (R1.9)

$N+OH \rightarrow NO+H$ (R1.10)

$N+O_2 \rightarrow NO+O$ (R1.11)

$NH+O \rightarrow NO+H$ (R1.12)

$NH+OH \rightarrow N+H_2O$ (R1.13)

$CN+O_2 \rightarrow NCO+O$ (R1.14)

$HCN+O \rightarrow NCO+H$ (R1.15)

$HCN+OH \rightarrow NCO+H_2$ (R1.16)

$NCO+O \rightarrow NO+CO$ (R1.17)

1.2.5.3 Fuel NOx

Fuel NOx comes from the nitrogen-containing compounds oxidation in char (char-N) during combustion in coal splitting and staging process, which is the main contributor to formation of NOx emissions. There are two types for the NO formation during char oxidation [102, 103]: the first way is char-N reacts with O_2 generating NO directly and the reduction of NO on the char occurs subsequently; for the other pathway, HCN and HNCO are generated first, which will undergo the oxidation process forming NO finally. Overall, the first pathway domains on the NO formation during char combustion, the reaction mechanisms are [11]:

$C(N) + O_2 \rightarrow NO + C(O)$ (R1.18)

$2C_f + NO \rightarrow C'(N) + C(O)$ (R1.19)

$C'(N) + NO \rightarrow N_2 + C(O)$ (R1.20)

$C'(N) + C'(N) \rightarrow N_2 + 2C_f$ (R1.21)

where, C_f denotes a free carbon site, C'(N) is a nitrogen surface species, differing from the char-N site C(N) [11]. The N_2 formation is mainly through R1.18 when the temperature ranging from 900K to 1200K.

Pevida and co-workers investigated NO heterogeneous reduction on carbonaceous materials, and found that temperatures had significant influence on the mechanisms of NO reduction process by char [104]. The mechanisms can be analyzed under three different temperature ranges [104]:

(1) Low temperature ($T < 250°C$) reduction mechanisms

NO chemisorption prevails below 250°C, where is no char gasification by NO. The process is shown in the following reactions:

$C_{ac} + 2NO \rightarrow N_2 + C(O_2)$ (R1.22)

$C_{ac} + 2NO \rightarrow 2C(N) + C(O_2)$ (R1.23)

Besides, as shown in Figure 1.11, $(NO)_2$ production occurs before NO dissociative chemisorption, which will react with char to form N_2 and $C(O_2)$ subsequently. The reactions are:

$C_{ac} + (NO)_2 \rightarrow N_2 + C(O_2)$ (R1.24)

$C_{ac} + (NO)_2 \rightarrow 2C(N) + C(O_2)$ (R1.25)

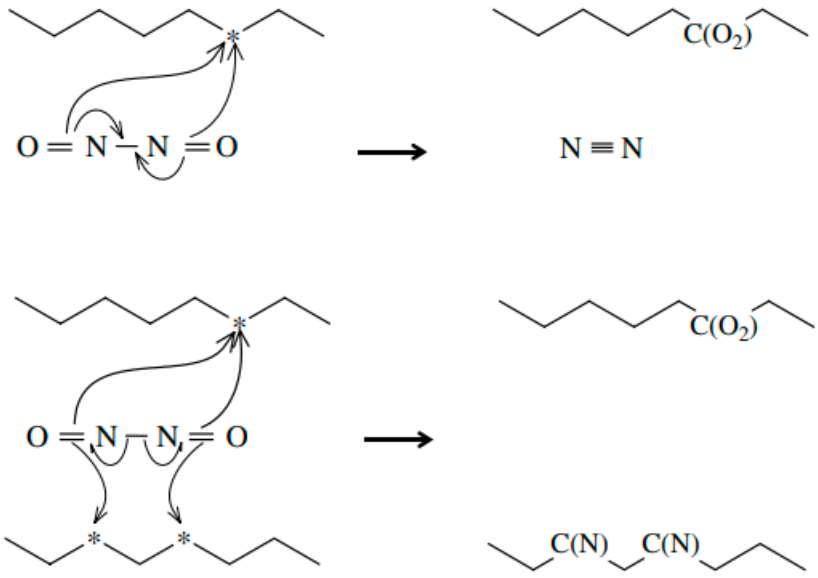

Figure 1.11 Schematic of NO chemisorption [104].

(2) Medium temperature (250°*C* < *T* < *750°C*) reduction mechanisms

With temperatures ranging from 250°C to 750°C, the reactions of char gasification and NO chemisorption by NO occur simultaneously, and the gasification reaction gradually prevails with temperature increasing. However, the rate of this desorption reaction is slow at low temperatures, which restricts the adsorption of NO on the char. Thus, the reaction rate is determined by the desorption reaction:

$C(O_2) \rightarrow CO_2 + C_{ac}$ (R1.26)

(3) High temperature (750°*C* < *T* < *1000°C*) reduction mechanisms

At this temperature range, char gasification by NO domains for the N_2 and CO_2 generation. The following reactions describe the process:

$2C_{ac} + NO \rightarrow C(N) + C(O)$ (R1.27)

$C(N) + NO \rightarrow N_2 + C(O)$ (R1.28)

$C_{ac} + C(O) + NO \rightarrow C(O_2) + C(N)$ (R1.29)

$C(O_2) \rightarrow CO_2 + C_{ac}$ (R1.30)

During the combustion process, char-N oxidation and NO reduction on the surface of char occur simultaneously. And the NO yield decreases with the bulk gas NO concentration [105], particle size [106, 107], pressure [108, 109], and char reactivity [110-114]. Increased particle size and pressure can increase NO residence time in the pores benefiting NO abatement. The instantaneous NO formation increases during char is burning out because the particle becomes smaller and more porous causing larger amounts of NO to escape inhibiting the reduction process [102, 115, 116].

1.2.6 NO Reduction by HCN and NH_3

According to earlier research, the coal pyrolysis gas contains two different forms of nitrogenous species: hydrogen cyanide (HCN) and ammonia (NH_3) [94, 117]. Thus, this thesis mainly focuses on the investigation of NO abatement process by HCN as well as NH_3 in this thesis.

In the SNCR process, where NH_3 is utilised to reduce NOx pollutants under fuel-lean circumstances, and the processes of NO removal by NH_3 have been intensively researched before [118, 119]. Results showed that the primary channel for NO abatement is interactions between NO and NH_2 radicals generated from NH_3, and the relevant reactions are shown below [119]:

$NH_3 + OH \rightarrow NH_2 + H_2O$ (R1.31)

$NH_2 + NO \rightarrow N_2 + H_2O$ (R1.32)

$NH_2 + NO \rightarrow N_2H + H_2O$ (R1.33)

$N_2H + O_2 \rightarrow N_2 + HO_2$ (R1.34)

$N_2H \rightarrow N_2 + H$ (R1.35)

$N_2H + O_2 \rightarrow N_2 + O_2 + H$ (R1.36)

Whereas, when temperature rises, the levels of active OH, O, and H radicals increase, which causes NH_3 molecules to oxidize and finally produce NO. The oxidation processes are shown as follows [119]:

$NH_2 + O \rightarrow HNO + H$ (R1.37)

$HNO + OH \rightarrow NO + H_2O$ (R1.38)

$NH_2 + OH \rightarrow NH + H_2O$ (R1.39)

$NH + NO \rightarrow N_2O + H$ (R1.40)

$N_2O + O \rightarrow NO + NO$ (R1.41)

As a result, there is an optimum temperature at which NO levels are at their lowest. The temperature is normally around 1250K and its range is relatively narrow [120, 121]. However, the boilers usually operate under varying loads and are not available in this temperature range, thereby reducing the optimal temperature is often desirable [122]. An effective method to change the optimal temperature is the addition of gas additives during reduction process, such as H_2 [121, 123], CO [124, 125], CH_4 [126] and Na_2CO_3 [127, 128]. Researchers have determined that the nitrogen-free parts in coal pyrolysis gas are composed of H_2, CO and hydrocarbons (C_xH_y) [70, 129]. Therefore, *we* mainly focused on the performance of additives CH_4, CO and H_2 during the NO reduction process in the current thesis.

The additives during NO abatement process bring a lot of active radicals like H and OH, which benefits the NO reduction and thus optimal temperature decreases with the addition of additives [130, 131]. The reactions related to the addition of H_2 (R1.42-R1.43), CO (R1.44-R1.45) and CH_4 (R1.46-R1.51) are as follows [130, 131]:

$$OH + H_2 \rightarrow H_2O + H \quad \text{(R1.42)}$$

$$O + H_2 \rightarrow OH + H \quad \text{(R1.43)}$$

$$CO + OH \rightarrow CO_2 + H \quad \text{(R1.44)}$$

$$CO + O_2 + H_2O \rightarrow CO_2 + 2OH \quad \text{(R1.45)}$$

$$CH_4 + OH \rightarrow CH_3 + H_2O \quad \text{(R1.46)}$$

$$CH_3 + NO_2 \rightarrow CH_3O + NO \quad \text{(R1.47)}$$

$$CH_3O \rightarrow CH_2O + H \quad \text{(R1.48)}$$

$$CH_2O + OH \rightarrow HCO + H_2O \quad \text{(R1.49)}$$

$$HCO + O_2 \rightarrow CO + HO_2 \quad \text{(R1.50)}$$

$$HO_2 + NO \rightarrow NO_2 + OH \quad \text{(R1.51)}$$

Besides, NO removal performance is also affected by NH_3 and O_2 concentrations. Specially, ur Rahman and co-workers studied the influence of NH_3 concentrations on NO reduction efficiency with NH_3/NO ratio ranging from 0.8 to 2.4 [132]. They concluded that 1.6 is the optimum NH_3/NO ratio for a maximum reduction of NO. Klippenstein and co-workers performed a series of simulations for SNCR process with O_2 concentrations from 0.5% to 50% [118]. Results indicate that optimal temperature and maximum amount of NO removal decreases simultaneously as O_2 concentrations increase in the system, while the width of the temperature window increases.

Though many researchers have made great efforts on SNCR process, there are still limitations and blanks to apply those results on NO reduction by coal pyrolysis gas process. Firstly, the NO reduction process by HCN molecules has never been considered before. In addition, the above studies were carried out under fuel-lean conditions differing from the optimum air/fuel ratio of coal splitting and staging process, which could affect the NO removal performance with NH_3. Besides, there has been no comprehensive comparison of the NO removal behaviours of HCN and NH_3. Finally, the amount of NO molecules was used to gauge the effectiveness of the removal process in previous studies. However, the system still has a large number of species that possess nitrogen, which will also contaminate the ecosystem. The production of N_2 is a more reasonable method to gauge how effectively nitrogen-containing reactants reduce. Therefore, more research on NO elimination using HCN and NH_3 is required.

1.3 Research methods

1.3.1 Experimental Methods

The experimental devices for pyrolysis and NO reduction include shock tube [91], thermo-gravimetric analysis (TGA) [133], fixed-bed reactor [134], wire-mesh reactor [135], drop tube furnace [136] and fluidized Bed [137], electron spin resonance (ESR) [138, 139], solid pyrolysis/synchrotron vacuum ultraviolet photoionization mass spectrometry (Solid-Py/SVUV-PIMS) [140], tubular reactor [131], swirl flame combustor [141], quartz flow reactor [124]. These experimental methods are mostly focused on the study of main stable products and kinetic parameters of overall reactions, while the detection of intermediates or radicals and the analysis of reaction mechanisms are difficult due to the limitations of current experimental techniques. Atomistic-scale computational techniques can reveal the underlying mechanisms of chemical reactions and obtain intermediate structures that are difficult or impossible to obtain using current measurement methods. The two basic techniques are molecular dynamics (MD) and quantum mechanics (QM) simulations.

1.3.2 Quantum Mechanics (QM) Methods

The basic principle of the quantum chemistry method is to solve the

Schrodinger equation, and then obtain the description of the electronic level of the system [142]. At present, ab initio and density functional theory (DFT) are the most commonly utilised approaches in QM.

Ab initio is the earliest method in QM by Robert Parr and co-workers [143]. Using the variation principle, the wave function of the system electron is expressed as a function of atomic orbitals [142]. The wave function of the atomic orbit is a combination of some specific mathematical functions [142]. The types of Wavefunction-based approaches are Hartree–Fock theory, second-order Moller–Plesset perturbation theory (MP2), methods based on the coupled-cluster ansatz and multireference perturbation methods [142]. Though this calculation method is extremely accurate, the calculation speed with this method is very slow and the system that can calculate is extremely small. For DFT, the wave function is replaced by the electron density, where exchange and correlation functionals are employed to describe the electron correlation energy [144]. Compared with Ab initio, the calculation speed of DFT is faster and the accuracy is the same as Ab initio.

In recent years, the improvement of algorithms and compute speed has greatly enhanced the speed and accuracy of QM. However, QM is still only suitable to calculate small systems because of its high compute cost, which is usually smaller than 100 atoms [145].

1.3.3 Molecular Dynamics (MD) Simulation

Molecular dynamics (MD) is a technique for calculating the equilibrium and transport properties of a classical many-body system [146]. The movement of atoms/molecules is calculated by Newtonian motion mechanics. The potential energy of simulated system is obtained using molecular force fields or interatomic potentials.

As observed in Figure 1.12, the main steps for MD are as follows: (1) Specify the initial velocity and position of all atoms. (2) Predict next forces and positions of all atoms. (3) Calculate and output quantities of interest. (4) Move time and step forward. (5) Repeat the process from step 2.

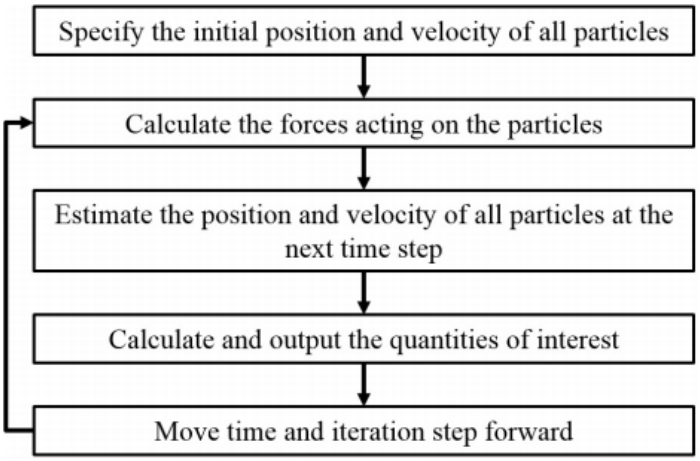

Figure 1.12 Main steps for conducting the MD simulation [147].

The force field is the function of potential energy of systems that is used for estimating the forces between atoms in simulated systems. Classical force fields include but not limited to AMBER (assisted model building with energy minimization) [148], CHARMM (chemistry at Harvard macromolecular mechanics) [149] and CVFF (consistent valence force field) [150]. Afterwards, to calculate the properties of molecules more accurately, the second-generation force fields CFF (consistent force field) [151] and MMFF (Merck Molecular Force Field) [152] were developed. The parameters in force fields are mainly derived from experimental data and QM calculations. The selection of the force field is according to the application of each force field, which is essential for accurate results.

However, MD is not suitable to simulate the chemical process. To solve this problem, reactive force field (ReaxFF) molecular dynamics (MD) was developed to study the chemical reactions in the present work, which can simulate chemical processes with an affordable computational cost and high accuracy [153, 154]. More details of ReaxFF MD are introduced in Chapter 2.

1.4 Aim of the Research

The aim of current research is to investigate the nitrogen migration during coal splitting and staging process as well as assisted combustion by EF and ozone by ReaxFF MD simulations. Specifically studied was how water affected the pyrolysis of nitrogen-containing chemicals in coal (Chapter 3). Also, the influence of temperatures, oxygen content, nitrogen-containing species content and nitrogen-free species in coal pyrolysis gas on the NOx reduction process by

nitrogenous species was explored (Chapter 4). Finally, the effects of EF and ozone on the pollutants during the combustion process of nitrogenous compounds in coal (Chapter 5) were investigated. Those findings could improve the understanding of the details of the NOx regulating process by those technologies and contribute to the development of control strategies for operating conditions that result in lower NOx emissions from coal combustion.

Chapter 2 Methodology

2.1 Reactive Force Field (ReaxFF) Molecular Dynamics (MD)

ReaxFF was first developed by van Duin and co-workers [155]. Figure 2.1 shows the hierarchy of computational methods. As observed, QM can describe chemical reactions, but the simulation systems are usually smaller. Classic MD can be applied in large systems but cannot simulate chemical reactions. ReaxFF solves this problem well, as it can simulate chemical reactions in large systems. During the simulation process, the chemical bonds between atoms can be broken and formed according to the bond order parameters which are upgraded every MD step [155]. Bond order is calculated based on interatomic distances, which are shown as follows [156]:

$$BO'_{\mathrm{ij}} = BO_{ij}^{\sigma} + BO_{ij}^{\pi} + BO_{ij}^{\pi\pi} = exp\left[P_{bo1}\left(\frac{r_{ij}}{r_0^{\sigma}}\right)^{P_{bo2}}\right] + exp\left[P_{bo3}\left(\frac{r_{ij}}{r_0^{\pi}}\right)^{P_{bo4}}\right] + exp\left[P_{bo5}\left(\frac{r_{ij}}{r_0^{\pi\pi}}\right)^{P_{bo6}}\right] \quad (2.1)$$

where, BO_{ij}^{σ}, BO_{ij}^{π} and $BO_{ij}^{\pi\pi}$ represent single, double and triple bond orders, respectively. r_{ij} is the interatomic distance, r_0^{σ}, r_0^{π} and $r_0^{\pi\pi}$ are the equilibrium lengths for single, double and triple bond. Besides, P_{bo1} to P_{bo6} are empirical parameters.

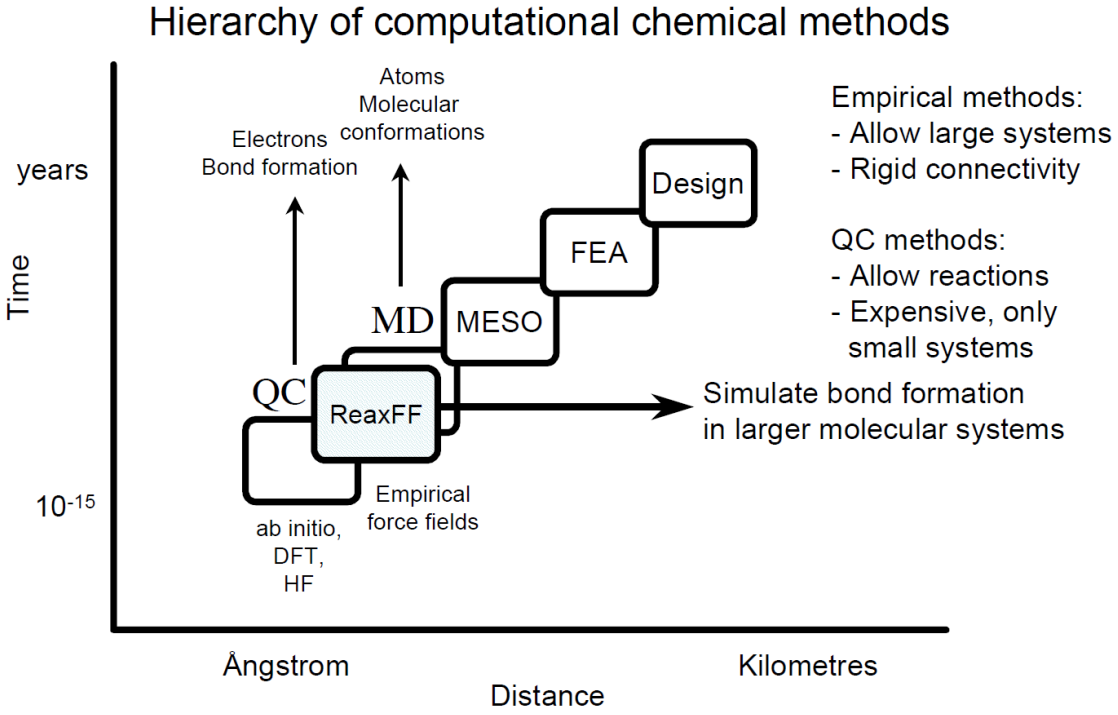

Figure 2.1 Computational methods hierarchy [157].

The total energy expression of the system is shown in Equation 2.2 [156]:

$$E_{system}=E_{bond}+E_{over}+E_{under}+E_{val}+E_{pen}+E_{tors}+E_{conj}+E_{vdWaals}+E_{Coulomb} \quad (2.2)$$

E_{system}: the total potential energy of the system

E_{bond}: the energy of the bonds between atoms

E_{over}: energy penalty for the bond energy of over-coordinated atoms

E_{under}: energy penalty for the bond energy of under-coordinated atoms

E_{val}: bond angle energy related to the three-body interaction energy

E_{pen}: energy penalty for atoms forming two double bonds with surrounding atoms

E_{tors}: dihedral angle energy related to the four-body interaction energy

E_{conj}: conjugation energy for aromatic structures in the system

$E_{vdWaals}$: non-bonded interactions between molecules

E_{Colomb}: coulomb interaction expressed by the charge of atoms and the distance of atoms

Among them, E_{bond}, E_{over}, E_{under}, E_{val}, E_{pen}, E_{tors} and E_{conj} are bond-order-dependent contributions. $E_{vdWaals}$ and $E_{Coulomb}$ are bond-order-independent contributions. The functions of each term in Equation 2.2 are shown in Equation (2.3 to 2.11) [156]. The detailed introduction of variables and parameters can refer to previous work [156].

$$E_{bond} = -D_e^{\sigma}\cdot BO_{ij}^{\sigma}\cdot exp\left[P_{be,1}\left(1-\left(BO_{ij}^{\sigma}\right)^{P_{be,2}}\right)\right] - D_e^{\pi}\cdot BO_{ij}^{\pi} - D_e^{\pi\pi}\cdot BO_{ij}^{\pi\pi} \quad (2.3)$$

$$E_{over} = P_{over}\cdot\Delta_i\cdot\left(\frac{1}{1+exp(\lambda_6\cdot\Delta_i)}\right) \quad (2.4)$$

$$E_{under} = -P_{under}\cdot\frac{1+exp(-\lambda_7\cdot\Delta_i)}{1+exp(-\lambda_8\cdot\Delta_i)}\cdot f_6\left(BO_{ij,\pi},\Delta_j\right) \quad (2.5)$$

$$E_{val} = f_7\left(BO_{ij}\right)\cdot f_7\left(BO_{ik}\right)\cdot f_8\left(\Delta_j\right)\left(k_a - k_a exp\left[-k_b\left(\Theta_0-\Theta_{ijk}\right)^2\right]\right) \quad (2.6a)$$

$$f_7\left(BO_{ij}\right) = 1-exp\left(-\lambda_{11}\cdot BO_{ij}^{\lambda_{12}}\right) \quad (2.6b)$$

$$f_8\left(\Delta_j\right) = \frac{2+exp\left(-\lambda_{13}\cdot\Delta_j\right)}{1+exp\left(-\lambda_{13}\cdot\Delta_j\right)+exp\left(P_{v,1}\cdot\Delta_j\right)} * \left[\lambda_{14}-\left(\lambda_{14}-1\right)\cdot\frac{2+exp\left(-\lambda_{15}\cdot\Delta_j\right)}{1+exp\left(-\lambda_{15}\cdot\Delta_j\right)+exp\left(P_{v,2}\cdot\Delta_j\right)}\right] \quad (2.6c)$$

$$E_{pen} = \lambda_{19}\cdot f_9\left(\Delta_j\right)\cdot exp\left[-\lambda_{20}\left(BO_{ij}-2\right)^2\right]\cdot exp\left[-\lambda_{20}\left(BO_{jk}-2\right)^2\right] \quad (2.7a)$$

$$f_9\left(\Delta_j\right) = \frac{2+exp\left[-\lambda_{21}\cdot\Delta_j\right]}{1+exp\left[-\lambda_{21}\cdot\Delta_j\right]+exp\left[\lambda_{22}\cdot\Delta_j\right]} \quad (2.7b)$$

$$E_{tors} = f_{10}\left(BO_{ij},BO_{jk},BO_{kl}\right)\sin\Theta_{ijk}\sin\Theta_{jkl}\left[\frac{1}{2}V_1\left(1+\cos\omega_{ijkl}\right)+\right.$$

$$\frac{1}{2}V_2 exp\left[P_{tor1}\left(BO_{jk}-1+f_{11}(\Delta_j,\Delta_k)\right)^2\right]*\left(1-\cos 2\omega_{ijkl}\right)+\frac{1}{2}V_3\left(1+\cos 3\omega_{ijkl}\right)\Big] \tag{2.8a}$$

$$f_{10}(BO_{ij},BO_{jk},BO_{kl})=\left(1-e^{-\lambda_{23}BO_{ij}}\right)\left(1-e^{-\lambda_{23}BO_{jk}}\right)\left(1-e^{-\lambda_{23}BO_{kl}}\right) \tag{2.8b}$$

$$f_{11}(\Delta_j,\Delta_k)=\frac{2+exp\left[-\lambda_{24}\cdot(\Delta_j+\Delta_k)\right]}{1+exp\left[-\lambda_{24}\cdot(\Delta_j+\Delta_k)\right]+exp\left[-\lambda_{25}\cdot(\Delta_j+\Delta_k)\right]} \tag{2.8c}$$

$$E_{conj}=f_{12}(BO_{ij},BO_{jk},BO_{kl})\lambda_{26}\left[1+\left(\cos^2\omega_{ijkl}-1\right)\cdot\sin\Theta_{ijk}\cdot\sin\Theta_{jkl}\right] \tag{2.9a}$$

$$f_{12}(BO_{ij},BO_{jk},BO_{kl})=e^{-\lambda_{27}\cdot\left(BO_{ij}-1.5\right)^2}\cdot e^{-\lambda_{27}\cdot\left(BO_{jk}-1.5\right)^2}\cdot e^{-\lambda_{27}\cdot(BO_{kl}-1.5)^2} \tag{2.9b}$$

$$E_{vdWaals}=D_{ij}\cdot\left\{exp\left[\alpha_{ij}\left(1-\frac{f_{13}(r_{ij})}{r_{vdW}}\right)\right]-2\cdot exp\left[\frac{1}{2}\alpha_{ij}\left(1-\frac{f_{13}(r_{ij})}{r_{vdW}}\right)\right]\right\} \tag{2.10a}$$

$$f_{13}(r_{ij})=\left[r_{ij}^{\lambda_{29}}+\frac{1}{\lambda_{\omega}}^{\lambda_{28}}\right]^{\frac{1}{\lambda_{28}}} \tag{2.10b}$$

$$E_{Coulomb}=C\cdot\frac{q_i\cdot q_j}{\left\{r_{ij}^3+\left(\frac{1}{\gamma_{ij}}\right)^3\right\}^{\frac{1}{3}}} \tag{2.11}$$

It is clear from Figure 2.2 that many common elements in the periodic table are available for ReaxFF parameter sets. As Figure 2.3 shows, there are two branches of ReaxFF parameter sets: (1) the combustion branch and (2) the aqueous branch [158]. The ReaxFF parameter sets are transferable on the same branch, but they are untransferable between branches [158]. Thus, the appropriate force field should be selected according to the research system, which is essential to get positive results from ReaxFF MD simulations.

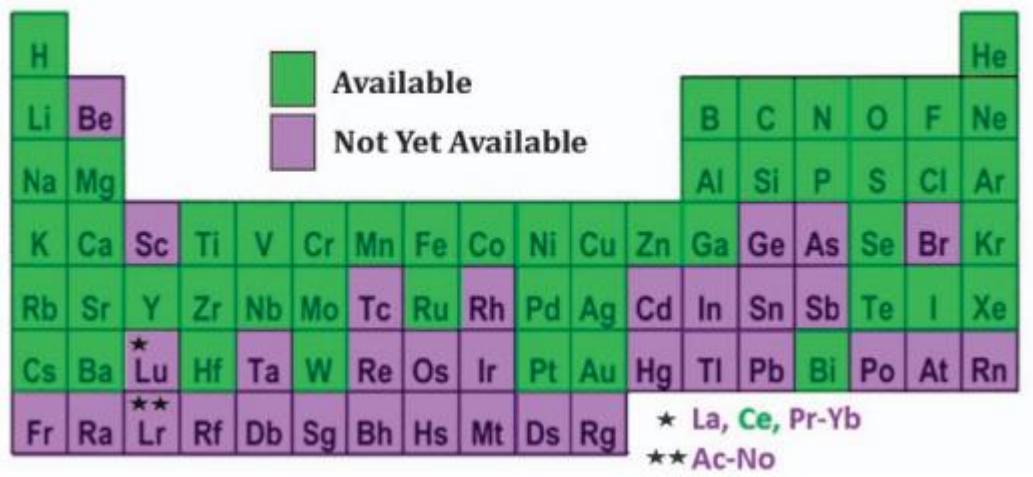

Figure 2.2 Elements distribution for ReaxFF [158].

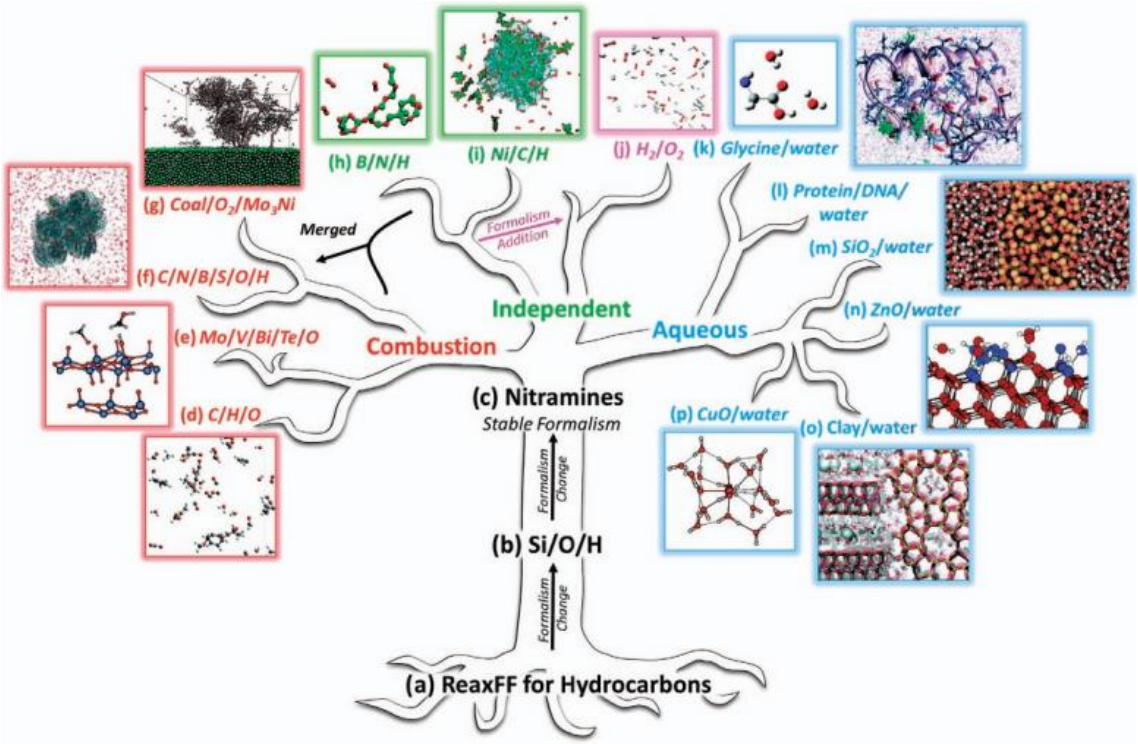

Figure 2.3 ReaxFF development tree, where parameter sets on a common 'branch' are fully transferable with one another [158].

2.2 Integration method and boundary conditions

2.2.1 Charge Distribution

Charge equilibration methods (QEq) is an effective algorithm proposed by Rappé and Goddard in 1991, which can estimate the electrostatic potential of molecules and periodic frameworks by assigning point charges to each atom [159-162]. Electronegativity expression is as follows:

$$\chi_i = \chi_i^0 + J_i^0 q_i + \sum_{i=1}^{N} J_{ij} q_i \quad (2.12)$$

where, χ_i is electronegativity, i, j is the atom number, q is the atomic charge, J_i^0 is self-Coulomb interaction (or atomic hardness) [163]. J_{ij} is the electrostatic potential between atom i and atom j. The minimum energy is found if $\chi_1 = \chi_2 = \cdots = \chi_i$.

2.2.2 Velocity-Verlet Integration

Velocity-Verlet integration is a numerical method used to integrate Newton's equations of motion [164]. In 1967, Verlet proposed this algorithm based on the Taylor expansion of the particle's coordinate variable (t), which are:

$$r_i(t+\Delta t) = r_i(t) + \frac{dr_i(t)}{dt}\Delta t + \frac{1}{2!}\frac{d^2}{dt^2}r_i(t)\Delta t^2 + \frac{1}{3!}\frac{d^3}{dt^3}r_i(t)\Delta t^3 + O(\Delta t^4) \quad (2.13)$$

Changing ∆t to -∆t gives:

$$r_i(t-\Delta t) = r_i(t) - \frac{dr_i(t)}{dt}\Delta t + \frac{1}{2!}\frac{d^2}{dt^2}r_i(t)\Delta t^2 - \frac{1}{3!}\frac{d^3}{dt^3}r_i(t)\Delta t^3 + O(\Delta t^4) \quad (2.14)$$

Adding these two expansions gives:

$$r_i(t+\Delta t) = -r_i(t-\Delta t) + 2r_i(t) + \frac{d^2}{dt^2}r_i(t)\Delta t^2 + O(\Delta t^4) \quad (2.15)$$

Misusing these two expansions gives:

$$v_i(t) = \frac{1}{2\Delta t}[r_i(t+\Delta t) - r_i(t-\Delta t)] \quad (2.16)$$

However, the position and velocity of particles are not available at the same value of the time variable using Verlet algorithm. In addition, the formula 2.16 contains the l/∆t term. Since a small ∆t value is usually selected in actual calculation, it is easy to cause errors during calculation. To solve this issue, Swope and co-workers developed Velocity-Verlet algorithm by explicitly incorporating velocity [165]. The functions are as follows:

$$r_i(t+\Delta t) = r_i(t) + v_i(t)\Delta t + \frac{1}{2}a_i(t)\Delta t^2 \quad (2.17)$$

$$v_i(t+\Delta t) = v_i(t) + \frac{1}{2}\Delta t[a_i(t+\Delta t) - a_i(t-\Delta t)] \quad (2.18)$$

This method is easy to use and has high accuracy and stability, thus Velocity-Verlet algorithm is used in the current research.

2.2.3 Ensembles

Ensemble is a collection of systems with the same computational conditions, including: NVT (canonical ensemble: constant number of substance N, volume V and temperature T), NVE (microcanonical ensemble: constant number of particles N, volume V, and total energy E), etc [166]. The choice of the ensemble is based on the research needs. The NVT ensemble is selected in the current thesis because of its compatibility with experiments.

The common methods for temperature control are Berendsen thermostat and Nosé-Hoover thermostat. Berendsen thermostat is an algorithm that rescales velocities of particles in molecular dynamics simulations to control the simulation temperature, inhibiting the fluctuations of temperatures which are present in the

canonical ensemble [167]. For the Nosé-Hoover thermostat, the temperature in the system is controlled by changing the Hamiltonian variable (an operator describing the total energy of the system) of the system, which is extremely efficient for controlling a system to the target temperature [168]. Therefore, the Nose-Hoover temperature control method is selected for the control of the system temperature, and the temperature damping constant is set to 100 fs.

2.2.4 Boundary Conditions

The models of molecular dynamics are cubic boxes containing a certain number of molecules. The scale range of molecular dynamics simulation is generally in the nanometre scale. If aperiodic boundary conditions are applied in simulated systems, the distribution of atoms in the system could be affected by boundary effects, leading to the inaccuracy of the calculation results. Therefore, periodic boundary conditions are adopted to eliminate surface effects with little influence on the thermodynamic properties and local structures of simulated systems [169, 170].

Figure 2.4a shows the arrangement and moving direction of system seats in a 2D box. The box in the centre represents the simulated system, and the surrounding boxes have the same arrangement and motion with the simulated system, which is called a periodic mirror system. When any particle in the computing system moves out of the box, a particle must move in from the opposite direction, as shown in particle 2. Such constraints keep the number of particles in the system constant.

When calculating intermolecular forces, the nearest mirror image method is used. As shown in Figure 2.4b, the calculation of the force between particles 1 and 2 is through particle 1 and its closest mirror to particle 2. Particle 2 in box D is the closest to particle 1 in all mirror systems. Similarly, the intermolecular force between particles 3 and 1 is calculated by particle 3 in central box and particle 1 in the box E.

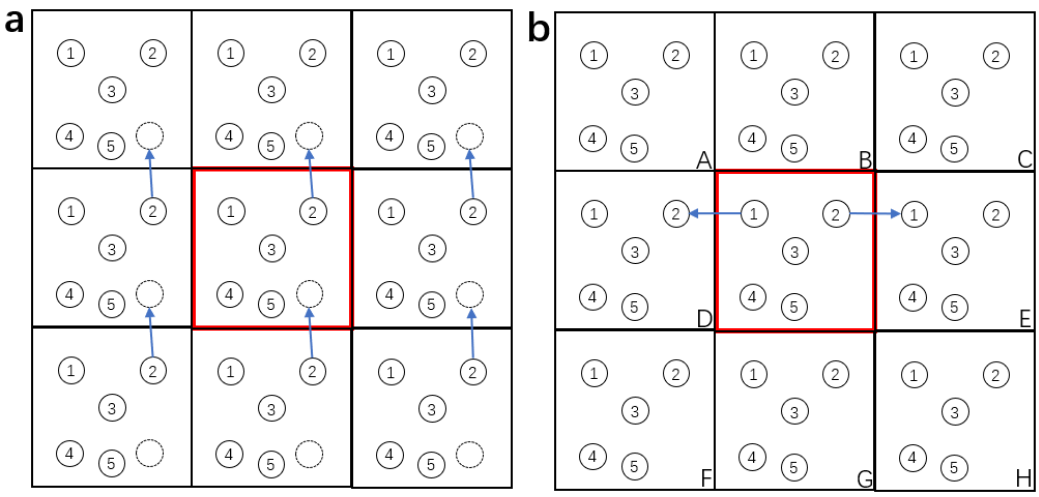

Figure 2.4 Schematic diagram of periodic boundary condition in two dimension. (a) Movement of particles. (b) Nearest images of particles.

2.3 Steps of ReaxFF MD Simulation

Steps to use ReaxFF MD simulations include system construction, energy minimization as well as system equilibration, chemical process simulations and data analysis.

2.3.1 System Construction

The first step is to establish models of target molecules in software Avogadro [171], which is a free, open-source, cross-platform, three-dimensional, molecular editor [171]. Then, the initial models are established in software Packmol [172] using the molecular models established in Avogadro. Finally, VMD (Visual Molecular Dynamics) [173] is used to convert models established in Packmol into data files, which are input files for LAMMPS (Large-scale Atomic/Molecular Massively Parallel Simulation) [174] simulations.

2.3.2 Energy Minimization and System Equilibration

Energy minimization and system equilibration are essential before reactive simulation. The purpose of energy minimization and system equilibration is to optimize the structure of molecules in the system and let the system reach a stable state (system potential energy remains stable). The conjugate gradient algorithm and NVT ensemble are chosen for energy minimization and system equilibration, respectively.

2.3.3 Chemical Process Simulations

The NVT ensemble with the Nosé-Hoover thermostat and REACX package is chosen for simulations. The choice of timestep and simulation duration values is according to the purpose of research and simulated systems. Generally speaking, simulation results are more accurate with the smaller the value of timestep. However, the computational costs will greatly increase. In addition, to avoid accidental errors during the simulations, all simulations are repeated three times, and the average values are taken as the final results.

2.3.4 Data Analysis

For output results, many quantities such as the potential energy and temperature can be obtained directly. However, post-processing is needed to obtain some information such as bonding information and dynamic trajectories. The bonding information is extracted using a script named mol_fra.c in LAMMPS. For another important result, the dynamic trajectories of atoms are obtained using additional software VMD [173]. The reaction pathways are analysed using Chemical Trajectory Analyzer (ChemTrayzer) scripts with the bond order cutoff of 0.3 [175]. The net flux (NF) indicates how often the reaction was observed during the simulation time, which is calculated by the occurrence difference between the forward reaction and the reverse reaction [176].

2.4 Validation, Simulation Parameters and Random Errors of ReaxFF MD

The ReaxFF parameters used in this work were previously parametrized against a training set of QM-derived data that combined a variety of C/H/O/N-containing compound properties (bond dissociation, geometry distortion, IR spectra, condensed phase properties) with a variety of nitrogen-containing material reactions [177-181]. The ReaxFF was also approved by describing N/H processes including N-N single, double, and triple bond dissociation; H-N-H, H-N-N, and N-N-N angle strain connections as along with H-H bond dissociation [177, 179]. The above validations support the mechanisms observed in this thesis. In addition, ReaxFF MD is considered to be a first-principal simulation method. Provided that the chosen force field C/H/O/N are adequately validated and the

numerical procedures are correct, as in the case of my study, the results are accurate and reliable. This is especially true when the phenomena studied are of atomic or nanoscales, such as chemical reactions. No other methods are able to reveal more details or are more accurate than ReaxFF MD under the same physical conditions. Whenever possible, the simulation findings are compared with experimental results, theoretical and other numerical data. However, quantitative comparison between MD and experimental results is not possible in most cases, as experiments are often conducted under different conditions and suffer from a high degree of uncertainty.

MD is computationally expensive. ReaxFF MD is even more expensive because the spatial and temporal scales of chemical reactions are extremely small. These methods are only possible on supercomputers. Even on today's supercomputers, ReaxFF MD can only simulate a system consisting of tens to thousands of molecules. The physical time simulated is tens or hundreds of nanoseconds. To shorten the simulation time and save computational cost of ReaxFF MD, an effective and reliable strategy is to artificially increase the temperature of the system under study. This approach has been frequently employed in ReaxFF MD simulations, which are considered to be acceptable and would not change the reaction mechanisms significantly [182]. This approach has been verified to reproduce reaction mechanisms observed in experiments [94, 154, 183].

ReaxFF MD simulation is a realisation of the physicochemical system, which may contain random errors. According to Figure 1.12, the basic principle of MD is to calculate the movement of atoms/molecules by Newtonian motion mechanics. The initial positions of the particles have a great influence on the simulation results as it will affect the forces on the particles and correspondingly the movements of particles are changed. That is also recognized as the chaotic nature of MD simulations, which also has been corroborate by recent studies [184-187]. To eliminate such noises, an effective and reliable computational route, ensemble method, is adopted here [188-191]. An ensemble approach employs a set of independent MD simulations (also called 'replicas'), to obtain the required averages and associated parameters [188]. The utilisation of ensembles and temporal averaging for systems in equilibrium is the main component of such simulations [188].In the current thesis, all simulations are carried out three times with randomly varying starting positions of reactants, and the average values are

used as final results. In all figures, the error bars represent the Standard Error (SE) of three independent replicas.

Chapter 3 Effects of water on pyridine pyrolysis

3.1 Simulation Details

Table 3.1 presents the details of the simulated systems. The computing domain in each case is a cubic box. Only 20 pyridine molecules are present in System 1. To study the influence of water on pyridine pyrolysis, 20-500 H_2O molecules are introduced to systems 2 to 8. Figure 3.1 presents the system configurations during pyridine pyrolysis in water-free (a) and water-containing (b) environments. As shown in Equation 3.1, α presents the ratio of the numbers of water, $n(H_2O)$, to pyridine, $n(C_5H_5N)$. The density of each system is 0.3 g/cm^3 in all cases with varying box sizes.

$$\alpha = \frac{n(\mathrm{H_2O})}{n(\mathrm{C_5H_5N})} \tag{3.1}$$

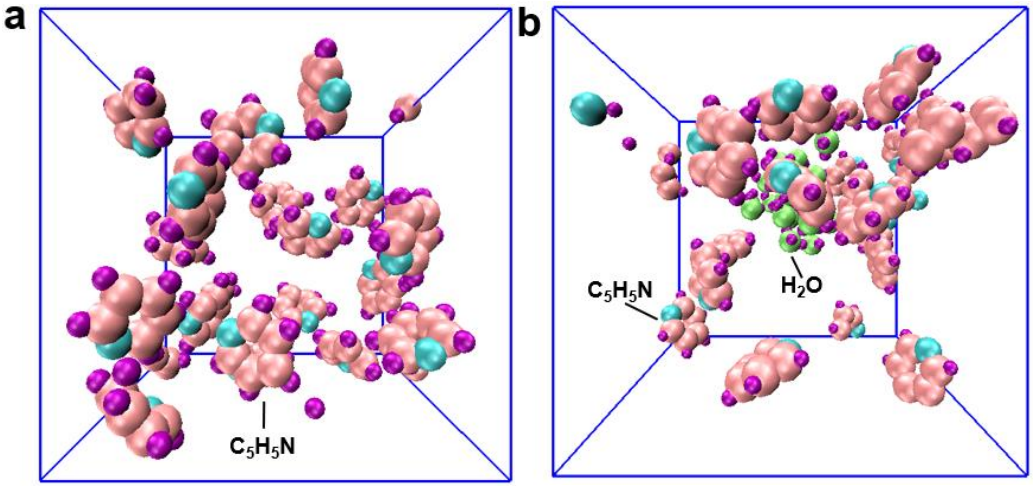

Figure 3.1 System configurations during pyridine pyrolysis. (a) α = 0 (b) α = 1.

Table 3.1 Case set-ups

System	Number of C_5H_5N molecules	Number of H_2O molecules	α	Density (g/cm^3)	Box size(Å)
1	20	0	0	0.3	20.61
2	20	20	1	0.3	22.07
3	20	40	2	0.3	23.36
4	20	60	3	0.3	24.52
5	20	80	4	0.3	25.58
6	20	100	5	0.3	26.56
7	20	200	10	0.3	30.62
8	20	500	25	0.3	38.85

The bond order cutoff and timestep values were set to 0.3 and 0.1 fs, respectively. Energy minimization as well as system equilibration were performed before "production" simulations. Temperatures were kept the same at 1000 K for 50 ps first. Subsequently, temperatures were increased to 3000 K (heating rate: 100 K/ps) and then maintained constant. The simulation lasts for a total of 1000 ps.

3.2 Results

3.2.1 Influence of Water on Pyridine Consumption

According to Figures 3.2a and 3.2b, at least 90% of C_5H_5N molecules are consumed during the first stage up to 600 ps in all simulations. To identify the impacts of water on pyridine consumption rates, the quantity of pyridine consumed at three different periods is presented in Figure 3.2 (c). Results indicate that H_2O accelerates pyridine consumption within the first 200 ps. The promotion influence of water is also observed during the oxidation process of ethanol and methane and char pyrolysis [70, 154, 192]. Reactions related to the consumption of pyridine molecules without water addition are as follows:

$C_5H_5N + H \rightarrow C_5H_6N$ (R3.1)

$C_5H_5N \rightarrow C_5H_4N + H$ (R3.2)

$C_5H_5N + H \rightarrow C_5H_4N + H_2$ (R3.3)

Whereas, under water addition cases, OH radials are generated from

reactions:

$H_2O \rightarrow OH + H$ (R3.4)

$H_2O + H \rightarrow OH + H_2$ (R3.5)

The presence of OH radials bring new reactions for pyridine consumption:

$C_5H_5N + OH \rightarrow H_2O + C_5H_4N$ (R3.6)

$C_5H_5N + OH \rightarrow C_5H_6NO$ (R3.7)

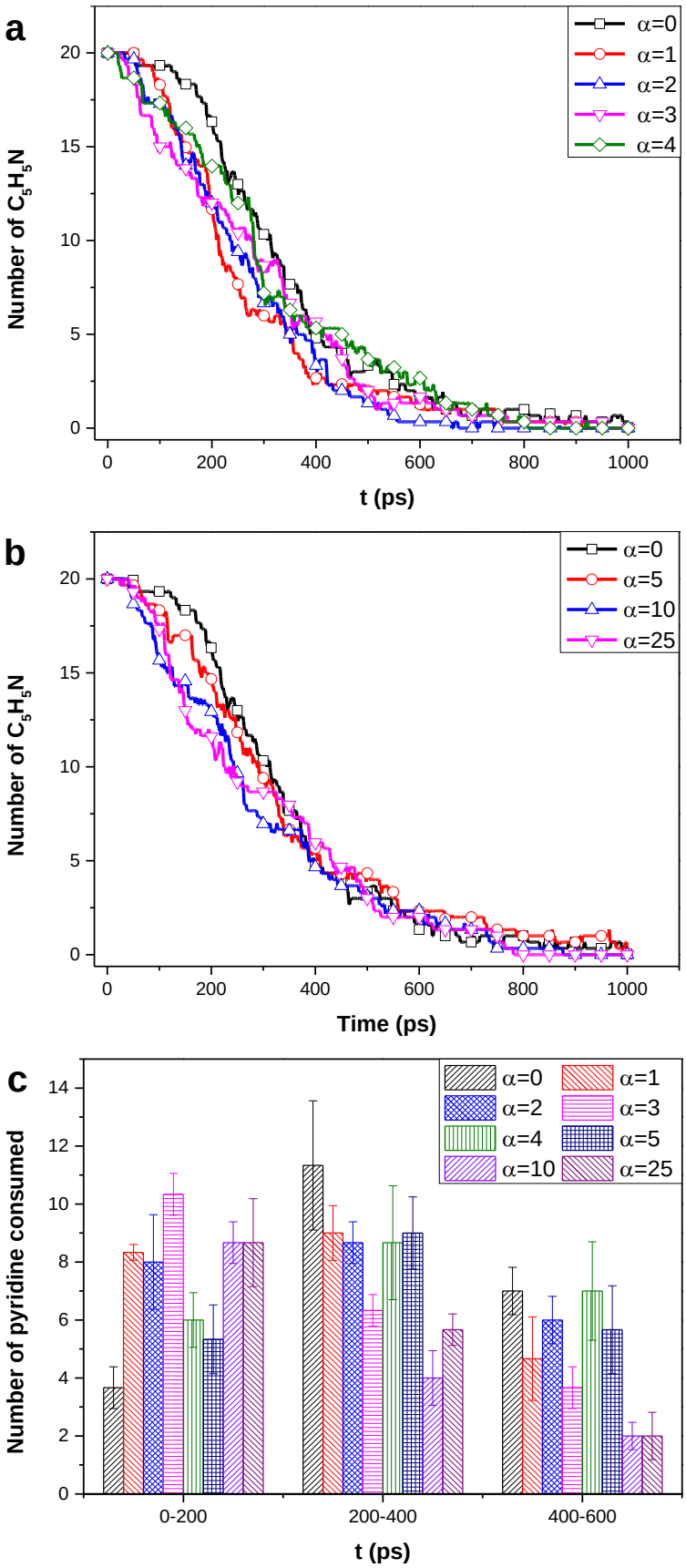

Figure 3.2 Time evolution of C_5H_5N under changing water concentrations and number of pyridine consumed at different periods. (a) α = 0-4. (b) α = 0&5-25. (c) consumption number of pyridine.

Overall, water molecules promote the formation of active OH intermediates during the pyrolysis process, thus accelerating pyridine consumption. However, water presents negative effects on pyridine consumption rates after 200 ps. That will be explained in Section 3.2.3, where the behaviors of polycondensation compounds under varying α values were explored.

3.2.2 Influence of Water on Intermediates

Figures 3.3a and b present the number of species during pyridine pyrolysis in α = 0-25 as time goes. Overall, the species number firstly rises to a peak point and subsequently decreases with time going on in all cases. Besides, the species number under water addition cases is much larger than that in the water-free case, which indicates that H_2O molecules participate in a variety of intermediate reactions and produce new intermediates throughout pyridine pyrolysis. That agrees well with the findings in Section 3.2.1 that H_2O brings active OH intermediates and accelerates pyridine consumption during pyridine pyrolysis. In addition, when α is greater than 5, the change of species number is insignificant with α rising in the system.

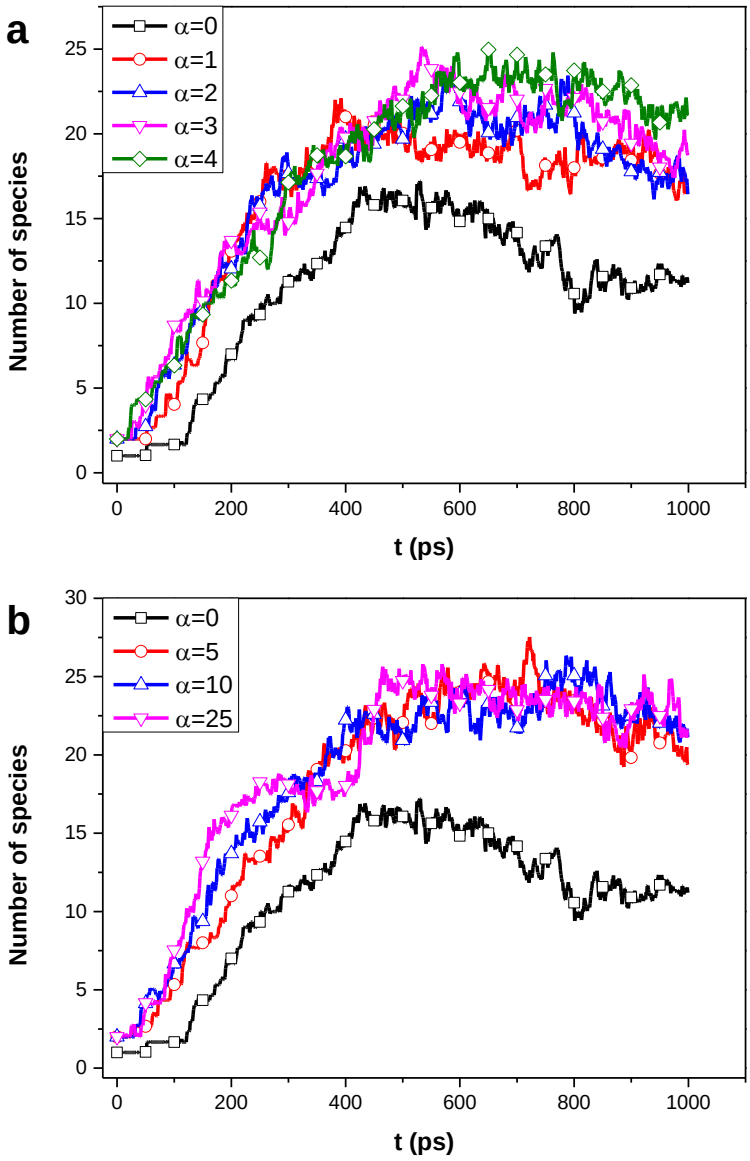

Figure 3.3 The number of species evolving through time with varying α values. (a) α = 0-4. (b) α = 0&5-25.

To further understand the impact of H_2O on the intermediates from pyridine pyrolysis, the main intermediates under varying α values were explored as observed in Table 3.2. It is clear that H_2, NH_3, CN, HCN, C_4H_2 and C_4H_3 are common intermediates in all cases. C_4H_4. CO, CHNO, CH_2NO, C_2H_2O and C_2H_3O are only detected in water-containing conditions.

CNO, CHO, CHO_2 and C_2HO_2 are found when α is larger than 2. CO_2 is observed for α over 4-25. C_4H_3O has been found in instances with α values ranging from 5 to 25. C_3H_4O and C_4H_4O are spotted with α of 10 or 25. C2O2 is found in α = 3, 4, 5, and 25 cases. C_3H_2O and C_3H_3O occur in cases with α of 4,

5, 25 and α = 5, 25, respectively.

Table 3.2 Key intermediates under varying α values. Different symbols are for clarifying the effects of H_2O on intermediates. •: α = 0-25, ♦: α = 1-25, ♠: α = 2-25, Δ: α = 4-25, □: α = 5-25, ×: α = 10-25, ⊗: α = 3-5&25, ⊕: α = 4&5&25, ♥: α = 5&25.

α	0	1	2	3	4	5	10	25
H_2	•	•	•	•	•	•	•	•
NH_3	•	•	•	•	•	•	•	•
CN	•	•	•	•	•	•	•	•
HCN	•	•	•	•	•	•	•	•
C_4H_2	•	•	•	•	•	•	•	•
C_4H_3	•	•	•	•	•	•	•	•
C_4H_4	•	•	•	•	•	•	•	•
CO		♦	♦	♦	♦	♦	♦	♦
CHNO		♦	♦	♦	♦	♦	♦	♦
CH_2NO		♦	♦	♦	♦	♦	♦	♦
C_2H_2O		♦	♦	♦	♦	♦	♦	♦
C_2H_3O		♦	♦	♦	♦	♦	♦	♦
CNO			♠	♠	♠	♠	♠	♠
CHO			♠	♠	♠	♠	♠	♠
CHO_2			♠	♠	♠	♠	♠	♠
C_2HO_2			♠	♠	♠	♠	♠	♠
CO_2					Δ	Δ	Δ	Δ
C_4H_3O						□	□	□
C_3H_4O							×	×
C_4H_4O							×	×
C_2O_2				⊗	⊗	⊗		⊗
C_3H_2O					⊕	⊕		⊕
C_3H_3O						♥		♥

3.2.3 Influence of Water on Polycondensation Compounds

Apart from the decomposition process, polycondensation reactions exist simultaneously during coal pyrolysis. In rising order of C atom numbers, the products are gas (C_0-C_5), tar (C_5-C_{40}) and char (C_{40+}) [61]. The influence of water on polycondensation processes in the pyrolysis process is revealed in this section.

Figures 3.4a - 3.4c show the proportion of C, H and N in C_5+ at the end of simulations. The percentages of C, H and N in C_5+ fall dramatically as the number of H_2O increases during the pyrolysis process and few C_5+ compounds are detected in the α = 25 case, agreeing well with previous experimental works [70, 71]. That means water molecules significantly limit polycondensation processes and change nitrogen migration to char, tar, and gas. Furthermore, the polycondensation process happens mostly after 200 ps based on the products analysis during the pyrolysis process. This explains the phenomenon in Section 3.2.1 that H_2O has a clear inhibitory impact on pyridine reduction after 200 ps. Figure 4.4d presents structures of C_5+ as α increases. As α increases from 0 to 10, the proportion of C atoms decreases considerably (from C_{21} to C_6) in the polycondensation products. Also, a rise of H_2O addition during pyridine pyrolysis enhances the presence of O atoms in polycondensation products.

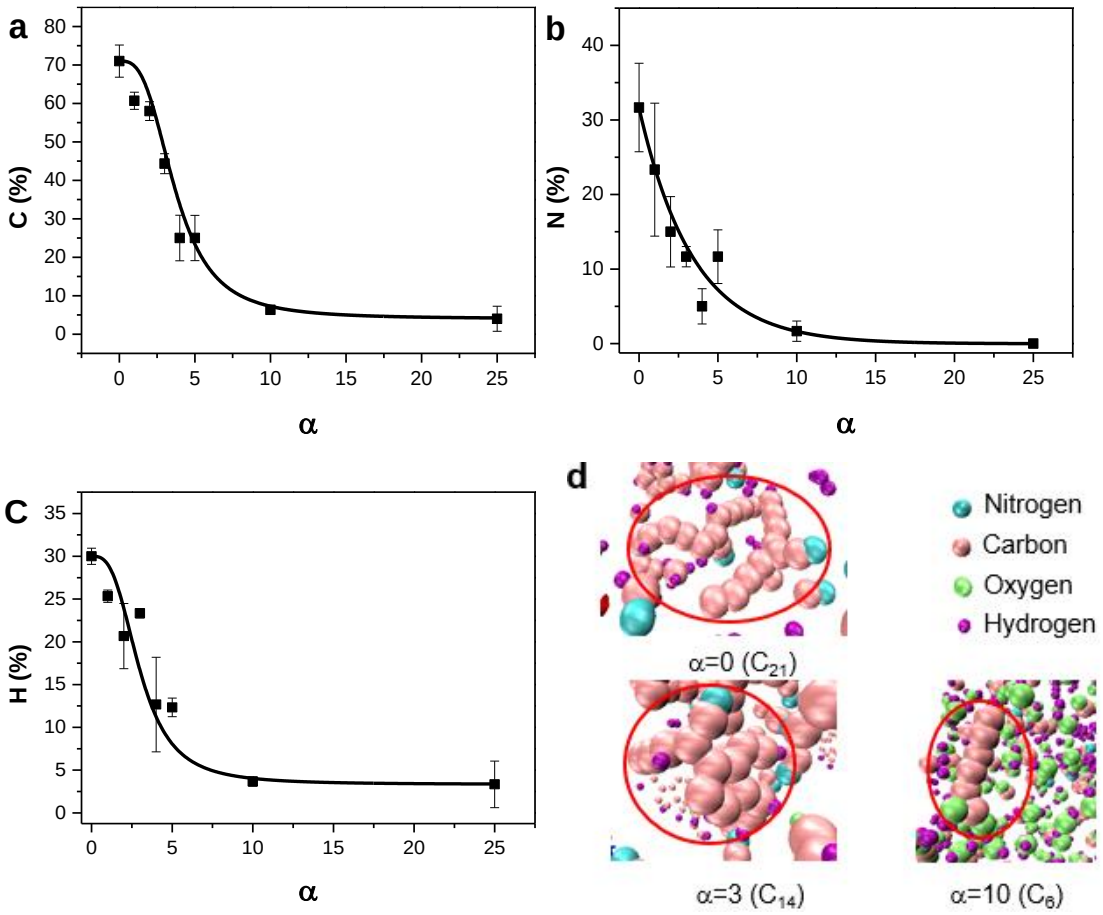

Figure 3.4 The percentages of elements in C_5+ and structures of C_5+ under varying α values. (a) C; (b) N; (c) H; (d) structures of C_5+.

3.2.4 Influence of Water on Ring-opening Process

In terms of earlier studies [91, 92], ring-opening reactions are the first step during the pyrolysis process. Figure 3.5a illustrates the schematics of four different types of ring-opening processes identified in our simulations. In the type A case, o-C_5H_5N first reacts with H atom generating the intermediate o-C_5H_6N, which opens the ring generating a chain C_5H_6N. Type B is the case when C_5H_5N molecules directly open rings to form the chain C_5H_5N. Type C happens when pyridine loses an H atom, after that, ring-opening reactions take place, which is also corroborated by earlier studies [91-93, 154]. In type D, C_5H_5N molecules combine with OH derived from water to generate oxygen-containing intermediates, which subsequently undergoes ring-opening process. Following that, chain intermediates (C_5) undergo thermal decomposition, yielding HCN, CN, C_4H_4 and C_4H_3. The influence of H_2O on those intermediates is further explored in Section 3.2.5.

Figure 3.5b illustrates the percentages of ring-opening types under varying

α values. The percentages of type A and type B during pyridine pyrolysis reduce as the system's water addition increases. In addition, the proportion of type C climbs to a maximum at α = 10 and subsequently drops as the number of water increases. The type D during pyridine pyrolysis occurs only when the water concentrations are at high level. Under the water-free condition, the C_5H_6N and C_5H_4N are generated through reactions R3.1-R3.3. However, the addition of H_2O molecules results in the formation of OH particles via R3.4 and R3.5. Those OH radicals promote the production of C_5H_4N through R3.6. Correspondingly, water inhibits ring-opening processes via types A and B, however, it enhances ring-opening reactions by type C. When the value of α grows to 4, oxygen-containing intermediates (C_5H_6NO, C_5H_5NO, C_5H_4NO and C_5H_3NO) are observed during pyridine pyrolysis, and relevant reactions are below:

$C_5H_5N + OH \rightarrow C_5H_6NO$ (R3.7)

$C_5H_4N + H_2O \rightarrow C_5H_6NO$ (R3.8)

$C_5H_4N + H_2O \rightarrow C_5H_5NO + H$ (R3.9)

$C_5H_4N + HO \rightarrow C_5H_5NO$ (R3.10)

$C_5H_6NO \rightarrow C_5H_5NO + H$ (R3.11)

$C_5H_5NO + HO \rightarrow H_2O + C_5H_4NO$ (R3.12)

$C_5H_4NO \rightarrow C_5H_3NO + H$ (R3.13)

The results show that water molecules speed up the consumption of C_5H_4N and enhance the formation of oxygen-containing intermediates. That accounts for the proportion of type C during pyridine pyrolysis decreases in the α of 25 case and type D only happens in cases under a relatively high-water content.

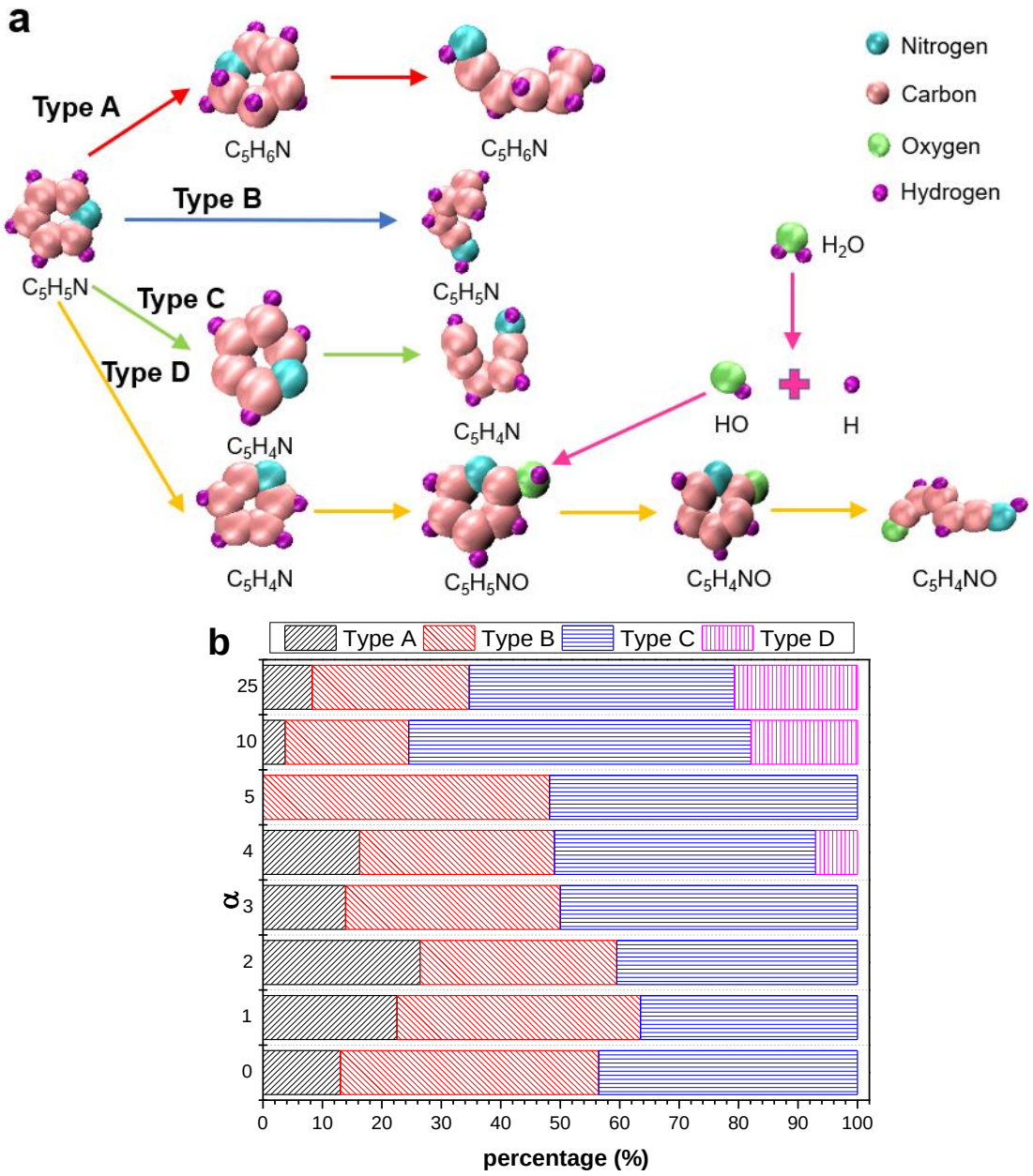

Figure 3.5 Schematic diagram and types of pyridine ring-opening process. (a) Snapshots of ring-opening process. (b) proportion of each type under different α values.

3.2.5 Influence of Water on Main Products

During pyridine pyrolysis, each pyridine molecule firstly undergoes ring-opening process, and then pyrolyzes to generate the key species including HCN, CN, C_4H_4 and C_4H_3, which is consistent with earlier findings [91-93, 154]. In this section, the influence of H_2O on those intermediates and the main products (NH_3, H_2 and CO) during pyridine pyrolysis was studied.

The influence of H_2O on the numbers of CO, H_2, NH_3 and HCN at the end of

simulations is shown in Figure 3.6. The production of H_2, CO, and NH_3 increases as the content of H_2O rises, agreeing well with previous work [66]. The yield of HCN presents a non-linear trend with water concentrations. When α is in the range of 0-3, the number of HCN stays constant. A parabolic shape is observed as α grows reaching the peak point at α = 10. As observed in Section 3.2.3, water inhibits the polycondensation reactions and promotes the generation of H_2, CO, and NH_3. To further illustrate how water affects the yields of main products, reaction pathways of intermediates under varying α values are investigated subsequently.

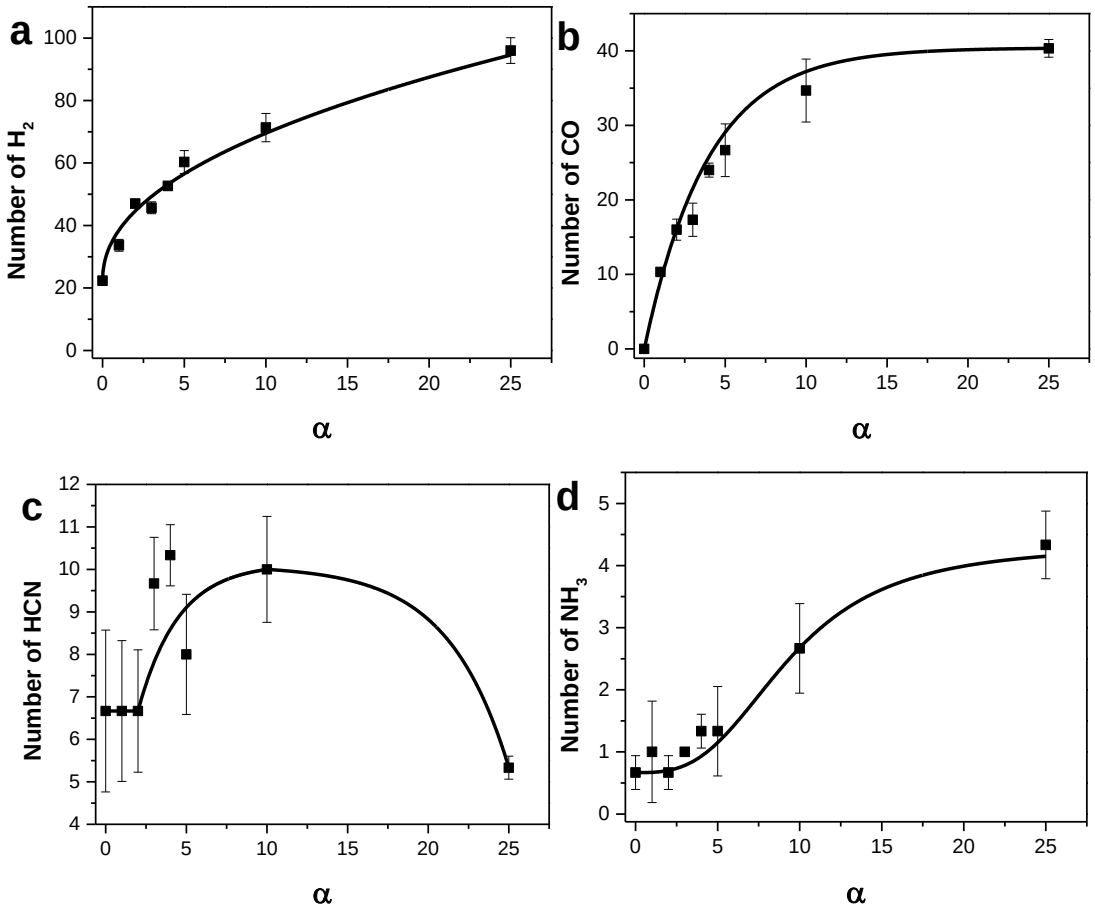

Figure 3.6 Influence of H_2O on the yields of key products. (a) H_2. (b) CO. (c) HCN. (d) NH_3.

During pyridine pyrolysis in the α of 0 case, H_2 is produced primarily from H radical by R3.14. In the cases of water addition, the addition of H_2O promotes the H_2 formation via R3.5.

$$H + H \rightarrow H_2 \quad \text{(R3.14)}$$

The effects of H_2O on reaction pathways of nitrogenous intermediates are

shown in Figure 3.7a. It is clear that NH_3 derives from HCN and CN along the channel HCN → CNH → NH → NH_2 →NH_3 during pyrolysis process in both water and water-free cases [94, 193]. Also, N_2 is not found in our simulations as the pathway from HCN/CN to N_2 occurs at high temperatures [94]. Under water addition conditions, pathways HCN → CH_2NO and CH_2NO → CHNO are formed through reactions:

$CHN + OH \rightarrow CH_2NO$ (R3.15)

$CH_2NO \rightarrow CHNO + H$ (R3.16)

Reactions R3.17 to R3.20 are found during pyridine pyrolysis with α of 2-25. In addition, R3.21 occurs when α value is larger than 4.

$CN + OH \rightarrow CHNO$ (R3.17)

$CN + H_2O \rightarrow CHNO + H$ (R3.18)

$CNHO \rightarrow CNO + H$ (R3.19)

$CH_2NO \rightarrow NH_2 + CO$ (R3.20)

$CNHO \rightarrow CO + NH$ (R3.21)

Taking the findings from Figures 3.6c and 3.6d together, it can be concluded that the contribution of OH to HCN consumption via R3.15 is dominant when α is 0, 1 and 25, which accounts for water has an insignificant influence on HCN production. However, in α = 2-10 cases, water molecules increase the HCN yield at the end of simulations owing to their promotional effects on pyridine pyrolysis. Moreover, OH radicals enhance the generation of new paths for NH and NH_2 generation (R3.20-R3.21), and both are key precursors to NH_3. H_2O also promotes the transfer from NH_2 to NH_3 via R3.22. Thus, the number of NH_3 shows an upward trend with water addition during pyridine pyrolysis.

$H_2O + NH_2 \rightarrow NH_3 + HO$ (R3.22)

Figure 3.7b illustrates the mechanisms of nitrogen-free intermediates during pyridine pyrolysis under varying α cases. It is clear that C_4H_4 and C_4H_3 are the key initial nitrogen-free species in all conditions [94]. Furthermore, C_2H_2 and C_2H mainly derive from the pyrolysis process of C_4H_4 and C_4H_3. C_4H_2 is generated through the loss of one H atom from C_4H_3.

Besides, under water-addition conditions, oxygen-containing intermediates are found from the reactions between OH radicals and intermediates (C_4H_3, C_4H_2, C_2H_2 and C_2H), which will further convert to CO finally. However, there are significant differences in the reaction pathways regarding CO generation at

different water concentrations. Specifically, when water concentrations in systems are low (α = 1-4), OH mostly reacts with C_2 molecules to produce oxygen-containing intermediates via the following reactions:

$C_2H + OH \rightarrow C_2H_2O$ (R3.23)

$C_2H_2 + OH \rightarrow C_2H_3O$ (R3.24)

And C_2H_3O, C_2H_2O and CHO are important precursors generating CO when α ranges from 1 to 4. For α of 2-25, CO converts to CHO_2 via R3.25:

$CO + OH \rightarrow CHO_2$ (R3.25)

CO_2 is produced by the thermal decomposition of CHO_2 by R3.26 in α = 4-25 cases.

$CHO_2 \rightarrow CO_2 + H$ (R3.26)

In the cases with α of 5-25, the reactions between OH and C_3 and C_4 intermediates are observed via R3.27-R3.29:

$C_3H_3 + OH \rightarrow C_3H_4O$ (R3.27)

$C_4H_2 + OH \rightarrow C_4H_3O$ (R3.28)

$C_4H_3 + OH \rightarrow C_4H_4O$ (R3.29)

And C_4H_2O, C_4H_3O, C_3H_3O, C_3H_2O and C_2O_2 are important precursors to generate CO. Besides, the pathway $HCN \rightarrow CH_2NO \rightarrow CO$ is found under water-containing conditions.

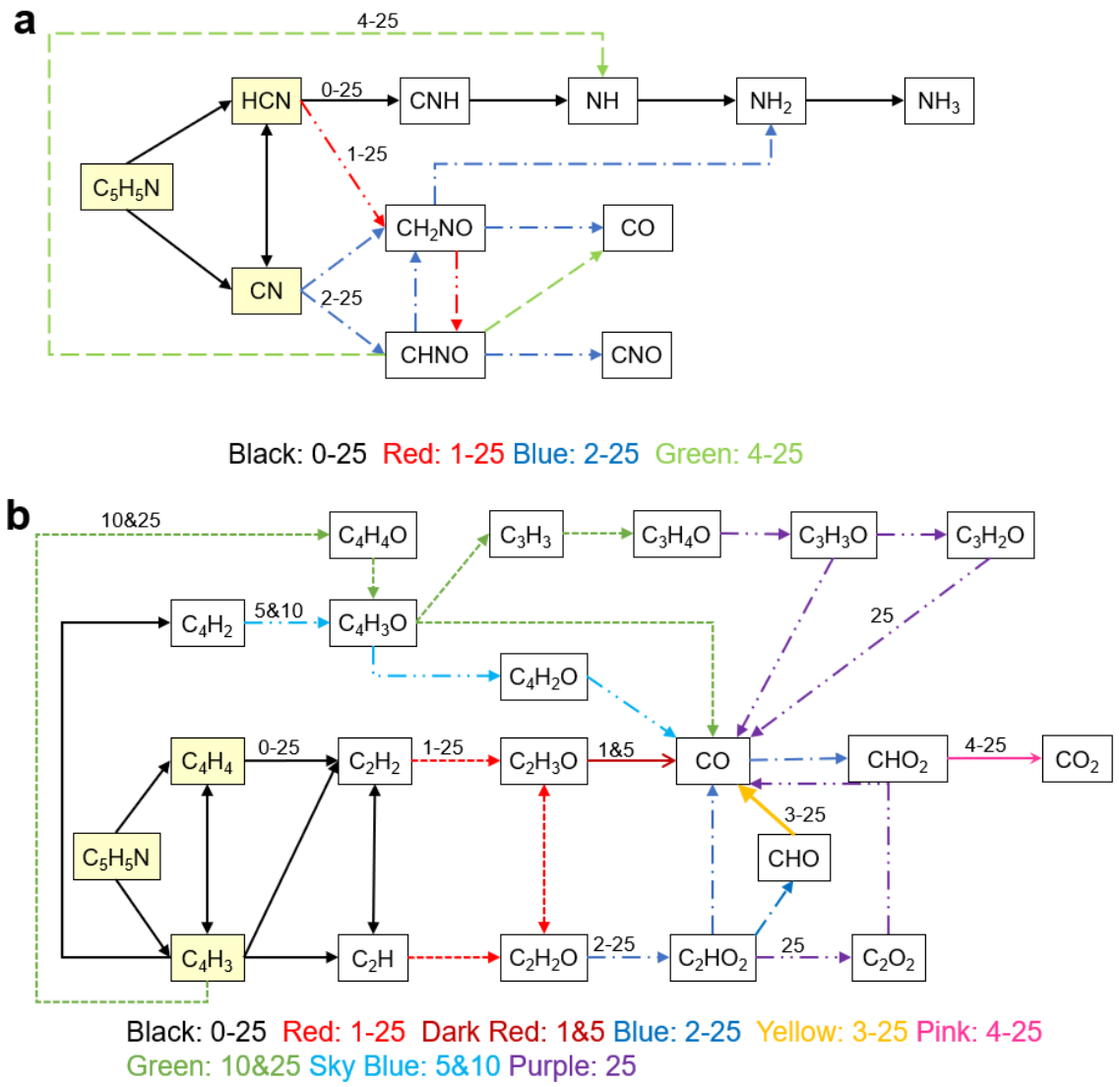

Figure 3.7 Influence of H_2O on pathways during pyridine pyrolysis. (a) nitrogenous species. (b) nitrogen-free species. The numerical numbers represent values of α. Boxes in yellow are the start of reactions.

3.3 Discussion

In this section, the impacts of H_2O molecules on the pyridine pyrolysis process were explored via ReaxFF MD simulations. The novel intermediates and reactions were revealed that had not been described in earlier studies [66, 95]. Furthermore, the impacts of H_2O on the pyridine consumption rates and ring-opening reactions of pyridine were explained at atomic scales. According to our simulation results, it can be concluded that water addition is an effective method to modify the pyridine pyrolysis process, which may be used to enhance NOx removal behaviors for the coal splitting and staging process.

Specifically, nitrogenous species in coal pyrolysis gas occupy a vital position

in the NOx removal performance during the coal splitting and staging process [7, 194, 195]. In addition, although nitrogen-containing compounds perform better in terms of NOx removal than nitrogen-free species, nitrogen-free species also affect the conversion from NOx to N_2 [196, 197]. According to the simulation results, water molecules significantly modify the numbers and types of nitrogen-containing and nitrogen-free compounds in pyrolysis gas, which can be used to achieve maximum NOx reduction performance by controlling the components in pyrolysis gas.

In general, water has a monotonic influence on the pyridine pyrolysis process, which benefits the control process of pyridine pyrolysis. However, non-monotonic behaviors also occur in terms of water concentrations in intermediate species (C_2O_2, C_3H_2O, and C_3H_3O) and consumption rates of pyridine. When α is lower than 10, C_2O_2, C_3H_2O, and C_3H_3O are formed via condensation reactions (CO reacts with CO, C_2H_2 and C_2H_3, respectively). Considering the yields of C_2O_2, C_3H_2O, and C_3H_3O are found to be minimal and their contributions to the pathway from NOx to N_2 are minor [172, 173], thereby their impacts on NOx reduction could be ignored. In addition, the non-monotonic behavior with respect to pyridine consumption rates and water content indicates that different control measures are necessary as the pyrolysis process goes on in real life.

Chapter 4 Mechanisms of NO Removal by HCN and NH_3

4.1 Effects of temperature on NO removal performance

4.1.1 Simulations details

To investigate the NO abatement by HCN and NH_3 processes, two systems with configurations of 120NO/120HCN/90O_2 and 120NO/120NH_3/30O_2 are produced with the density of 0.15 g/cm^3, respectively. The reactant equivalence ratios are obtained from the reduction equation as follows:

$$4NO + 4NH_3 + O_2 \rightarrow 4N_2 + 6H_2O \quad (4.1)$$

$$4NO + 4HCN + 3O_2 \rightarrow 4N_2 + 2H_2O + 4CO_2 \quad (4.2)$$

The bond order, time step and total simulation time are 0.3, 0.1 fs and 1000 ps, respectively. At the start, each system goes through 20 ps of energy minimization and equilibration at 40 K to optimise the initial geometric configuration. After that, the simulated system is heated to final temperatures (2400 K to 3400 K with 200 K increments) and maintained at target temperatures.

4.1.2. Results

4.1.2.1 Comparison of NO Reduction by HCN and NH_3

Figures 4.1a and 4.1b indicate that high temperatures accelerate HCN and NH_3 consumption significantly. NH_3 is reduced quicker than HCN molecules in all cases. When it comes to NO molecules, high temperatures can improve NO reduction capabilities by NH_3. However, in HCN cases, the numbers of NO almost keep the same between 2400 K and 3000 K, and slightly decline with temperature rising over 3000 K. Furthermore, as shown in Figures 4.1e and 4.1f, the yield of N_2 rises with temperature increasing in both HCN and NH_3 conditions, and there is considerably more N_2 production when NO is removed by NH_3 than by HCN. That indicates NH_3 outperforms HCN in terms of NO reduction. To further understand the NO reduction process, reaction pathways are studied in Sections 4.1.2.2 and 4.1.2.3 subsequently.

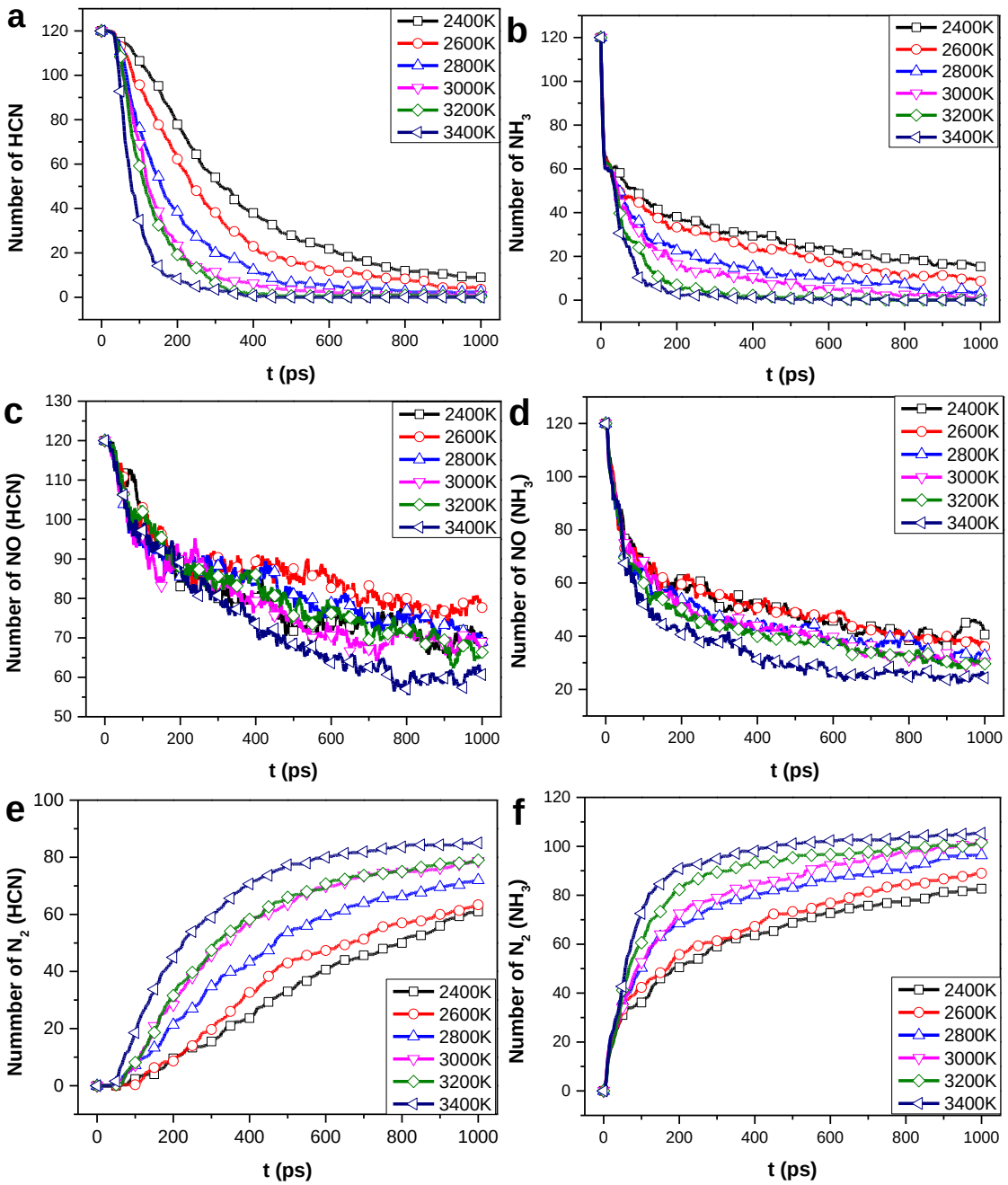

Figure 4.1 Time evolution of main species of NO reduction from 2400 K to 3400 K. (a) HCN; (b) NH_3; (c) NO removal by HCN; (d) NO removal by NH_3; (e) N_2 in HCN condition; (f) N_2 in NH_3 condition.

4.1.2.2 Mechanisms of NO Reduction by HCN

Figure 4.2 depicts the pathways of NO removal by HCN at temperatures ranging from 2400 K to 3400 K. It can be noticed that high temperatures encourage novel N_2 production routes, such as N →N_2, HN_2 →N_2, CN_2O_2 → N_2 at 2600 K-3400 K and NH → N_2 at 3400 K. HCN presents three distinct contributions to the NO reduction process.

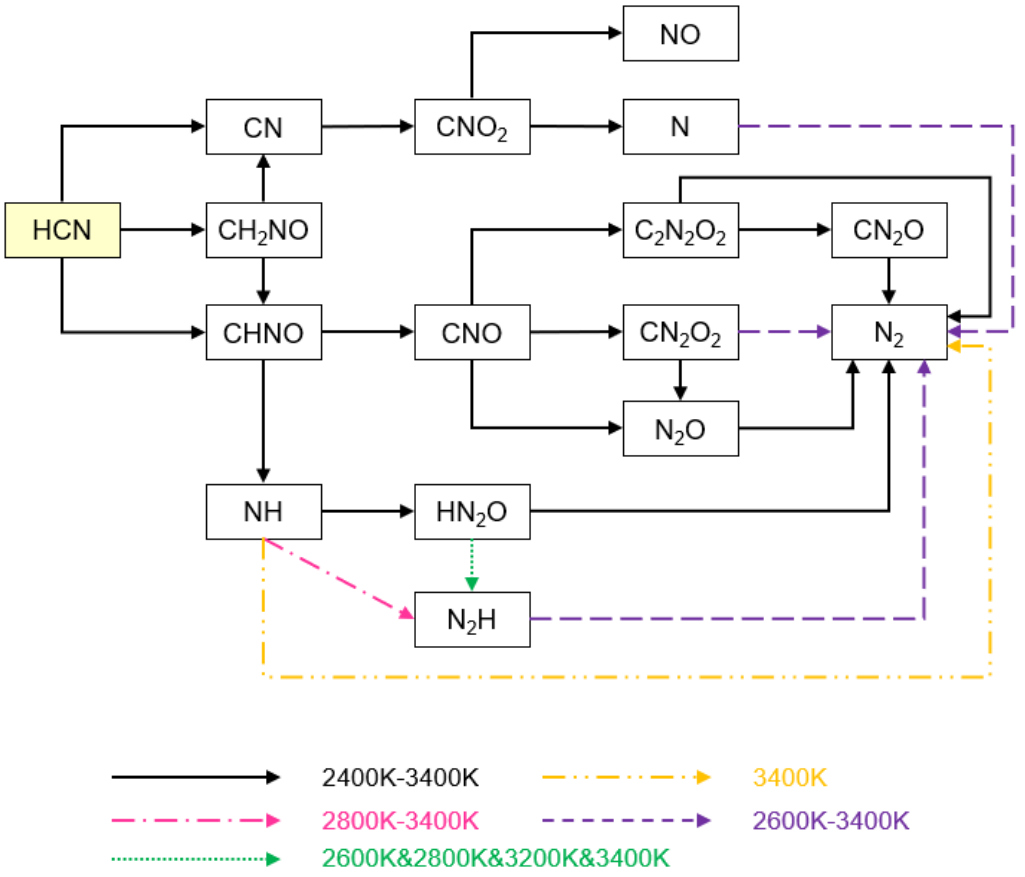

Figure 4.2 Pathways during NO removal with HCN. The starting species is HCN in the yellow box.

Firstly, a part of HCN is oxidized forming NO via the pathway HCN → CN → CNO_2 → NO, which has reserve impacts on NO removal. The second pathway is N_2 generation by channels HCN → CHNO → CNO → $C_2N_2O_2$ → CN_2O → N_2 and HCN → CHNO → CNO → $C_2N_2O_2$ → N_2. The key intermediate $C_2N_2O_2$ is formed via R4.1.

$$CNO + CNO \rightarrow C_2N_2O_2 \quad (R4.1)$$

CNO is produced via the oxidation of HCN. As a result, although N_2 is generated, it makes no contribution to NO abatement. Thirdly, HCN is converted to radicals N, NH, and CNO via oxidation and decomposition processes, which then react with NO via R4.2 to R4.7 to produce N_2.

$$CNO + NO \rightarrow CN_2O_2 \quad (R4.2)$$

$$CNO + NO \rightarrow CO + N_2O \quad (R4.3)$$

$$NH + NO \rightarrow HN_2O \quad (R4.4)$$

$$NH + NO \rightarrow N_2H + O \quad (R4.5)$$

$$NH + NO \rightarrow N_2 + H + O \quad (R4.6)$$

$N + NO \rightarrow N_2 + O$ (R4.7)

Besides R4.6 and R4.7, the following are the primary reactions related to N_2 generation from N_2O, HN_2O, CN_2O, $C_2N_2O_2$, CN_2O_2 and HN_2 during NO reduction by HCN:

$N_2O \rightarrow N_2 + O$ (R4.8)

$NO + N_2O \rightarrow N_2 + NO_2$ (R4.9)

$HN_2O \rightarrow N_2 + HO$ (R4.10)

$CN_2O \rightarrow N_2 + CO$ (R4.11)

$C_2N_2O_2 \rightarrow N_2 + CO + CO$ (R4.12)

$CN_2O_2 \rightarrow N_2 + CO + O$ (R4.13)

$N_2H + CO_2 \rightarrow N_2 + CHO_2$ (R4.14)

$N_2H \rightarrow N_2 + H$ (R4.15)

To better understand how temperature influences the numbers of NO and N_2 at the end of simulations, Tables 4.1 and 4.2 analyse the NFs of the key reaction pathways related to N_2 and NO.

Table 4.1 Net flux (NF) of key channels for NO consumption and generation during NO abatement with HCN at 2400 K to 3400 K.

Pathways	2400 K	2600 K	2800 K	3000 K	3200 K	3400 K
$CNO \rightarrow CN_2O_2$	46	54	34	46	48	43
$CNO \rightarrow N_2O$	15	19	25	18	20	18
$NH \rightarrow HN_2O$	11	13	15	17	12	21
$N \rightarrow N_2$	0	5	8	6	9	12
$NH \rightarrow N_2H$	0	0	11	11	6	7
$NH \rightarrow N_2$	0	0	0	0	0	12
Total NO consumption	72	91	93	98	95	113
$CNO_2 \rightarrow NO$	37	51	57	60	43	55
Net consumption	35	40	36	38	52	58

Table 4.2 Net flux (NF) of key channels for N_2 generation during NO abatement with HCN at 2400 K to 3400 K.

Pathways	2400 K	2600 K	2800 K	3000 K	3200 K	3400 K
$N_2O \rightarrow N_2$	39	40	36	54	50	44
$HN_2O \rightarrow N_2$	13	15	14	19	9	6
$CN_2O \rightarrow N_2$	17	14	19	19	21	15
$C_2N_2O_2 \rightarrow N_2$	11	12	10	19	11	14
$CN_2O_2 \rightarrow N_2$	0	11	13	17	30	30
$N \rightarrow N_2$	0	5	8	6	9	12
$N_2H \rightarrow N_2$	0	6	15	8	11	13
$NH \rightarrow N_2$	0	0	0	0	0	12
Total	80	103	115	142	141	146

As observed Table 4.1, the net NF of NO reduction nearly remains constant between 2400 K and 3000 K and increases when the temperature exceeds 3000K. This is consistent with the variations in NO numbers at various temperatures illustrated in Figure 4.1c. Furthermore, NO abatement and generation occur concurrently during NO abatement with HCN. Overall, the NF of NO removal rises with rising temperature due to the enhancement of combinations between NO and NH&N (R4.4-R4.7), but the promotion effects of temperature on the reaction between CNO and NO are insignificant. The NO formation is derived from the CNO_2 pyrolysis via R4.16.

$CNO_2 \rightarrow NO + CO$ (R4.16)

The NF of R4.16 follows a parabolic trend and peaks around 3000 K, which accounts for the amount of NO nearly remains the same between 2400 K and 3000 K.

The NF of the key reaction channels for N_2 generation under NO removal with HCN cases is shown in Table 4.2. The total NF of N_2 generation rises dramatically with increasing temperatures, which accounts for that high temperature enhances the yields of N_2 during NO reduction process. In detail, the rise in N_2 generation is mostly by the enhancement of channels $CN_2O_2 \rightarrow N_2$ (R4.13), $N \rightarrow N_2$ (R4.7), $N_2H \rightarrow N_2$ (R4.14&R4.15), and $NH \rightarrow N_2$ (R4.6).

In summary, as temperature rises, NO abatement and N_2 production increase by the promotion of channels:

a. $HCN \rightarrow CN \rightarrow CNO_2 \rightarrow N \rightarrow N_2$

b. $HCN \rightarrow CNHO \rightarrow NH \rightarrow N_2$

c. $HCN \rightarrow CNHO \rightarrow NH \rightarrow HN_2O \rightarrow N_2H \rightarrow N_2$

d. $HCN \rightarrow CNHO \rightarrow NH \rightarrow N_2H \rightarrow N_2$

e. $HCN \rightarrow CNHO \rightarrow CNO \rightarrow CN_2O_2 \rightarrow N_2$

4.1.2.3 Mechanisms of NO Reduction by NH_3

According to Figure 4.3, the key species for NO removal are NH, NH_2 and NH_3 via R4.17-R4.34. And R4.17 only happens at 2600 K-3400 K.

$NH_3 + NO \rightarrow HN_2O + H_2$ (R4.17)

$NH_3 + NO \rightarrow H_2N_2O + H$ (R4.18)

$NH_3 + NO + HO \rightarrow H_2N_2O + H_2O$ (R4.19)

$NH_2 + NO \rightarrow H_2N_2O$ (R4.20)

$NH + NO \rightarrow HN_2 + O$ (R4.21)

$NH + NO \rightarrow N_2 + H + O$ (R4.22)

$NH + NO \rightarrow HN_2O$ (R4.23)

$N_2H + NO \rightarrow N_2 + HNO$ (R4.24)

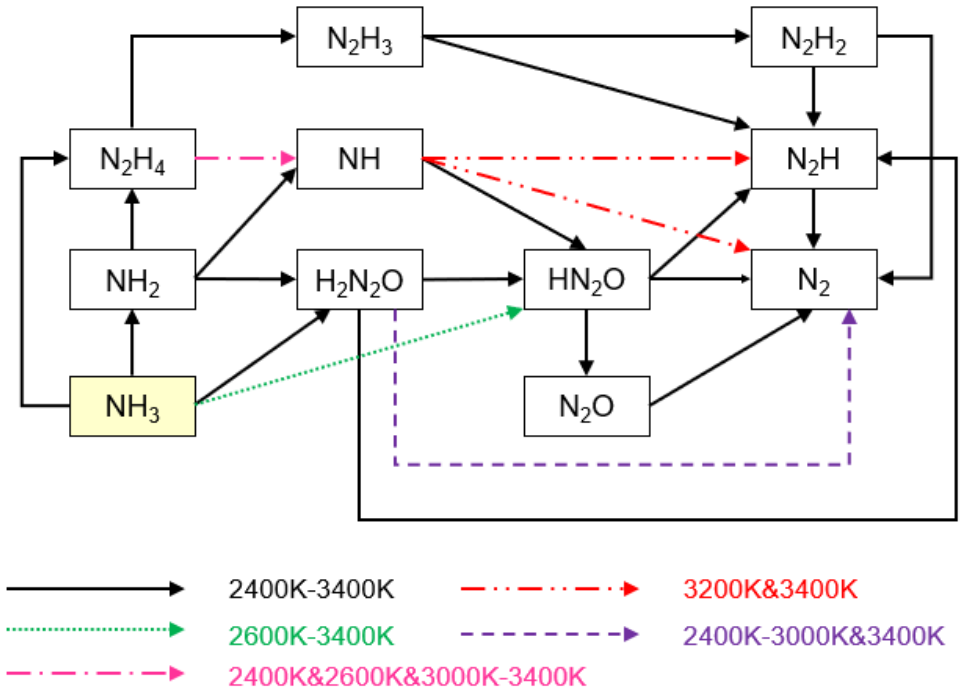

Figure 4.3 Channels of NO removal with NH_3. The beginning species is NH_3 in the yellow box.

N_2 is formed by reactions:

$HN_2O \rightarrow N_2 + HO$ (R4.25)

$HN_2O \rightarrow N_2 + H + O$ (R4.26)

$N_2H \rightarrow N_2 + H$ (R4.27)

$N_2H + HO \rightarrow N_2 + H_2O$ (R4.28)

$N_2H + NO \rightarrow N_2 + HNO$ (R4.29)

$N_2H_2 \rightarrow N_2 + H_2$ (R4.30)

$N_2O \rightarrow N_2 + O$ (R4.31)

$H_2N_2O \rightarrow N_2 + H_2O$ (R4.32)

$H_2N_2O \rightarrow N_2 + H + HO$ (R4.33)

$NH + NO \rightarrow N_2 + H + O$ (R4.34)

$NH \rightarrow N_2$ takes place between 3200 K and 3400 K, while $H_2N_2O \rightarrow N_2$ occurs under 2400 K-3000 K and 3400 K conditions. In addition, the channels related to N_2 generation $NH_3 \rightarrow NH_2 \rightarrow H_2N_2O \rightarrow N_2H \rightarrow N_2$ and $NH_3 \rightarrow NH_2 \rightarrow H_2N_2O \rightarrow N_2$ are also supported by earlier research [118, 119].

Additionally, there are reaction pathways of N_2 formation from NH_3 without NO removal. First, N_2H_4 is generated via R4.35-R4.36, which will be transformed to N_2 via $N_2H_4 \rightarrow N_2H_3 \rightarrow N_2H \rightarrow N_2$ and $N_2H_4 \rightarrow N_2H_3 \rightarrow N_2H_2 \rightarrow N_2$.

$NH_2 + NH_2 \rightarrow N_2H_4$ (R4.35)

$NH_3 + NH_3 \rightarrow N_2H_4 + H + H$ (R4.36)

$NH_3 + NH_3 + O_2 \rightarrow N_2H_4 + HO_2 + H$ (R4.37)

To further understand the effects of temperature on the numbers of NO and N_2 in products finally, the contributions of each channel associated with NO removal and N_2 generation at varying temperatures were investigated, as illustrated in Tables 4.3 and 4.4. The total NF of NO abatement and N_2 generation rises with increasing temperatures, agreeing well with the final amount of NO and N_2 with temperatures ranging from 2400 K to 3400 K.

Table 4.3 Net flux (NF) of key channels for NO consumption during NO reduction with NH_3 at 2400 K-3400 K.

Pathways	2400 K	2600 K	2800 K	3000 K	3200 K	3400 K
NH → HN_2O	12	16	31	34	35	47
NH_3 → H_2N_2O	18	16	16	18	26	21
NH_2 → H_2N_2O	71	69	65	60	27	34
NH_3 → HN_2O	0	4	5	7	3	7
NH → HN_2	0	0	0	0	16	15
NH → N_2	0	0	0	0	7	13
Total	101	105	117	119	114	137

Table 4.4 Net flux (NF) of key channels for N_2 generation during NO reduction with NH_3 at 2400 K-3400 K.

Pathways	2400 K	2600 K	2800 K	3000 K	3200 K	3400 K
HN_2O → N_2	41	46	53	53	57	49
N_2H → N_2	50	60	58	58	72	78
N_2H_2 → N_2	13	11	20	18	24	17
N_2O → N_2	11	15	9	15	13	20
H_2N_2O → N_2	13	3	8	18	0	7
NH → N_2	0	0	0	0	7	13
Total	128	135	148	162	173	184

As shown in Table 4.3, the pathway NH → HN_2O via R4.23 plays a dominant role to the rise in NO reduction as temperature increases. And NH_2 → H_2N_2O through R4.20 is essential for NO removal especially at 2400 K-3000 K. Furthermore, high temperatures present reverse effects on the combination of NH_2 and NO. At 3200 K-3400 K, channels NH → N_2H via R4.21 and HN → N_2 through R4.22 are enhanced.

With temperatures ranging from 2400 K to 3400 K, HN_2O → N_2 via R4.25-R4.26 and N_2H → N_2 via R4.27-R4.29 are promoted with the increase of temperature. The pathway N_2H_2 → N_2 via R5.30 is slightly enhanced over 2400 K to 3400 K. Regarding the channel N_2O → N_2 via R4.31, its contribution to N_2 production nearly keeps constant from 2400 K to 3200 K and rises at 3400 K. At 3200 K-3400 K, the channel NH → N_2 through R4.34 is enhanced between 3200 K to 3400 K.

According to the above study, it is concluded that high temperatures enhance N_2 generation, NO consumption and NO removal by NH_3 via the following channels:

f. $NH_3 \rightarrow NH \rightarrow HN_2O \rightarrow N_2$

g. $NH_3 \rightarrow NH \rightarrow N_2H \rightarrow N_2$

h. $NH_3 \rightarrow NH \rightarrow N_2$

4.1.3 Discussion

In this part, ReaxFF MD is used to explore the mechanisms of NO abatement with HCN and NH_3 at various temperatures, which are important in NOx reduction via coal pyrolysis gas. To better regulate NOx emissions, it is crucial to examine the NO removal behaviours of HCN and NH_3 in the light of existing publications.

In earlier research [118, 119, 130, 198], the amount of NO is used to indicate NOx removal effectiveness. Whereas nitrogenous species can also be converted to NOx in the burnout zone, emitting pollutants into the atmosphere. As a result, as shown in Figure 4.4, the amount of N_2 generated in simulations is employed as an indication to indicate the reduction behaviours of nitrogenous reactants. The increase of temperature significantly improves NOx control effectiveness in both HCN and NH_3 conditions, and NH_3 has approximately 19.1% more capacity than HCN for NO removal from 2400 K to 3400 K. Furthermore, the optimum temperature is not detected in the simulation results during NO reduction via NH_3, that is inconsistent with the phenomenon reported in the ammonia based SNCR method [118, 119, 130, 198]. This is because SNCR operates in excess oxygen atmospheres, and high temperatures encourage NH_3 oxidation resulting in decreased NO reduction efficiency. Whereas, in the reburning zone, NO molecules are reduced under fuel-rich circumstances where the oxidation of nitrogen-containing species is supressed. Thereby, the NO removal with NH_3 behaviours is not limited as temperatures rise.

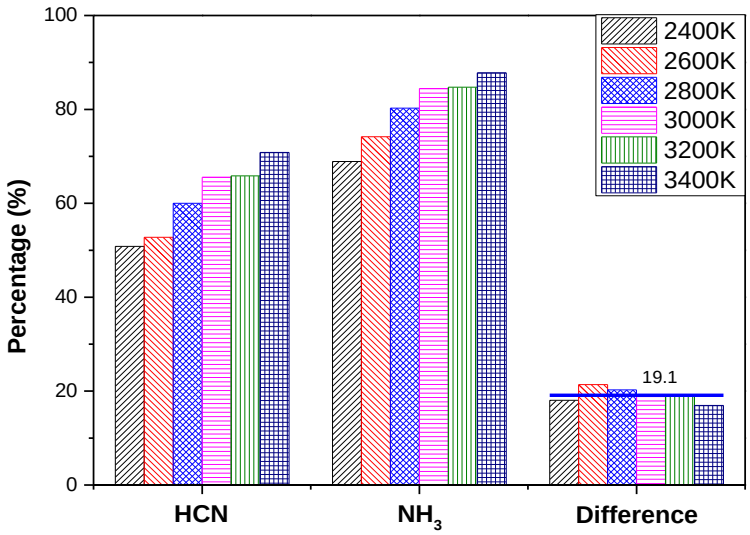

Figure 4.4 Reduction efficiency of nitrogen-containing reactants.

According to above findings, increasing reactive temperatures is an efficient way to increase the NOx removal behaviours of coal pyrolysis gas. Increasing the NH_3 content in coal pyrolysis gas can also benefits the control of NOx emissions, which may be accomplished by raising pressure, temperature and water content during coal pyrolysis [94, 117].

4.2 Effects of Oxygen and HCN/NH_3 on the NO Removal Performance

4.2.1 Simulation Details

The reactant equivalence ratios are computed using the reduction equation, as indicated in Equations (4.1) and (4.2). (4.2). A molar ratio, *λ*, is proposed to aid analysis, as demonstrated in Equations (4.3) and (4.4), respectively. As indicated in Equation (4.5), *R* is the ratio of the number of HCN or NH_3 to that of pyridine.

$$\lambda = \frac{4n(\mathrm{O_2})}{3n(\mathrm{NO})} \tag{4.3}$$

$$\lambda = \frac{4n(\mathrm{O_2})}{n(\mathrm{NO})} \tag{4.4}$$

$$R = \frac{n(\mathrm{HCN\ or\ NH_3})}{n(\mathrm{NO})} \tag{4.5}$$

where *n*(NO), *n*(O_2) and *n*(HCN or NH_3) means the amount of NO, O_2 and HCN or NH_3, respectively.

Table 4.5 summarises the simulated mixes. Cases 1 and 4 are for comparison when NO is reduced by HCN and NH_3 with *λ* and *R* values of 1. Cases 2 and 3 are designed to study the impact of O_2 concentrations and HCN/NO ratios on NO abatement performance by HCN, where *λ and R* ranges from 0.0 to 0.8 and 1.2 to 2.0 with a 0.2 increment, respectively. Similarly, Cases 5 and 6 are used to investigate the impact of the number of O_2 and NH_3 molecules on NO reduction behaviour by NH_3 under varying *λ* and *R* values. The density of all simulations is kept at 0.15 g/cm^3.

Table 4.5 Case set-ups.

ID	# of NO	# of HCN	# of NH_3	# of O_2	λ	R
1	120	120	0	90	1.0	1.0
2	120	120	0	0-72	0.0-0.8	1.0
3	120	144-240	0	90	1.0	1.2-2.0
4	120	0	120	30	1.0	1.0
5	120	0	120	0-24	0.0-0.8	1.0
6	120	0	144-240	30	1.0	1.2-2.0

To optimize the initial configuration of reactants, each system goes through 20 ps of energy reduction and equilibration at 40 K. Following that, the systems are heated to 3000 K and then held at that temperature. For all simulations, the time step and the overall simulation time are 0.1 fs and 1000 ps, respectively.

4.2.2 Results

4.2.2.1 Effects of λ Values on NO Removal Performance by HCN and NH_3

Figures 4.5a and b illustrate the amount of NO and N_2 produced during NO reduction by HCN and NH_3 at various λ values. The number of NO grows when O_2 concentrations rise, and the rising trend is more pronounced when NO is eliminated by HCN rather than NH_3. High O_2 concentrations hinder N_2 production in NO reduction by NH_3 conditions. However, during NO reduction by HCN, N_2 production presents a parabolic pattern, culminating at λ = 0.6. This result is consistent with experimental investigations showing that the best NOx reduction efficiency by coal pyrolysis gas occurs under fuel-rich conditions [5].

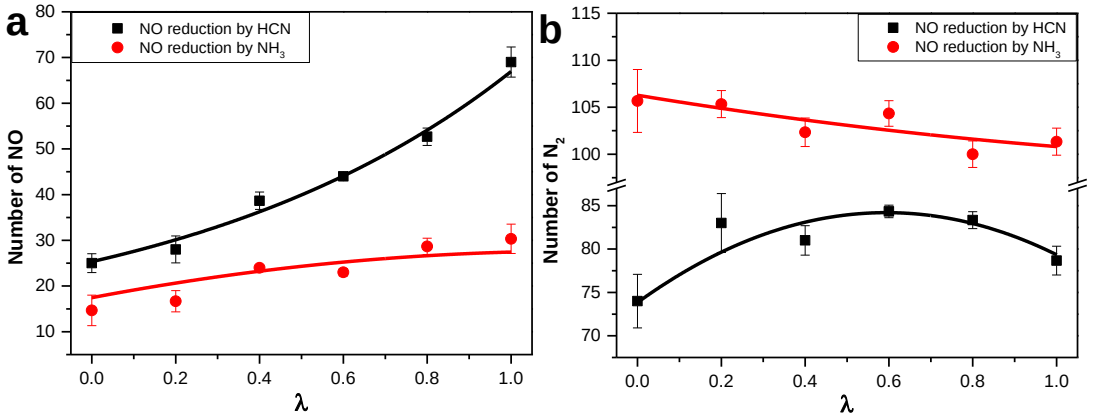

Figure 4.5 Numbers of (a) NO and (b) N_2 for λ ranging from 0 to 1 at the end of simulations.

Figure 4.6 presents chemical pathways at various λ levels to gain a further understanding of how O_2 influences NO reduction by HCN and NH_3. In all circumstances, CNO, NH, and N are key intermediates for NO consumption, as shown in Figure 4.6a. In λ = 0.0-0.2 conditions, the responses of NO consumption by HCN and CN are detected. The formation of NO and N from intermediate CNO_2 is found with λ = 0.2-1.0 & 0.4-1.0. When λ values are 0.0, 0.4, and 0.6, CN_2 will react with NO to create CN_3O. Thermal breakdown of intermediates HN_2O, HN_2, N_2O, and CN_2O for N_2 molecules is observed in λ = 0.0-1.0 conditions. CNO and N reactions with NO production occur in λ = 0.6 and 0.0-1.0, respectively. The pathway $CN_3O \rightarrow N_2$ is found in situations with λ from 0.0 to 0.6. The thermal breakdown of $C_2N_2O_2$ and CN_2O_2 is discovered with λ = 0.2-1.0.

Figure 4.6b shows the chemical pathways involved in NO elimination by NH_3. The primary intermediates are the same in all circumstances, however the reaction routes alter during the NO reduction process at varied O_2 concentrations. When λ values are 0.0-1.0, the major intermediates to consume NO molecules are NH_3, NH_2, and NH, whereas HN_2O, N_2H, and N_2H_2 are significant precursors to N_2 production. The pathway $N_2H_3 \rightarrow N_2$ is found with λ = 0.0. $NH_3 \rightarrow HN_2O$ and $N_2H_2 \rightarrow$ NH are not identified with at 0.6 and 0.2, respectively. When values are between 0.0 and 0.4, the pathways NH $\rightarrow N_2H_3$, NH $\rightarrow N_2H$, and $H_2N_2O \rightarrow N_2H$ occur. The conversion from NH_3 to NH is found in λ = 0.0 and 0.2 cases.

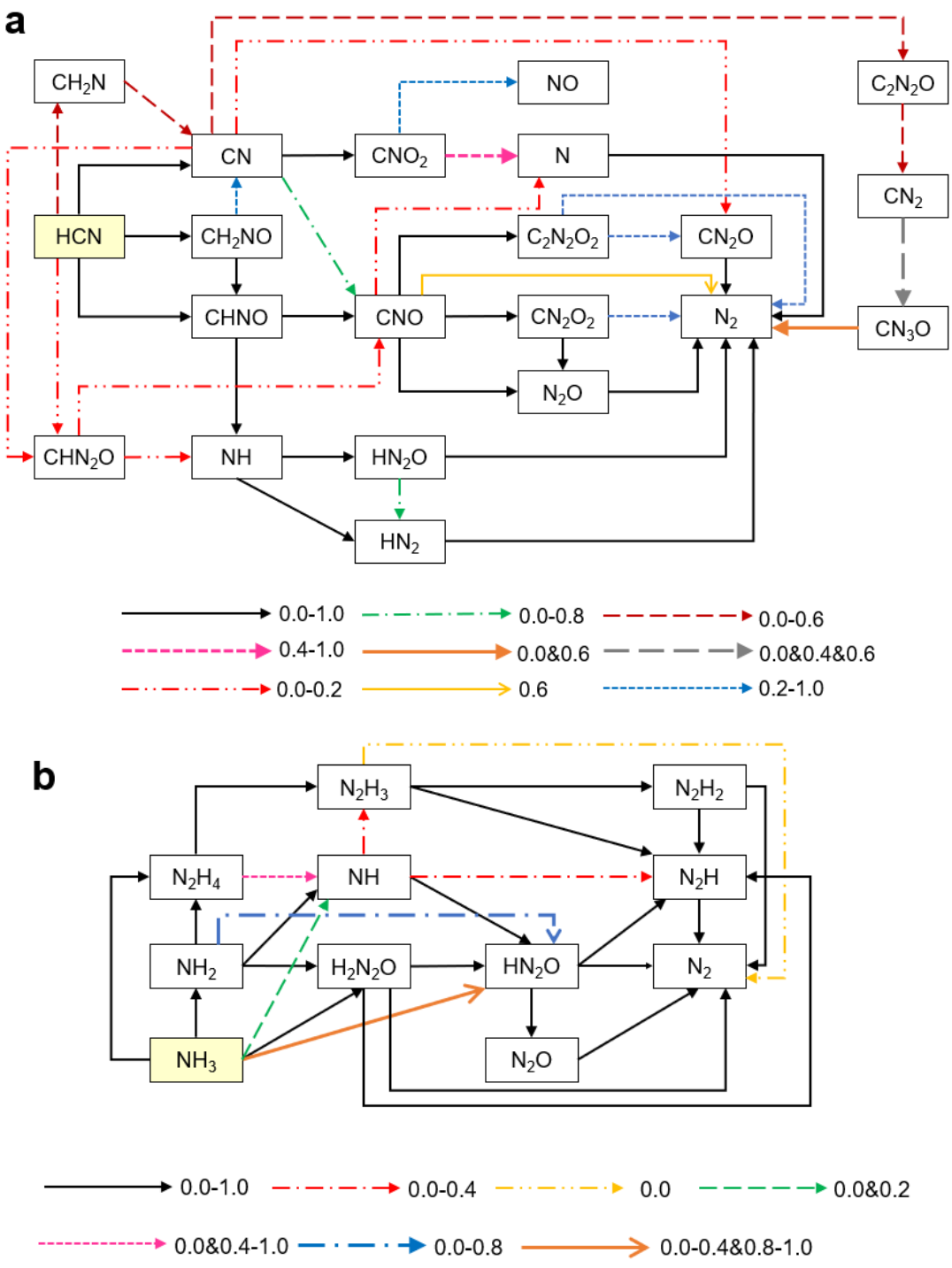

Figure 4.6 Reaction pathways of NO abatement by (a) HCN and (b) NH_3 under varying λ values. HCN and NH_3 are the starting molecules in yellow boxes.

Tables 4.6 and 4.7 study the NF of key pathways related to N_2 and NO during NO abatement with HCN and NH_3, respectively, to further discover how O_2 impacts the numbers of NO and N_2 at the conclusion of reactions. As shown in Table 4.6, the NF of NO consumption varies about 95 with λ ranging from 0.0 to 1.0. However, NO generation by route $CNO_2 \rightarrow NO$ is promoted at high O_2

concentrations during NO reduction by HCN, resulting in a decrease in net NO consumption with rising λ, which is consistent with the fluctuation of NO numbers at different λ values in Figure 4.5a. Although the impact of O_2 on the NF of NO consuming is negligible, the NFs of pathways associated with NO consumption varies at different λ levels. Specifically, a reduction in O_2 concentrations inhibits the NO consumption routes CNO → CN_2O_2 and CNO → N_2O, but increases NO consumption via intermediates HCN, CN, and CN_2. The NF of conversion from NH to HN_2O reaches its maximum value at λ = 0.4. The influence of O_2 on N → N_2 and NH → HN_2 are negligible.

In terms of N_2 formation, the NF of N_2 generation follows a similar pattern to the N_2 yield, which peaks at λ = 0.6. Among the N_2 production routes, O_2 favours the pathways CN_2O → N_2, $C_2N_2O_2$ → N_2, and CN_2O_2 → N_2 when λ ranges from 0.0 to 1.0. The contribution of N_2O → N_2 is nearly unchanged with of 0.2-1.0, but it is considerably inhibited at λ of 0.0 case. Over λ = 0.0-0.6, O_2 molecules have an insignificant effect on the conversion of N_2H to N_2, while in λ = 0.8-1.0 conditions, they inhibit this process. As λ increases, the NF of N → N_2 varies slightly as λ increases. The NF of N_2 production from HN_2O reaches its maximum with λ of 0.6. In addition, CNO → N_2 and CN_3O → N_2 are discovered with λ = 0.6 and 0.0&0.6, respectively.

Table 4.6 Net flux (NF) of key channels linked with NO and N_2 during NO abatement with HCN at λ = 0-1.

Pathways	0	0.2	0.4	0.6	0.8	1
HCN → CHN_2O	13	2	0	0	0	0
CN → CHN_2O	11	7	0	0	0	0
CN → CN_2O	15	6	0	0	0	0
CNO → N_2	0	0	0	11	0	0
CN_2 → CN_3O	7	0	10	10	0	0
CNO → CN_2O_2	20	22	38	30	48	46
CNO → N_2O	4	9	15	14	13	18
N → N_2	5	7	6	6	8	6
NH → HN_2O	13	20	23	22	22	17
NH → HN_2	7	7	8	9	5	11
Total NO consumption	95	80	100	102	96	98
CNO_2 → NO	0	8	14	31	45	60
Net NO consumption	95	72	86	71	51	38
CNO → N_2	0	0	0	11	0	0
CN_3O → N_2	10	0	0	7	0	0
N_2O → N_2	20	48	45	42	45	54
HN_2O → N_2	18	15	24	26	20	19
CN_2O → N_2	8	11	11	17	16	19
$C_2N_2O_2$ → N_2	0	8	7	13	14	19
CN_2O_2 → N_2	0	11	5	12	13	17
N → N_2	5	7	6	6	8	6
N_2H → N_2	24	32	16	23	17	8
N_2 generation	85	132	114	157	133	142

Table 4.7 shows a declining trend with rising values for the NFs of NO consumption and N_2 generation, which is consistent with the changes in NO and N_2 quantities seen in Figure 4.5. Overall, with λ varying from 0.0 to 1.0, the NF of NO reduction by NH radical almost stays the same. The pathway NH → HN_2O is

weakened when λ is less than 0.4 because NH is converted to N_2H. As O_2 concentrations rise, the contribution of NH_2 to NO abatement declines noticeably. In contrast to $NH_2 \rightarrow HN_2O$, $NH_2 \rightarrow H_2N_2O$ has a parabolic trend that reaches its lowest point at λ = 0.6. Additionally, when the amount of O_2 rises, the reactions between NO and NH_3 molecules are slightly impeded. O_2 has an insignificant impact on the channels $HN_2O \rightarrow N_2$, $N_2O \rightarrow N_2$, and $H_2N_2O \rightarrow N_2$ in terms of N_2 production. When λ is high, $N_2H \rightarrow N_2$ and $N_2H_2 \rightarrow N_2$ are inhibited, which reduces the production of N_2. Additionally, the pathway $N_2H_3 \rightarrow N_2$ is observed with λ of 0.0.

Table 4.7 Net flux (NF) of key channels linked with NO and N_2 during NO removal with NH_3 at λ = 0-1.

Pathways	0	0.2	0.4	0.6	0.8	1
$NH \rightarrow HN_2O$	33	21	21	32	38	34
$NH \rightarrow N_2H$	7	7	14	0	0	0
$NH_2 \rightarrow H_2N_2O$	89	69	61	44	54	60
$NH_2 \rightarrow HN_2O$	4	12	8	22	14	0
$NH_3 \rightarrow HN_2O$	11	13	10	0	7	7
$NH_3 \rightarrow H_2N_2O$	22	29	22	20	23	18
Total NO consumption	166	151	136	118	136	119
$HN_2O \rightarrow N_2$	53	58	52	49	54	53
$N_2H \rightarrow N_2$	66	76	64	61	69	58
$N_2H_2 \rightarrow N_2$	30	34	28	17	23	18
$N_2O \rightarrow N_2$	23	18	21	19	26	15
$H_2N_2O \rightarrow N_2$	13	5	7	12	2	18
$N_2H_3 \rightarrow N_2$	11	0	0	0	0	0
Total N_2 formation	196	191	172	158	174	162

In summary, O_2 has a detrimental effect on NO reduction in conditions of NO reduction with HCN because it encourages HCN oxidation, which produces NO molecules via $HCN \rightarrow CN \rightarrow CNO_2 \rightarrow NO$. The intermediates for NO removal vary from CN, HCN, and CN_2 to CNO with λ rising, even while the NF of NO molecules consumption almost keeps the same under different O_2 concentrations. Besides, O_2 encourages the formation of the CNO radical greatly, which can then react with NO or itself to produce N_2. However, the N_2 yield reaches its maximum

when λ is 0.6 since λ values larger than 0.6 prevent the generation of N_2 from HN_2O, N_2H, CN_3O, and CNO. Additionally, O_2 inhibits N_2 production and NO removal behaviours when NO is reduced by NH_3. This is due to the weakening of NO consumption by NH_3 and NH_2 forming H_2N_2O or HN_2O when O_2 concentrations rise. Furthermore, the weakening of the pathway $NH_3/NH_2/NH \rightarrow H_3N_2 \rightarrow H_2N_2 \rightarrow N_2$ caused by an increase in O_2 reduces the generation of N_2.

4.2.2.2 Effects of *R* Values on NO Reduction Performance by HCN and NH_3

As shown in Figure 4.7, raising *R* values in both NO reduction by HCN and NH_3 situations improves the NO reduction and N_2 generation performance. With *R* rising from 1.0 to 2.0, the reduction efficiencies of reactants containing nitrogen increase by 7.7% and 3.8%, respectively. However, their profiles show downward tendencies when *R* is greater than 1.6, which is consistent with earlier research [198].

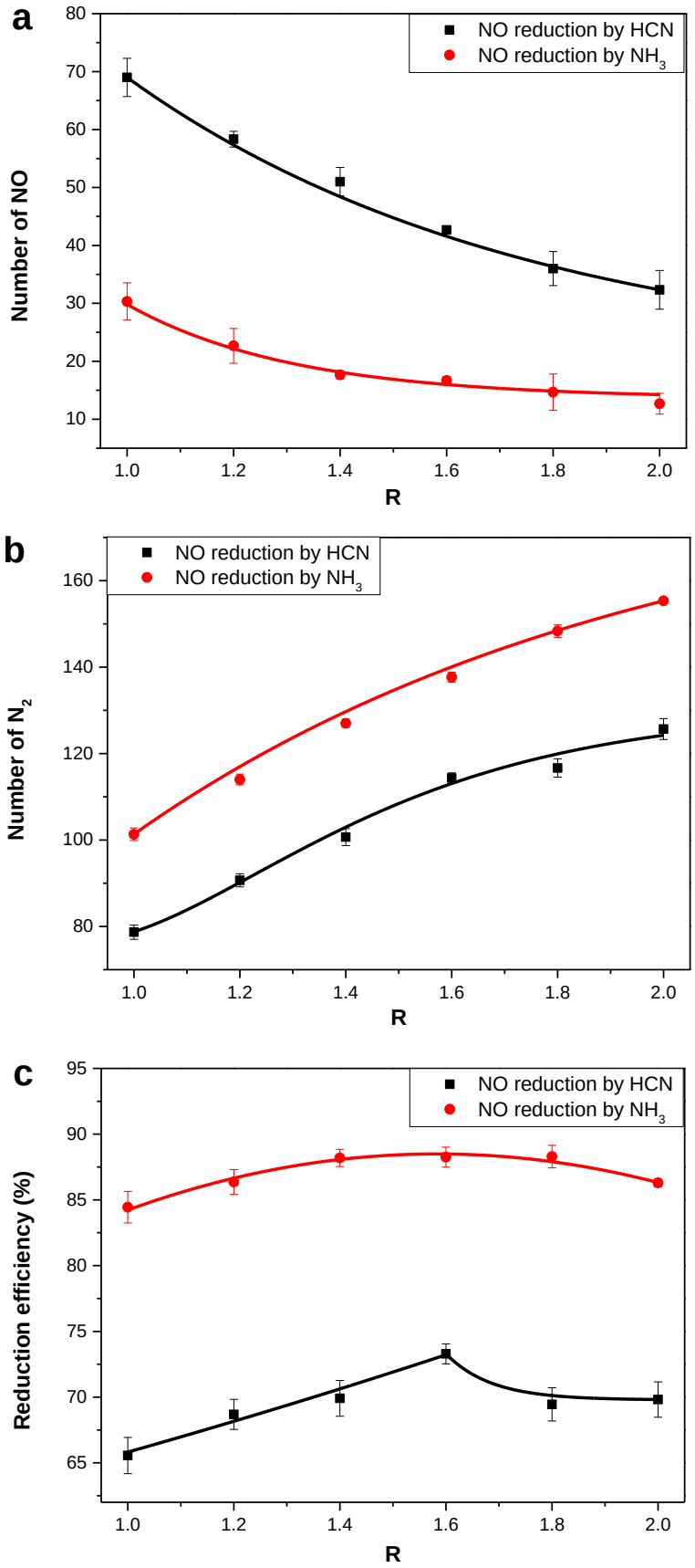

Figure 4.7 The final number of (a) NO, (b) N_2 and (c) reduction efficiency at R = 1.0-2.0. Here, reduction efficiency is the ratio of nitrogen element in N_2 to nitrogen-containing reactants at the end of reactions.

Figure 4.8a presents reaction pathways of NO reduction by HCN with changing *R* values. High *R* values enhance the generation of novel intermediates and paths to N_2. In particular, the routes CN → C_2N_2O → CN_2 → CN_3O → N_2, CN → CNO, CNO → N, and HN_2O → N_2H are found as *R* is greater than 1.2. In *R* = 1.6–2.0 situations, the conversion of NH to N_2 and HN_2O to N_2O takes place. There are two routes that produce N_2 when *R* values are 1.8 and 2.0: CN → CHN_2O → N_2 and CN_2 → C_2N_3O → N_2. In the instance where *R* = 1.6, there is no conversion from N to N_2. N_2 is formed from CNO with *R* = 1.2 & 1.6 & 1.8.

The primary intermediates stay the same when *R* values rise in NO reduction by NH_3 cases as illustrated in Figure 4.8b. However, distinct reaction paths exist for various *R* values. For example, when *R* value is over 1.2 and 1.8, respectively, the channels NH_2 → HN_2O and N_2H_3 → N_2 are discovered. N_2H_4 to NH conversion takes place between *R* = 1.0 and 1.8. In the range of *R* = 1.6 to 2.0, NH is formed from NH_3 and converted to N_2H_3, N_2H_2, and N_2H. The production of N_2 from H_2N_2O is not identified when *R* is 1.2.

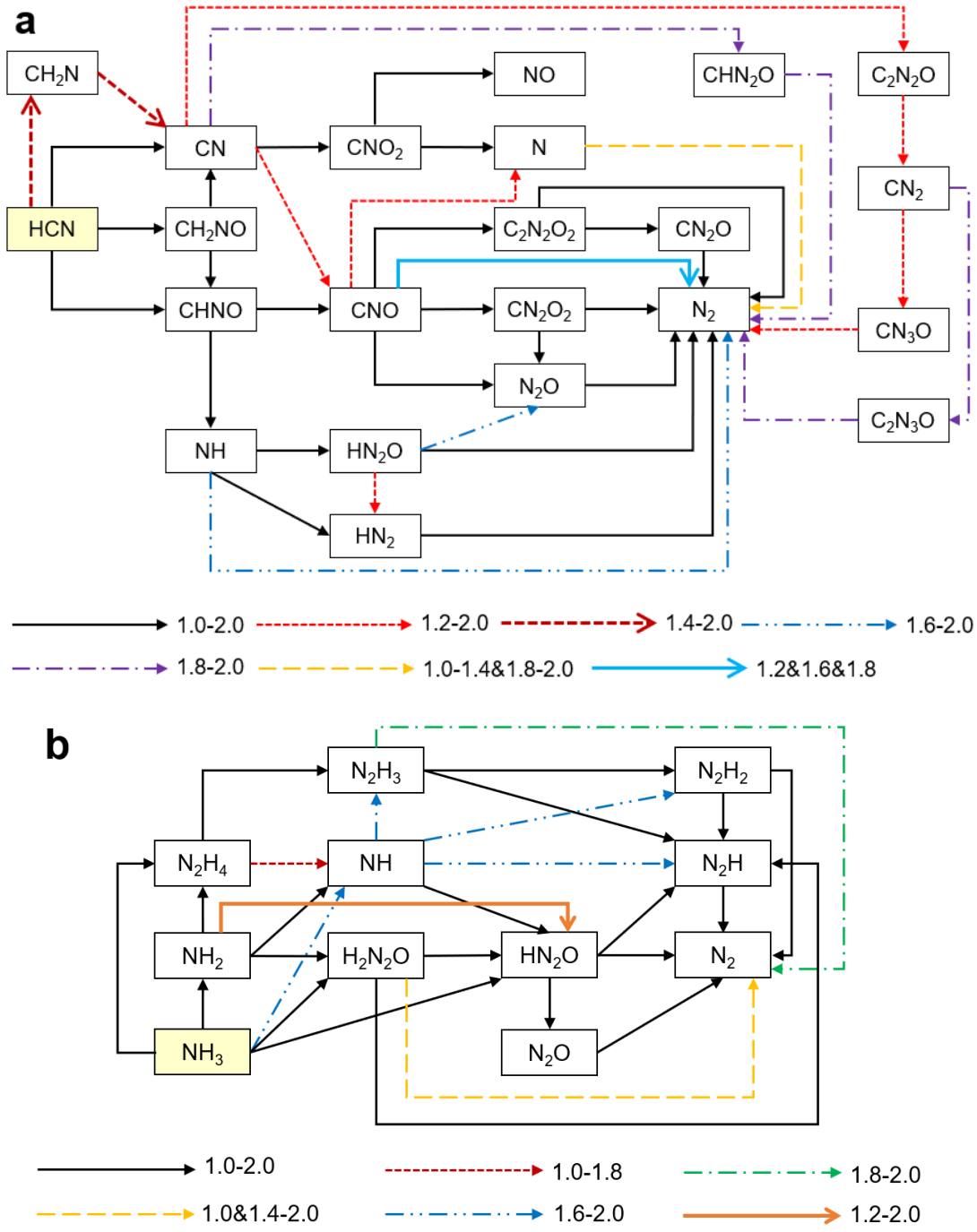

Figure 4.8 Reaction pathways of NO abatement by (a) HCN and (b) NH_3 under varying *R* values. HCN and NH_3 are the starting molecules in yellow boxes.

Figure 4.8 presents the alteration of chemical channels during NO abatement by HCN and NH_3 at various *R* values, however the reason why high *R* values improve NO reduction effectiveness remains unknown. The net flux (NF) of the key channels related with NO and N_2 after NO reduction using HCN and NH_3 with *R* changing from 1.0 to 2.0 is investigated subsequently.

As shown in Table 4.8, the NF of NO removal improves greatly as *R*

increases, whereas NO production from CNO_2 reduces slightly, which explains why high *R* values improve NO reduction behaviours by HCN. *R* values have minimal effect on the NF of N → N_2. CNO's contribution to NO removal reaches the highest point in the *R* = 1.4 condition because of the channels CNO → CN_2O_2 and CNO → N_2O. The channels of NO consumption via CN, CN_2, and NH are encouraged with *R* rising. In detail, the NF of NH → HN_2O increases from *R* = 1.0 to 1.6, but drops when *R* exceeds 1.6. The conversion from NH to N_2H and NH to N_2 is promoted in *R* = 2.0 and 1.6-2.0 cases, respectively. In terms of N_2 generation, high HCN/NO ratios boost N_2 production from CHN_2O, C_2N_3O, CN_3O, N_2H, and NH. *R* values present insignificant effects on the NF of CNO → N_2, N_2O → N_2, and N → N_2. High HCN/NH_3 ratios inhibit CN_2O_2 → N_2 significantly. N_2 production from CNO → $C_2N_2O_2$/CN_2O → N_2 is promoted in *R* = 1.0-1.6, but weaken in *R* = 1.6-2.0 cases.

Table 4.8 Net flux (NF) of key channels linked with NO and N_2 during NO reduction with HCN at R = 1.0-2.0.

Pathways	1.0	1.2	1.4	1.6	1.8	2.0
$CN \rightarrow CHN_2O$	0	0	0	0	3	6
$CN_2 \rightarrow CN_3O$	0	10	7	18	14	22
$CNO \rightarrow N_2$	0	14	0	6	5	0
$CNO \rightarrow CN_2O_2$	46	38	60	47	34	45
$CNO \rightarrow N_2O$	18	10	23	13	17	8
$N \rightarrow N_2$	6	10	10	0	8	8
$NH \rightarrow HN_2O$	17	24	40	43	31	35
$NH \rightarrow N_2H$	11	12	8	13	11	17
$NH \rightarrow N_2$	0	0	0	11	5	17
NO consumption	98	118	148	151	128	158
$CNO_2 \rightarrow NO$	60	54	55	49	45	45
Net NO consumption	38	64	93	102	83	113
$CHN_2O \rightarrow N_2$	0	0	0	0	13	8
$C_2N_3O \rightarrow N_2$	0	0	0	0	10	9
$CNO \rightarrow N_2$	0	14	0	6	5	0
$CN_3O \rightarrow N_2$	0	5	6	7	3	13
$N_2O \rightarrow N_2$	54	42	48	36	49	47
$HN_2O \rightarrow N_2$	19	26	32	41	29	36
$CN_2O \rightarrow N_2$	19	28	25	27	27	24
$C_2N_2O_2 \rightarrow N_2$	19	13	17	19	17	17
$CN_2O_2 \rightarrow N_2$	17	11	12	9	8	12
$N \rightarrow N_2$	6	10	10	0	8	8
$N_2H \rightarrow N_2$	8	19	21	28	31	37
$NH \rightarrow N_2$	0	0	0	11	5	17
N_2 generation	142	168	171	184	205	220

Regarding NO removal by NH_3, the NO abatement with NH_3 increases with R rising mostly through the $NH_3 \rightarrow H_2N_2O$, as shown in Table 4.9. The conversion of NH to HN_2O and HN_2 stays nearly constant under different R values. Furthermore, when the NH_3/NO ratio grows, the contribution of NH_2 to NO abatement (mostly via $NH_2 \rightarrow H_2N_2O$) decreases initially and then increases when R exceeds 1.4. In terms of N_2 production, high R values encourage the N_2

formation from N_2H_3, N_2H, and N_2H_2 to N_2. NH_3/NO ratios have insignificant effect on the conversion of HN_2O to N_2 with R = 1.0-1.8, however, improve $HN_2O \rightarrow N_2$ when R = 2.0. With increasing R, the NF of $N_2O \rightarrow N_2$ production drops marginally. Furthermore, the NF of pathway $H_2N_2O \rightarrow N_2$ reduces when R increases from 1.0 to 1.2, but increases when R exceeds 1.2.

Table 4.9 Net flux (NF) of key channels linked with NO and N_2 during NO removal with NH_3 at R = 1.0-2.0.

Pathways	1.0	1.2	1.4	1.6	1.8	2.0
$NH_3 \rightarrow HN_2O$	7	10	11	10	4	12
$NH_3 \rightarrow H_2N_2O$	18	27	48	45	34	66
$NH_2 \rightarrow H_2N_2O$	60	44	40	64	75	78
$NH_2 \rightarrow HN_2O$	0	8	12	8	12	2
$NH \rightarrow HN_2O$	34	37	36	30	28	24
$NH \rightarrow HN_2$	0	0	0	4	10	10
NO consumption	119	126	147	161	163	192
$HN_2O \rightarrow N_2$	53	53	53	54	50	66
$N_2H \rightarrow N_2$	58	91	98	137	144	145
$N_2H_2 \rightarrow N_2$	18	29	34	55	58	65
$N_2O \rightarrow N_2$	15	23	13	11	20	6
$H_2N_2O \rightarrow N_2$	18	0	8	6	14	22
$N_2H_3 \rightarrow N_2$	0	0	0	0	14	15
N_2 generation	162	196	206	263	300	319

To sum up, increasing the HCN/NO and NH_3/NO ratios can improve NO reduction behaviours, however the reduction efficiency peaks at R = 1.6. In detail, the promotion of NO reduction performance is by the reactions between NH radical with NO molecules, finally generating N_2. Furthermore, high R values stimulate N_2 production by introducing additional routes $HCN \rightarrow CN \rightarrow CHN_2O \rightarrow N_2$ and $HCN \rightarrow CN \rightarrow C_2N_2O \rightarrow CN_2 \rightarrow CN_3O \rightarrow N_2$. In addition, higher HCN/NO ratios promote "self-consumption" of HCN for N_2 synthesis through $HCN \rightarrow CNO \rightarrow C_2N_2O_2/CN_2O \rightarrow N_2$ and $HCN \rightarrow CN \rightarrow C_2N_2O \rightarrow CN_2 \rightarrow C_2N_3O \rightarrow N_2$. In terms of NO removal by NH_3, increasing the number of NH_3 molecules improves NO reduction performance mostly by boosting the interaction of NO molecules with NH_3 and NH_2 to form H_2N_2O, which eventually converts to N_2.

Besides, high *R* values benefit the "self-consumption" effect of NH_3 by the conversion of N_2H_3 and N_2H_2 to N_2, which is generated by the reactions of NH_3, NH_2, and NH.

4.2.3 Discussion

When NO is removed with HCN, O_2 promotes the formation of key intermediates (CNO and NH), which can then combine with NO to generate N_2. However, O_2 also has a negative impact on NO reduction due to NO generation from the oxidation of HCN, which accounts for the maximum N_2 formation in the λ = 0.6 condition.

O_2 molecules only present detrimental impacts on its behaviour when NO is reduced by NH_3. Unlike HCN, species NH_3, NH_2, and NH may combine with NO molecules to produce N_2 without first producing oxygen-containing intermediates. O_2 molecules, on the other hand, may mix with NHi species to generate macromolecules such as $N_2H_6O_2$, $N_3H_9O_4$, $N_4H_{12}O_8$, $N_5H_{15}O_8$, and $N_6H_{18}O_8$. That hinders the combination between NHi and NO molecules, explaining why O_2 has a detrimental impact on NO reduction.

Given that coal pyrolysis gas contains both HCN and NH_3, the ideal λ is about 0.6 depending on the percentage of HCN and NH_3, which is lower than the value (approximately 0.9) in earlier experimental research [5]. This might be due to the inhibition of nitrogen-free species on the NO reduction process in fuel-rich circumstances. Extended simulations with CH_4, CO, and H_2 additives during NO removal using HCN and NH_3 are necessary to gain a comprehensive understanding of the impacts of diverse nitrogen-free species (CH_4, CO, and H_2) on NO removal.

The "self-consumption" phenomenon happens in both HCN and NH_3 situations during the NO elimination procedure. That is, N_2 is formed from HCN or NH_3 molecules without combining NO molecules, resulting in inadequate reduction agents. Furthermore, oxidation of HCN generating NO is found in NO removal by HCN conditions, resulting in a decrease in NO reduction behaviours. As a result, increasing HCN/NO and NH_3/NO ratios can improve reduction behaviours, which reaches its peak when *R* is 1.6 in both HCN and NH_3 situations. In practise, the ratios of nitrogen-containing species to NO may be adjusted by controlling operational factors like temperature [7], pressure [94] and water

content [117] during coal pyrolysis.

4.3 Effects of Nitrogen-free Species (CH_4, CO and H_2) on NO Removal Performance by HCN and NH_3

4.3.1 Simulation Details

The reactant equivalence ratios are computed according to Equations (4.1) and (4.2). Each system contains 120NO and 120HCN or NH_3 to investigate the NO removal process by HCN or NH_3. To investigate the impact of nitrogen-free species on NO abatement by HCN and NH_3, simulated systems with CH_4, CO and H_2 addition are used under molar ratios of 0.5, 1.0, and 1.5 conditions. The density of all systems is kept constant at 0.15 g/cm^3.

Each system goes through 20 ps at 40 K of equilibration and energy minimization to optimize the starting configuration before "production simulation". The systems are then heated to 3000 K and temperatures are held constant. The time step and overall simulation time are chosen as 0.1 fs and 1000 ps, respectively, for all simulations.

4.3.2 Results

4.3.2.1 Nitrogen Distribution in Products during NO Reduction by HCN and NH_3 under Different Additives

Figure 4.9 presents the nitrogen distribution during NO abatement using HCN and NH_3 with various additions. Overall, nitrogen-free additions have a considerable impact on the yields of the key nitrogenous products (NO, N_2, HCN/CN, $C_xN_yO_z$ and NH_i).

As shown in Figures 4.9a and 4.9b, CH_4 promotes NO reduction in both HCN and NH_3 conditions. Besides, the conversion of NO to N_2 production is suppressed by CH_4 molecules in NO abatement by HCN and NH_3 cases. CH_4 enhances the fraction of HCN/CN, NH_i, and $C_xN_yO_z$ in both HCN and NH_3 conditions.

Figures 4.9c and 4.9d show how CO affects nitrogen distribution when NO is reduced by HCN and NH_3. The CO influence addition on NO consumption in HCN instances is negligible, whereas CO marginally inhibits NO consumption when NO is removed by NH_3. CO addition suppresses N_2 formation in both HCN and NH_3 conditions. The proportion of HCN/CN increases with CO addition in NO

removal by HCN cases. As shown in Figure 4.9c, the values of $C_xN_yO_z$ and NH_i are nearly identical. CO addition enhances the generation of $C_xN_yO_z$ and HCN/CN during NO reduction with NH_3, but has insignificant effect on NH_i generation.

Regarding the impacts of H_2 on NO removal behaviours, as shown in Figures 4.9e and 4.9f, H_2 considerably enhances NO consumption and N_2 generation in all cases. In the instance of NO removal by HCN, the addition of H_2 raises the percentages of HCN/CN and NH_i, while the $C_xN_yO_z$ content remains constant during H_2/NO values ranging from 0 to 5. NH_i concentration increases with H_2 addition when NO is removed by NH_3.

To summarize, the foregoing results show that the addition of nitrogen-free species can change the nitrogen distribution in products when NO is removed by HCN and NH_3. The channels are examined in order to further investigate mechanisms subsequently.

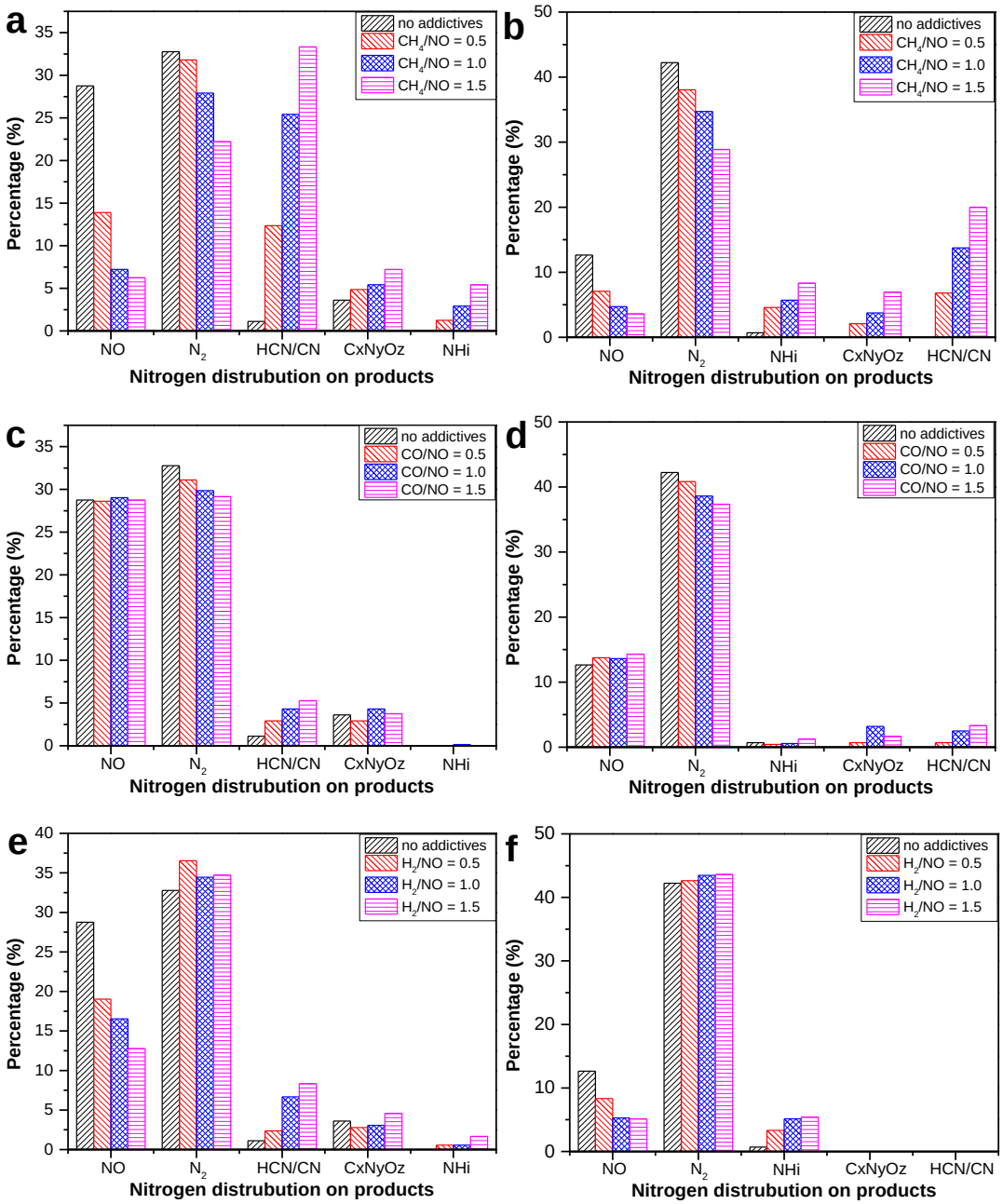

Figure 4.9 Nitrogen distribution on products during NO reduction process. (a) HCN with CH_4 addition. (b) NH_3 with CH_4 addition. (c) HCN with CO addition. (d) NH_3 with CO addition. (e) HCN with H_2 addition. (f) NH_3 with H_2 addition. $C_xN_yO_z$ present species containing C, N and O elements. NH_i is an umbrella term of NH_3, NH_2 and NH.

4.3.2.2 Effects of CH_4 Addition on Mechanisms of NO Abatement by HCN and NH_3

Figure 4.10a presents the reaction pathways of NO removal by HCN in the presence of CH_4 molecules. N, CNO, NH, and NH_2 are main intermediates formed during the oxidation and breakdown of HCN, which can eventually combine with NO molecules to generate N_2. The conversion from N to N_2 occurs

when the CH_4/NO molar ratios are 0 and 0.5. CNO participates in interactions with NO to produce CN_2O_2 and N_2O, and finally N_2. CNO → CN_2O_2 occurs in all conditions, however CNO → N_2O occurs only when the CH_4/NO molar ratios are 0 and 0.5. N_2 is formed from CNO with CH_4/NO ratio of 0. CH_4 presents insignificant influence on N_2 formation from processes in which NH combines with NO to produce HN_2O and N_2H. CH_4 enhances the formation of NH_2 intermediates in all cases. NH_2 consumes NO molecules when CH_4/NO molar ratios are 0.5 and 1.0.

Figure 4.10b shows that in NO reduction with NH_3 conditions, NH_3, NH_2, and NH are key species to consume NO forming intermediates such as H_2N_2O, HN_2O, and N_2H, which eventually convert to N_2. CH_4 has little effect on NO consumption via NH_2 → H_2N_2O and NH → HN_2O. NH_3 → H_2N_2O and NH_3 →HN_2O are not found in CH_4/NO ratio of 1.5 conditions. The conversion from NH to N_2H happens with CH_4/NO of 0.5. In all circumstances, the key precursors for N_2 generation are N_2H_2, N_2H, and HN_2O, however conversion from H_2N_2O to N_2 is not found with CH_4/NO ratio of 0.5. In addition, N_2H_2 and a portion of N_2H can be created directly from NH_i (NH_3, NH_2, and NH) species without NO reduction.

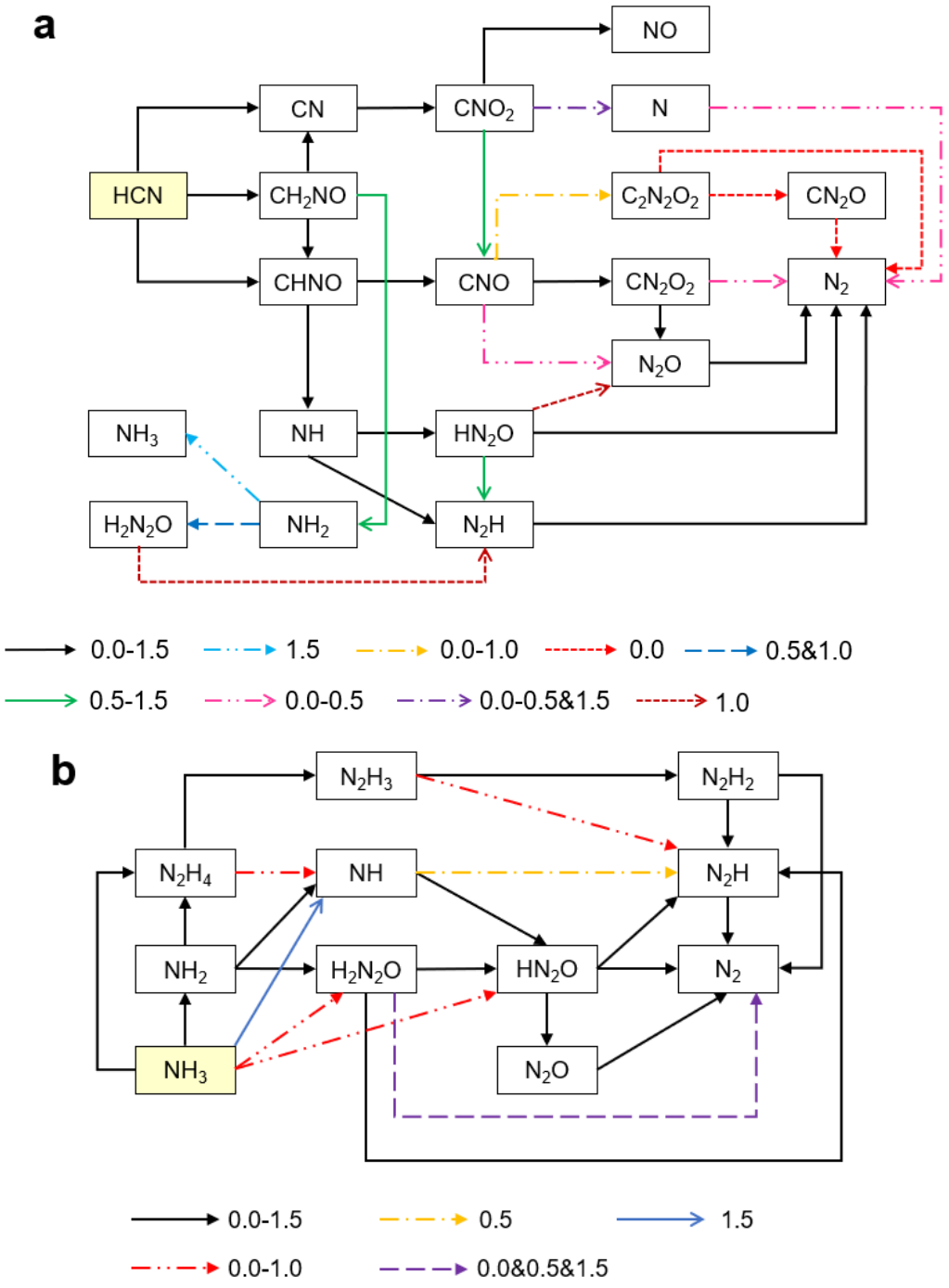

Figure 4.10 Reaction pathways of NO abatement by (a) HCN and (b) NH_3 with CH_4 addition. The numbers in the figure are the molar ratios of CH_4 to NO. HCN and NH_3 are the starting molecules in yellow boxes.

Table 4.10 shows the NF analysis of the primary pathways that is adopted to determine how CH_4 influences the NO removal behaviours with HCN and NH_3. CH_4 suppresses N_2 generation from reactions between CNO and NO or CNO via pathways CNO → CN_2O_2/N_2O → N_2 and CNO → $C_2N_2O_2$/CN_2O → N_2 when NO is removed with HCN. Under different CH_4/NO values, the NF of NH → HN_2O/N_2H

→ N_2 is nearly constant. In addition, the NF of CN → CNO_2 → NO and CN → CNO_2 → N → N_2 declines with CH_4 addition. In general, CH_4 inhibits the conversion of HCN to NO through CN_2O. Because of the inhibitory effect of CH_4 on NO formation, the number of NO consumption nearly remains constant under varying CH_4/NO ratios. Besides, the NO removal by NH and NH_3 is inhibited in NH_3 cases with CH_4 addition rising. The NF of NH_2 → H_2N_2O is at its lowest in the CH_4/NO ratio of 1 case. In terms of N_2 production, the contribution of HN_2O, N_2O, and H_2N_2O reduces when CH_4 is added; nevertheless, the NFs of N_2H → N_2 and N_2H_2 → N_2 fluctuate as CH_4/NO ratio rises. To summarise, the presence of CH_4 molecules inhibits the behaviours of NH_3 and HCN in converting NO to N_2. This is consistent with the variations in N_2 production in Figures 4.9a and 4.9b; the chemical effects of CH_4 on nitrogen-containing species are studied to determine the N distribution changes in NO, HCN/CN, $C_xH_yO_z$, and NH_i subsequently.

Table 4.10 Net flux (NF) of key channels for NO consumption and N_2 generation in the NO abatement process by HCN and NH_3 with varying CH_4/NO molar ratios.

NO reduction with HCN	0	0.5	1	1.5	NO reduction with NH_3	0	0.5	1	1.5
CNO → CN_2O_2	46	9	14	14	NH → HN_2O	34	27	18	15
CNO → N_2O	18	11	0	0	NH → N_2H	0	10	0	0
NH_2 → H_2N_2O	0	10	19	0	NH_3 → HN_2O	7	9	6	0
NH → HN_2O	17	17	9	22	NH_3 → H_2N_2O	18	12	10	0
NH → N_2H	11	9	9	8	NH_2 → H_2N_2O	60	36	30	59
N → N_2	6	5	0	0	NO consumption	119	94	64	74
NO consumption	98	61	51	44	HN_2O → N_2	53	45	37	31
CNO_2 → NO	60	28	22	7	N_2H → N_2	58	67	64	59
Net NO consumption	38	33	29	37	N_2H_2 → N_2	18	22	15	19
N_2O → N_2	54	33	16	12	N_2O → N_2	15	14	14	5
HN_2O → N_2	19	24	15	17	H_2N_2O → N_2	18	3	0	6
N_2H → N_2	8	11	23	17	N_2 formation	162	151	130	120
CN_2O → N_2	19	0	0	0					
$C_2N_2O_2$ → N_2	19	0	0	0					
CN_2O_2 → N_2	17	6	0	0					
N → N_2	6	5	0	0					
N_2 formation	88	79	54	46					

In NO removal by HCN cases, the addition of CH_4 enhances NO

consumption by producing HNO via R4.38 and R4.39.

$CH_4 + NO \rightarrow CH_3 + HNO$ (R4.38)

$C_aH_bN_cO_d + NO \rightarrow C_aH_{b-1}N_cO_d + HNO$ (R4.39)

HNO improves NH formation and CH_4 enhances the formation of NH_i through the conversion from CH_2NO to NH_2.

CH_3 has the abilities to react with CNO forming C_2H_3NO (R4.40), which can then be transformed to HCN/CN through the $C_2H_3NO \rightarrow CH_2N/CH_3N \rightarrow HCN/CN$ route. The addition of CH_4 lowers the quantity of OH, O, and O_2 by the formation of CO, hence reducing the consumption of HCN and CN via the $CN \rightarrow CNO_2$, $HCN \rightarrow CHNO$, and $HCN \rightarrow CH_2NO$ pathways. As a result, CH_4 molecules enhance the amounts of HCN and CN at the end of reduction processes. Furthermore, CH_4 enhances the reactions between hydrocarbons (C_xH_y) and nitrogen-containing species such as NO, HNO, and HCN/CN, raising the number of $C_xN_yO_z$ in products.

$CH_3 + CNO \rightarrow C_2H_3NO$ (R4.40)

$CH_3 + NH_2 \rightarrow CH_5N$ (R4.41)

When NO is removed with NH_3 molecules, CH_5N is produced by R4.40 in CH_4-containing cases, which can eventually be transformed to HCN and CN. Additionally, increased HNO production leads to the enhancement of NO consumption. HNO also limits the consumption of NH_i, lowering NO reduction behaviours. The amount of $C_xN_yO_z$ in products increases mainly due to the reactions between hydrocarbons (C_xH_y) and nitrogenous intermediates.

4.3.2.3 Effects of CO Addition on Mechanisms of NO Abatement by HCN and NH_3

The addition of CO molecules alters the chemical pathways in NO abatement by both HCN and NH_3 as shown in Figure 4.11. When NO is removed by HCN with CO addition, the routes $CN \rightarrow C_2NO_2 \rightarrow CNO$ and $HN_2O \rightarrow N_2H$ are discovered. $CNO \rightarrow N_2O$ happens when CO/NO ratios are 0, 0.5 and 1.5. $CHNO \rightarrow CHN_2O_2$ is observed in the CO/NO ratio of 0.5 case. NO consumption through $NH \rightarrow N_2H$ occurs when CO/NO ratio ranges from 0 and 1.5. N_2 production from interactions between N and NO is not identified in CO addition conditions, As to CO influence on the NO removal process by NH_3, CO suppresses the channels $N_2H_3 \rightarrow N_2H$ and $N_2H_2 \rightarrow N_2H$, which occur only when the molar ratio CO/NO is less than 1.5. The pathway $H_2N_2O \rightarrow N_2H$ occurs when the molar ratio CO/NO

ranges from 0.5 to 1.0. There is no N_2 production from H_2N_2O in the CO/NO ratio of 1.0 case.

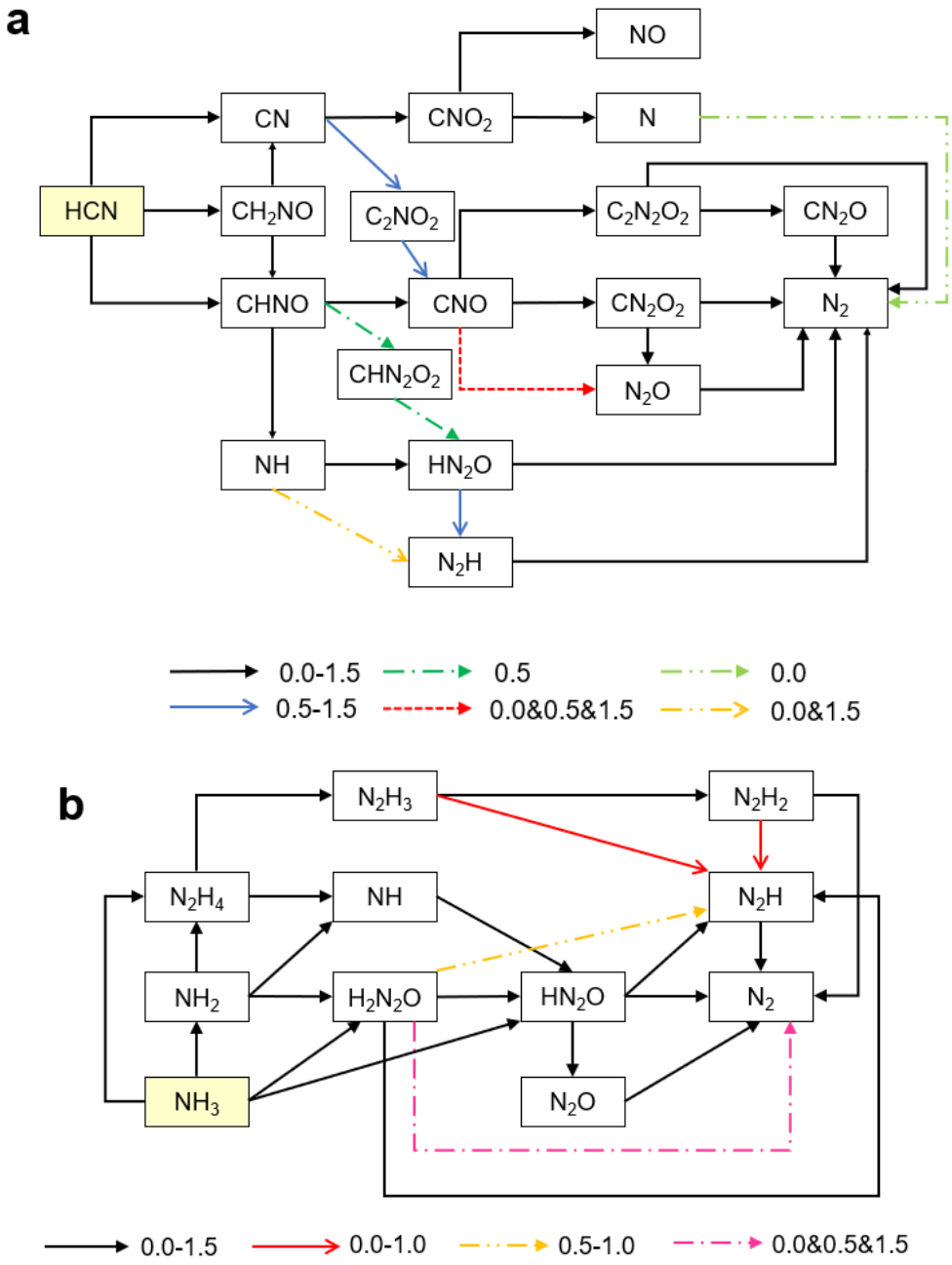

Figure 4.11 Reaction pathways of NO abatement by (a) HCN and (b) NH_3 with CO addition. The numbers in legends are the molar ratios of CO to NO. Boxes in yellow indicate species at the start of the reactions.

The effect of CO on the number of NO and N_2 is further demonstrated through NF analysis of NO and N_2 production reactions. CO reacts with oxygen-containing species (such as O_2, O, HO) to produce CO_2 when NO is removed by

HCN. CO_2 enhances the pathway CN → C_2NO_2 → CNO through reactions R4.41 and R4.42.

$$CN + CO_2 \rightarrow C_2NO_2 \quad (R4.41)$$

$$C_2NO_2 \rightarrow CNO + CO \quad (R4.42)$$

The reduction of O_2 prevents the pathway CN → CNO_2. As illustrated in Table 4.11, the NFs of CNO_2 → NO and CNO_2 → N → N_2 decrease with CO/NO ratios. CO inhibits the combination of CNO and NO, although it has a negligible effect on NO consumption by the NH radical. In total, the NF of net NO consumption fluctuates under varying conditions, which explains the NO trend in Figure 4.9c. When it comes to N_2 production, the NFs of $C_2N_2O_2$ → N_2 and CN_2O → N_2 reduce slightly with CO addition. CO weakens N_2 production through CNO → CN_2O_2/N_2O → N_2. CO speeds up the pathway N_2H → N_2, but slows down the conversion from HN_2O to N_2. The reactions between CO and oxygen-containing intermediates weaken the conversion of HCN/CN to species such as CNO_2, CH_2NO, and CHNO. CO has an insignificant influence on $C_xN_yO_z$ and NH_i generation and consumption, and the $C_xN_yO_z$ and NH_i concentrations are nearly constant in all circumstances.

In NO removal by NH_3 cases, CO reacts with NH_2 to generate CH_2NO, which is then transformed to CNO and CN (R4.43-R4.47). Thus, the concentrations of $C_xN_yO_z$ and HCN/CN rise.

$$CO + NH_2 \rightarrow CH_2NO \quad (R4.43)$$

$$CH_2NO \rightarrow CNO + H_2 \quad (R4.44)$$

$$CH_2NO \rightarrow CHNO + H \quad (R4.45)$$

$$CHNO \rightarrow CN + HO \quad (R4.46)$$

$$CNO + CO \rightarrow CO_2 + CN \quad (R4.47)$$

The capacity of $C_xN_yO_z$ to convert NO to N_2 is much lower than that of NH_i species, resulting in a fall in NO reduction performance in CO addition conditions. As indicated in Table 4.11, this finding accords with that the NFs of NO consumption and N_2 generation decreasing in CO addition situations. CO, in detail, has insignificant effect on NO consumption by NH_3 via channels NH_3 → HN_2O and NH_3 → H_2N_2O. As molar ratio CO/NO increases, the conversion of NH to HN_2O is weakened. The NF of NH_2 → N_2 rises first and subsequently falls, with the highest NF occurring at the CO/NO of 0.5 case. When it comes to the production of N_2, high CO addition inhibits the pathways HN_2O → N_2H and H_2N_2O → N_2. The effects of CO on the conversion from N_2H_2 to N_2 and N_2O to N_2 are insignificant.

Table 4.11 Net flux (NF) of key channels for NO consumption and N_2 generation in the NO abatement by HCN and NH_3 with varying molar ratios of CO to NO.

NO reduction with HCN	0	0.5	1	1.5	NO reduction with NH_3	0	0.5	1	1.5
CNO → CN_2O_2	46	36	43	37	NH → HN_2O	34	29	22	23
CNO → N_2O	18	13	0	14	NH_3 → HN_2O	7	6	5	3
CHNO → CHN_2O_2	0	11	0	0	NH_3 → H_2N_2O	18	11	18	14
N → N_2	6	0	0	0	NH_2 → H_2N_2O	60	71	29	39
NH → HN_2O	17	23	27	18	NO consumption	119	116	74	79
NH → N_2H	11	0	0	7	HN_2O → N_2	53	49	34	28
NO consumption	98	83	70	76	N_2H → N_2	58	60	48	45
CNO_2 → NO	60	51	39	32	N_2H_2 → N_2	18	17	18	16
Net NO consumption	38	32	31	44	N_2O → N_2	15	11	19	18
N_2O → N_2	54	39	30	24	H_2N_2O → N_2	18	7	0	8
CN_2O → N_2	19	19	18	16	N_2 generation	162	144	119	115
$C_2N_2O_2$ → N_2	19	13	13	16					
CN_2O_2 → N_2	17	15	15	14					
N → N_2	6	0	0	0					
HN_2O → N_2	19	14	16	15					
N_2H → N_2	8	11	17	19					
N_2 formation	142	111	109	104					

4.3.2.4 Effects of H_2 Addition on Mechanisms of NO Reduction by HCN and NH_3

The channels of NO abatement by HCN and NH_3 with H_2 molecules are shown in Figure 4.12. The presence of H_2 facilitates the transformation of NH_2 into H_2N_2O, NH into N_2, and HN_2O into N_2H. In circumstances where H_2/NO ratios are 0 and 1.5, respectively, N → N_2 and H_2N_2O → HN_2O are found. The conversions from NH to N_2H and $C_2N_2O_2$ to N_2 take place with the H_2/NO values ranging from 0 to 1.0. The pathway NH_2 → HN_2O is shown in the NO reduction by NH_3 conditions with H_2/NO ratio ranging from 0.5 to 1.0. The conversion from NH_3 to HN_2O is not observed in the H_2/NO ratio of 0.5 case. N_2 is produced from N_2O when H_2/NO ratios are 0.0 to 1.0.

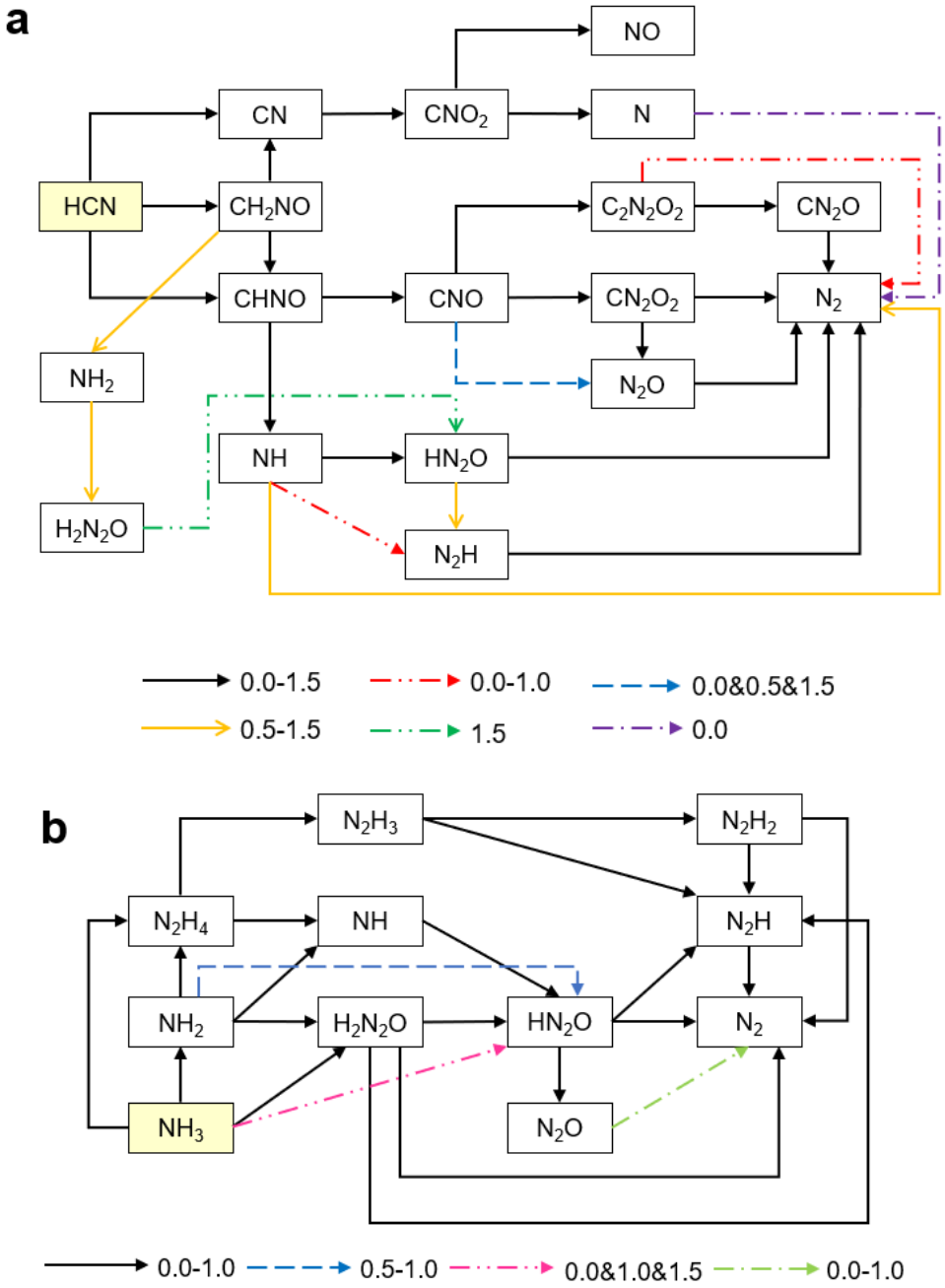

Figure 4.12 Reaction pathways of NO abatement by (a) HCN and (b) NH_3 with H_2 addition. The numbers in legends are the molar ratios of H_2 to NO. Boxes in yellow indicate species at the start of the reactions.

Table 4.12 presents the NF of the primary routes connected to NO consumption and N_2 production, which is adopt to further account for changes in nitrogen-containing products with H_2 addition during NO removal process. H_2 decreases the NF of CNO → CN_2O_2/N_2O and N → N_2 in NO reduction with HCN conditions, but it somewhat encourages NO removal by the NH radical and the generation of HN_2O, N_2, and N_2H. H_2 molecules benefit the channel CH_2NO →

$NH_2 \rightarrow H_2N_2O$. In terms of NO production, the channel $CN \rightarrow CNO_2 \rightarrow NO$ is markedly inhibited by the presence of H_2. Additionally, the contribution of the CNO radical to N_2 generation through $CNO \rightarrow C_2N_2O_2/CN_2O/CN_2O_2/N_2O \rightarrow N_2$ reduces with the presence of H_2. H_2 addition promotes N_2 formation from the NH radical through $NH \rightarrow N_2$, $NH \rightarrow HN_2O/N_2H \rightarrow N_2$. In NO removal by NH_3 cases, the NF of NO consumption rises significantly with the addition of H_2, whereas the conversion from NH and NH_2 to N_2 decreases with the addition of H_2 molecules. In addition, H_2 encourages the conversion of N_2H_2 to N_2, but has insignificant effect on N_2 formation from HN_2O and N_2H. H_2 molecules inhibit the conversion from H_2N_2O to N_2. As to the channel $N_2O \rightarrow N_2$, the NF almost stays the same across the range of H_2/NO = 0.0 to 1.0, but it drops to zero in the case of 1.5. The NO and N_2 concentration on the products in Figures 4.9e and 4.9f are discordant with the overall NF changes of NO consumption and N_2 generation in both the HCN and NH_3 conditions. The chemical reactions of H_2 connected with NO and N_2 are investigated in order to explain this phenomenon.

Table 4.12 Net flux (NF) of key channels for NO consumption and N_2 generation during NO abatement with HCN and NH_3 with varying molar ratios of H_2 to NO.

NO reduction by HCN	0	0.5	1	1.5	NO reduction by NH_3	0	0.5	1	1.5
$CNO \rightarrow CN_2O_2$	46	51	31	19	$NH \rightarrow HN_2O$	34	22	23	25
$CNO \rightarrow N_2O$	18	11	0	7	$NH_2 \rightarrow HN_2O$	0	11	8	2
$NH \rightarrow HN_2O$	17	26	25	27	$NH_2 \rightarrow H_2N_2O$	60	64	54	48
$NH \rightarrow N_2$	0	5	7	7	$NH_3 \rightarrow HN_2O$	7	0	12	6
$NH \rightarrow N_2H$	11	7	6	0	$NH_3 \rightarrow H_2N_2O$	18	26	18	58
$NH_2 \rightarrow H_2N_2O$	0	13	7	21	NO consumption	119	123	115	139
$N \rightarrow N_2$	6	0	0	0	$HN_2O \rightarrow N_2$	53	58	47	53
NO consumption	98	113	76	81	$N_2H \rightarrow N_2$	58	74	50	59
$CNO_2 \rightarrow NO$	60	29	14	2	$N_2H_2 \rightarrow N_2$	18	22	25	31
Net NO consumption	38	84	62	79	$N_2O \rightarrow N_2$	15	16	16	0
$HN_2O \rightarrow N_2$	19	32	25	36	$H_2N_2O \rightarrow N_2$	18	3	8	7
$NH \rightarrow N_2$	0	5	7	7	N_2 formation	162	173	146	150
$CN_2O \rightarrow N_2$	19	23	15	9					
$C_2N_2O_2 \rightarrow N_2$	19	11	11	0					
$CN_2O_2 \rightarrow N_2$	17	13	4	4					
$N_2O \rightarrow N_2$	54	39	32	34					
$N \rightarrow N_2$	6	0	0	0					
$N_2H \rightarrow N_2$	8	21	26	33					
N_2 formation	142	144	120	123					

H_2 molecules promote the formation of H radical, which improves the process of converting NO to HNO via R4.48. In both the NO removal with HCN and NH_3 conditions, that is the primary cause of the drop in NO content in products.

$$H + NO \rightarrow HNO \quad (R4.48)$$

Additionally, H_2 molecules promote the generation of HN_2O_2, which will ultimately form N_2 (R4.49-R4.51). These reactions explain how H_2 promotes N_2 generation during the NO reduction process.

$$N_2O_2 + H \rightarrow HN_2O_2 \quad (R4.49)$$

$$HNO + NO \rightarrow HN_2O_2 \quad (R4.50)$$

$$HN_2O_2 \rightarrow N_2 + O + HO \quad (R4.51)$$

HNO forms lower the formation of N_2 and NH_i as it is less reactive with nitrogen-containing species than NO. H_2 reduces the content of active species (like OH, O, and O_2) through the promotion of H_2O formation, which prevents the pathway HCN/CN → CNO_2/CHNO/CH_2NO. In circumstances when NO is

reduced by HCN and NH_3, the rise of HNO with H_2 addition also helps the generation of NH.

4.3.3 Discussion

In this section, ReaxFF MD is adopted to examine the impact of CH_4, CO, and H_2 on the effectiveness of HCN and NH_3 in reducing NO. The distribution of N element in products may be altered by changing the concentration of various nitrogen-free species, which shows that altering the nitrogen-free species in coal pyrolysis gas may be an effective strategy to enhance NO reduction efficiency.

In terms of NO reduction, the modelling results as well as findings from earlier research indicate that hydrocarbons perform better in NO decrease than H_2 and CO [196, 197]. The primary explanation is that the reactive H radicals in CH_4 can accelerate the transformation of NO into HNO. The effects of CO on NO content in products are negligible. N_2 is adopted as the indicator for NO removal efficiency since the nitrogen-containing intermediates (HCN/CN, NH_i, and $C_xN_yO_z$) in the reburn zone will generate NOx through oxidation process in the burnout zone.

Of the three additives, H_2 performs the best for N_2 production and CH_4 the poorest. The formation of N_2 is inhibited by CO and CH_4, whereas is enhanced by H_2 molecules. Thus, altering operating conditions during the coal pyrolysis process can reduce the CH_4 and CO contents, which can be a useful approach to increase NO reduction efficiency [94, 117]. Additionally, the nitrogen-free species' contribution to N_2 formation is noticeably less than that of the intermediates from HCN and NH_3, which agrees with other experimental findings that nitrogen species dominate the NOx removal behaviours by coal pyrolysis gas [5, 7].

Chapter 5 Assisted Pyridine Combustion

5.1 Pyridine Combustion Assisted by Electric Field

5.1.1 Simulation Details

Table 5.1 displays the initial parameters of the investigated systems. Every system contains 80 pyridine molecules, and the density of each system stays at 0.3 g/cm^3. The following global reaction is used to calculate the equivalency ratio (λ) of pyridine oxidation:

$$C_5H_5N+6.75O_2 \rightarrow 5CO_2+NO+2.5H_2O \quad (5.1)$$

System 1 simulates the pyridine combustion process under stoichiometric conditions (λ =1). Electric strengths ranging from 1 to 7.5 V/nm are applied in +X direction to investigate the effects of EF on pyridine combustion in systems 2-5,. Figure 5.1 displays the specifics of the system setups.

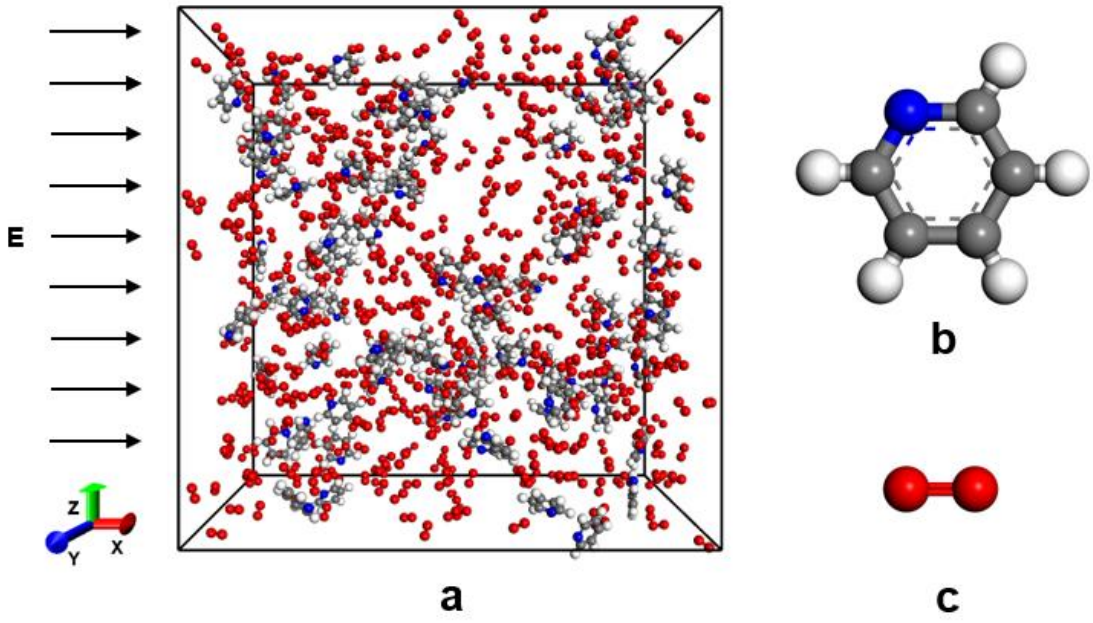

Figure 5.1 Simulated systems for pyridine combustion under different *E* values. (a) pyridine combustion system, (b) pyridine molecules, (c) oxygen molecules. H, C, N and O are represented in white, grey, blue and red, respectively.

Table 5.1 Case set-ups.

System	Number of C_5H_5N molecules	Number of O_2 molecules	E/V·nm^{-1}	Density (g/cm^3)	Box size (nm)
1	80	540	0	0.3	5.07
2	80	540	1	0.3	5.07
3	80	540	2.5	0.3	5.07
4	80	540	5	0.3	5.07
5	80	540	7.5	0.3	5.07

The cutoff and time step were set at 0.3 and 0.1 fs, respectively. First, at a temperature of 500 K for 100 ps, each system performed energy minimization and system equilibration. The system temperatures were then increased to 2600 K with heating rate of 100 K/ps. The system temperatures were then maintained constant after that. The simulation lasted for a total of 1000 ps. All data was logged every 100 fs.

5.1.2 Results

5.1.2.1 Time Evolution of Species Number and Reactants

The impacts of EF on consumption rates of reactants during oxidation are investigated using the temporal evolutions of C_5H_5N and O_2 with E ranging from 0 to 7.5 V/nm. Figures 5.2a and 5.2b shows that EF slows the consumption of C_5H_5N and O_2 at E = 0 to 2.5 V/nm, however, speeds up consumption rates between 2.5 to 7.5 V/nm. The species number in simulated systems with varied E values over 1000 ps is shown in Figures 5.2c and 5.2d. Overall, the number of species initially rises quickly to its highest value and then consistently declines after that. Additionally, when EF strength grows, more species can be generated during pyridine combustion. According to the aforementioned results, the application of EF changes the consumption rates of reactants and the number of species during pyridine combustion, which is consistent with earlier research [153, 199].

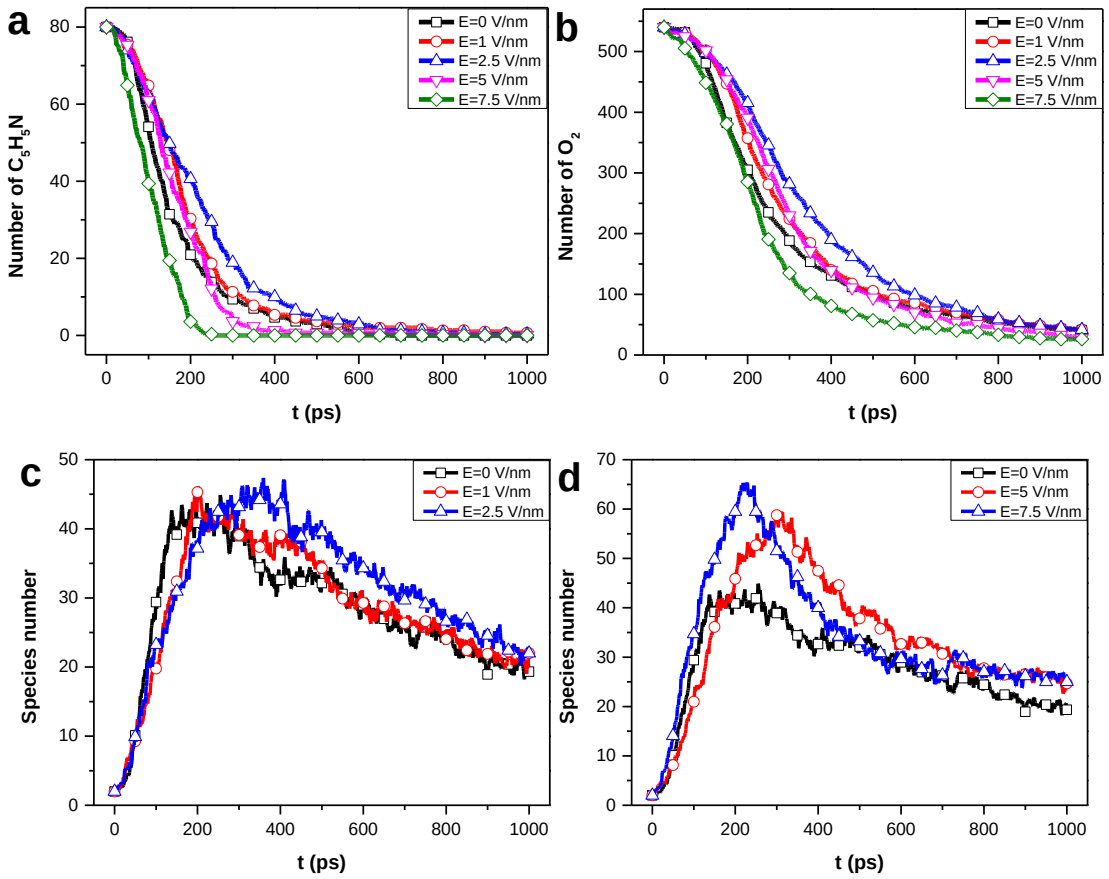

Figure 5.2 Time evolution of species number and reactants. (a) C_5H_5N; (b) O_2; (c) the number of species (E = 0-2.5 V/nm); (d) the number of species (E = 0&5&7.5 V/nm).

5.1.2.2 Influence of Electric Field on Nitrogenous Products (NO, NO_2 and N_2)

The influence of the EF on the production of important nitrogenous compounds is depicted in Figure 5.3. When the E value is between 0 and 7.5 V/nm, the yield of NO exhibits a decreasing trend with increasing EF strength. However, EF always has a negligible impact on the production of NO_2 and N_2 during pyridine combustion. The pattern of NOx (the total of NO and NO_2) fluctuations under varying EF strengths, which is also similar to that of NO since NO outweighs NO_2 in magnitude.

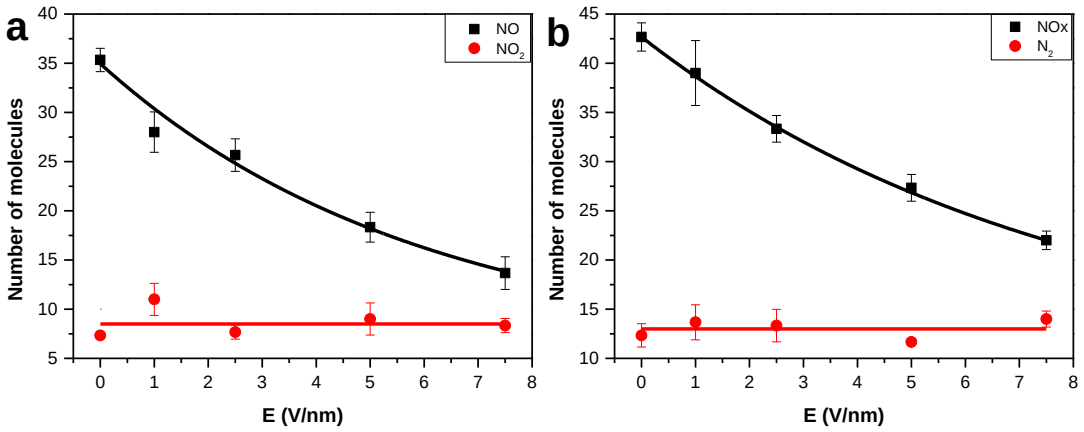

Figure 5.3 Influence of EF on the numbers of main nitrogenous products. (a) NO and NO_2; (b) NOx (NO + NO_2) and N_2.

Transfer pathways of the key nitrogenous intermediates with and without the application of EF were examined in order to explore how the EF alters the formation of important products. In most cases, oxygenation of pyridine molecules begins with the formation of oxygen-containing intermediates (C_5H_5NO, $C_5H_4NO_2$, C_5H_4NO, and $C_5H_3NO_2$). The chain species that result from those intermediates then open rings. The chain then breaks down into HCN, CN, CNO, and HNO, which undergo a series of reactions to transform into the primary products that contain nitrogen. The results on the pyridine oxidation reaction mechanisms are in good accord with earlier studies [193]. This thesis focuses on the chemical channels leading from CN, HCN, HNO, and CNO to important nitrogenous products (NO, NO_2 and N_2).

$C_2N_2O_2$ is a key intermediate for the production of N_2, which is produced by reaction R5.1 (CNO + CNO → $C_2N_2O_2$), as illustrated in Figure 5.4. When *E* values are from 0 to 5 V/nm, N_2 is generated by reactions R5.2 ($C_2N_2O_2$ → CN_2O + CO), R5.3 (CN_2O → N_2 + CO), and R5.4 ($C_2N_2O_2$ → N_2 + 2CO). However, N_2 is produced by the pathways $C_2N_2O_2$ → $C_2HN_2O_3$ → N_2 and CN_2O_2 → CHN_2O_3 → CHN_2O_2 → N_2 when the *E* value is 7.5 V/nm. The oxidation of pyridine leads to NO formation through five channels. Specially, NO is produced via the thermal breakdown of $CHNO_3$, CNO_2 as well as by the oxidation of HNO and CNO_3 with OH, O_2 and HO_2 in all cases. NO is formed by the channel CNO_2 → CNO_4 → NO at *E* = 2.5 and *E* = 7.5 V/nm. The production of HNO_2, HNO_3, NO_2, and CN_2O_2 consumes NO molecules in all cases. In all circumstances, NO_2 is formed by the channels NO → NO_2, NO → HNO_3 → NO_2 and NO → HNO_2 → NO_2 in all cases. The pathway for NO_2 consumption is through NO_2 → CNO_3. CNO/HCN →

$CHNO_2 \rightarrow CNO_2$ is found at E = 5 & 7.5 V/nm cases.

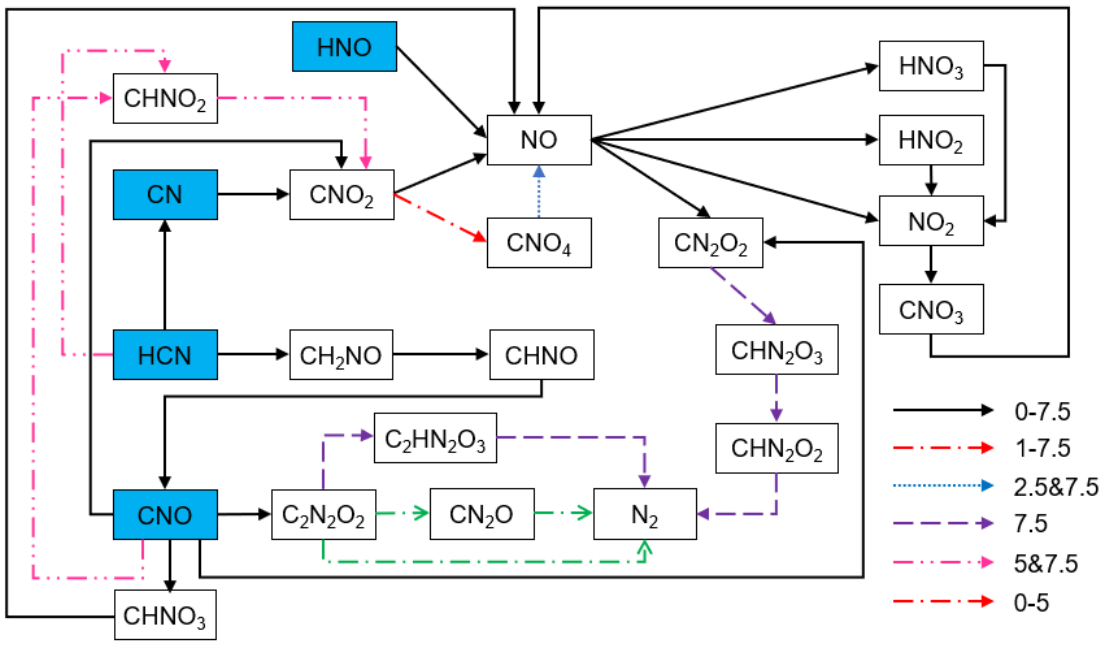

Figure 5.4 Influence of EF on channels of key nitrogenous species. The beginning intermediates are in blue boxes. The numerical values represent EF strengths.

The net flex (NF) values of important channels is listed in Table 5.2 to further show the contributions made by each channel to the formation of NO_2, NO and N_2. Overall, when the EF strength increases, the changes of net NF and yields of the three key products (N_2, NO_2 and NO) coincide, demonstrating the reliability of the NF analysis in a thorough understanding of chemical processes.

In detail, during pyridine combustion, an increase in EF strength prevents NO formation while benefiting NO consumption. Among them, EF has a negligible impact on the conversion from CNO_3 and CNO_2 to NO. The conversion from CNO_2 to NO through R5.5 ($CNO_2 \rightarrow CO + NO$), however, is weaken with E values, which explains the variations in total NO production under different circumstances. Regarding the consumption of NO, EF enhances the conversion of NO to CN_2O_2 and HNO_2, but has insignificant effect on the channels $NO \rightarrow NO_2$ and $NO \rightarrow HNO_3$. Therefore, $NO \rightarrow CN_2O_2$ via R5.6 ($NO + CNO \rightarrow CN_2O_2$) and $NO \rightarrow HNO_2$ through R5.7 ($NO + OH \rightarrow HNO_2$) is main pathway that promotes NO consumption with rising EF strength.

Over the range of E = 0-7.5 V/nm, EF has approximately the same effects on NO_2 consumption and formation. When the EF strength is between 0 and 1

V/nm, the production and consumption of NO_2 rise as the EF strength increases, but when *E* is over 1 V/nm, the conversion decreases with *E* value increasing. These findings suggest that both NO_2 formation and consumption together account for the insignificant impact of EF on net formation of NO_2. As *E* rises, R5.8 ($HNO_3 \rightarrow OH + NO_2$) and R5.9 ($OH + HNO_3 \rightarrow NO_2 + H_2O_2$) that produce NO_2 from HNO_3 are supressed. The rise in EF intensities improves the conversion of HNO_2 to NO_2 with *E* ranging from 0 to 1 V/nm. On the other hand, when *E* is between 1 and 7.5 V/nm, the generation of NO_2 is slightly inhibited by increasing EF strength. Therefore, as EF strength increases, HNO_3 and HNO_2 both contribute to NO_2 formation. The total NF of N_2 formation nearly stays constant throughout a range of EF strengths, despite the EF switching the channels of N_2 generation from CN_2O (R5.3) and $C_2N_2O_2$ (R5.4) to CHN_2O_2 via R5.10 ($CHN_2O_2 \rightarrow N_2 + CHO_2$) and $C_2HN_2O_3$ via R5.11 ($C_2HN_2O_3 \rightarrow N_2 + CHO_2 + CO$).

Table 5.2 Net flux (NF) of channels related to NO_2, NO and N_2 with *E* = 0-7.5 V/nm.

Pathways	0	1	2.5	5	7.5
$CNO_2 \rightarrow NO$	90	86	55	56	33
$HNO \rightarrow NO$	13	7	13	7	-1
$CHNO_3 \rightarrow NO$	14	5	9	22	18
$CNO_3 \rightarrow NO$	12	12	5	8	10
$CNO_4 \rightarrow NO$	0	0	11	0	2
Total NO generation	129	110	93	93	62
$NO \rightarrow CN_2O_2$	8	6	13	14	19
$NO \rightarrow NO_2$	3	4	4	9	-5
$NO \rightarrow HNO_3$	17	7	8	2	13
$NO \rightarrow HNO_2$	2	23	14	33	32
NO consumption	30	40	39	58	59
Net NO generation	99	70	54	35	3
$NO \rightarrow NO_2$	3	4	4	9	-5
$HNO_3 \rightarrow NO_2$	13	5	2	-3	2
$HNO_2 \rightarrow NO_2$	1	17	5	13	12
Total NO_2 generation	17	26	11	19	9
$NO_2 \rightarrow CNO_3$	7	11	4	2	1
Net NO_2 generation	10	15	7	17	8
$CN_2O \rightarrow N_2$	5	10	8	7	0
$C_2N_2O_2 \rightarrow N_2$	7	8	8	3	0
$CHN_2O_2 \rightarrow N_2$	0	0	0	0	7
$C_2HN_2O_3 \rightarrow N_2$	0	0	0	0	6
Total N_2 generation	12	18	16	10	13

5.1.2.3 Influence of Electric Field on Nitrogen-free Products (CO and CO_2)

The numbers of CO_2, CO and unburned carbon ($C_xH_yN_zO_n$) at various EF values are compared in Figures 5.5a–5.5c. When *E* values are from 0 to 7.5 V/nm cases, CO production is limited as the EF strength rises. However, when the EF rises, the amount of CO_2 initially remains the same between *E* = 0 and 2.5 V/nm while exhibiting an increased trend between *E* = 2.5 and 7.5 V/nm. The production of unburned carbon ($C_xH_yN_zO_n$) is also enhanced by a rise in EF. The CO and CO_2 reaction processes at various *E* values during pyridine combustion were investigated to show how the EF impacts the numbers of CO and CO_2.

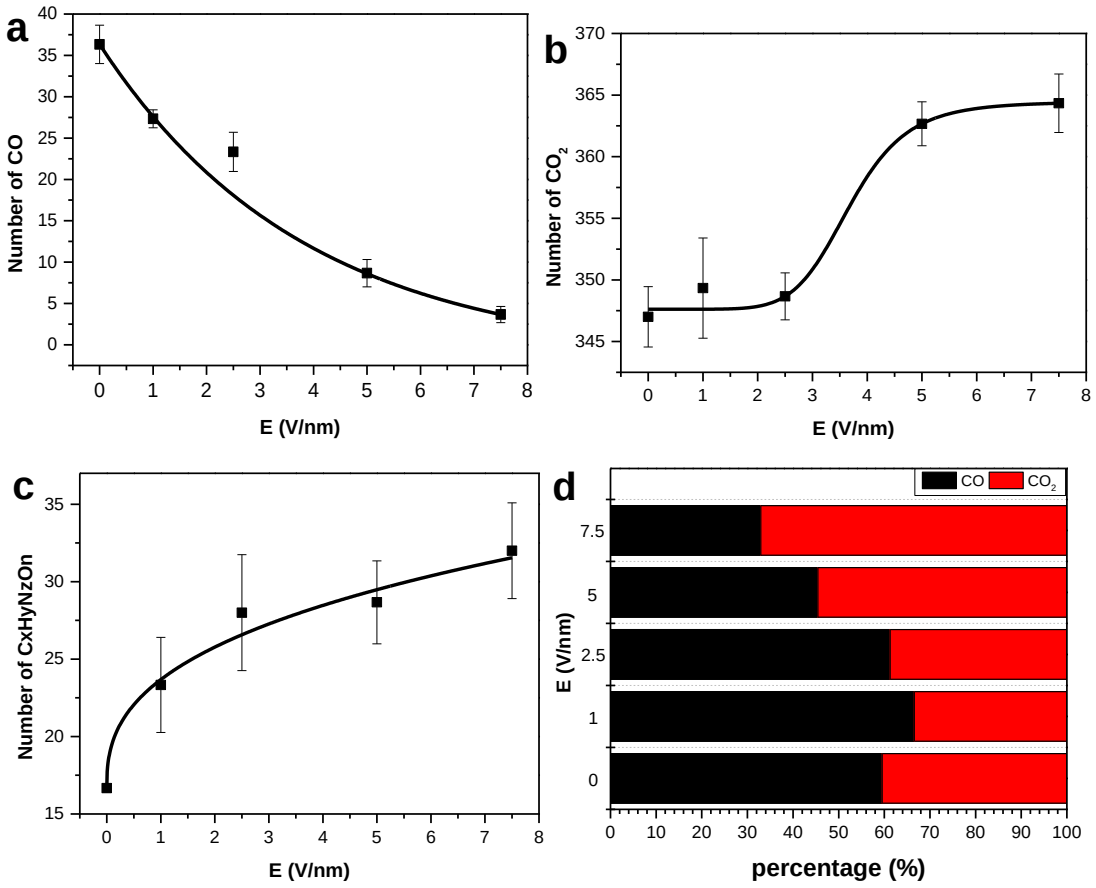

Figure 5.5 Influence of EF on key nitrogen-free products. (a) CO; (b) CO_2; (c) unburn carbons (CxHyNzOn); (d) percentages of CO and CO_2 formed by decomposition of oxygen-containing species.

The formation of CO and CO_2 occurred in two phases during the burning of pyridine. Pyridine molecules are first oxidized to produce intermediates that contain oxygen atoms, and then ring-opening processes create chain species. Through the reactions R5.12 ($C_xH_yN_zO_n \rightarrow C_{x-1}H_yN_zO_{n-2} + CO_2$) and R5.13 ($C_xH_yN_zO_n \rightarrow C_{x-1}H_yN_zO_{n-1} + CO$), those chained intermediates are thermally decomposed to produce CO and CO_2. Figure 5.5d shows that in the conditions of E = 1 & 2.5 V/nm, EF only marginally suppresses the formation of CO_2 resulting from the pyrolysis of oxygen-containing species. The rise in E values, however, dramatically improves R5.12 when the EF strength value exceeds 2.5. Following that, CO is converted to CO_2, which results in the generation of CO_2. Table 5.3 lists the NF of channels linked with CO_2 and CO under various EF strengths.

CO is consumed through pathway CO → CO_2/CO_3/CHO_2/CHO_3. R5.14-R5.22 are key reactions via which EF presents substantial inhibitory effects on the generation of CO_2, CO_3, and CHO_2 from CO.

$HO_2 + CO \rightarrow OH + CO_2$ (R5.14)

$O_2 + CO \rightarrow O + CO_2$ (R5.15)

$NO_2 + CO \rightarrow NO + CO_2$ (R5.16)

$O_2 + HO + CO \rightarrow HO_2 + CO_2$ (R5.17)

$O + CO \rightarrow CO_2$ (R5.18)

$HO + CO \rightarrow H + CO_2$ (R5.19)

$O_2 + CO \rightarrow CO_3$ (R5.20)

$HO + CO \rightarrow CHO_2$ (R5.21)

$H_2O_2 + CO \rightarrow OH + CHO_2$ (R5.22)

Additionally, variations in EF strength have an insignificant impact on the NF of conversion from CO to CHO_3 through R5.23 ($CO + HO_2 \rightarrow CHO_3$). With increasing EF intensities, the total NO consumption presents a declining trend. As previously indicated, EF benefits the generation of unburned carbon in all conditions and reduces the CO_2 produced by the pyrolysis of oxygen-containing species with E = 5 & 7.5 V/nm. Therefore, CO formation during pyridine oxidation is mostly inhibited, which accounts for the drop in CO number with increasing EF intensities.

Table 5.3 also shows that the major precursors to CO_2 formation are CO, CO_3, CO_4, CHO_2, CHO_3 and CHO_4. Specifically, under all conditions, EF intensities enhance the conversion of CO to CO_2 through R5.15–R5.19. Additionally, the NF of conversion from CO_3 to CO_2 presents a parabolic trend as E values rise and reaches its maximal point at E = 1 V/nm mainly through R5.23 ($CO_3 \rightarrow O + CO_2$). The EF enhances the pathway $CHO_2 \rightarrow CO_2$ when E is between 0 and 5 V/nm, while it reduces when E is between 5-7 V/nm. Under various circumstances, the reaction R5.24 ($CHO_2 + O_2 \rightarrow CO_2 + HO_2$) is vital for the pathway $CHO_2 \rightarrow CO_2$. As a result of R5.25 ($CHO_3 \rightarrow CO_2 + HO$) and R5.26 ($CO_4 \rightarrow CO_2 + O_2$), high EF also enhances the production of CO_2 from CHO_3 and CO_4. When the EF intensity is more than 1 V/nm, the NF of the conversion from CHO_4 to CO_2 through R5.27 ($CHO_4 \rightarrow CO_2 + HO_2$) first increases with E ranging from 0 to 1 V/nm, and then drops. Overall, the NF of CO_2 generation is slightly increased between E = 0 and 2.5 V/nm, while it falls between 2.5 and 7.5 V/nm. While CO_2 is produced via the pyrolysis of oxygen-containing species in circumstances where E = 1-2.5 V/nm, the encouraging effect of EF on CO_2 formation leads the nearly constant CO_2 production. The reaction R5.12 plays a dominant position on CO_2 production when E is greater than 2.5 V/nm, leading to

an increase in CO_2 yield.

Table 5.3 Net flux (NF) of channels linked with CO and CO_2 with *E* = 0-7.5 V/nm.

Pathways	0	1	2.5	5	7.5
$CO \rightarrow CO_2$	171	159	142	69	26
$CO \rightarrow CO_3$	259	258	236	213	205
$CO \rightarrow CHO_2$	126	84	84	47	26
$CO \rightarrow CHO_3$	21	21	30	10	10
Total CO consumption	577	522	492	339	267
$CO \rightarrow CO_2$	171	159	142	69	26
$CO_3 \rightarrow CO_2$	163	182	165	138	125
$CHO_2 \rightarrow CO_2$	101	115	127	147	97
$CHO_3 \rightarrow CO_2$	65	66	85	80	116
$CHO_4 \rightarrow CO_2$	10	0	16	26	27
$CO_4 \rightarrow CO_2$	0	0	0	7	20
Total CO_2 consumption	510	522	535	467	411

5.1.3 Discussion

ReaxFF MD is used to provide insight on the impacts of EF on pyridine combustion. Results show that EF contributes positively to the regulation of CO and NO emissions generation during pyridine combustion. In addition, the modifications of the principal products (CO_2, CO, NO_2, NO, and N_2) are explained at the atomic level.

By directing charge carriers to move in particular directions during fuel combustion, the EF can change the interactions between charged species [33]. Additionally, the reactivity of the mixture is increased by the collision of accelerating species with neutral molecules. In this way, EF modifies the fuels' combustion processes.

Additionally, the effectiveness of EF in reducing pollutants at various EF strengths is compared. The data above indicates that in the *E* = 7.5 V/nm case, where the numbers of CO, NO and NOx are lowered by 90%, 61% and 48% respectively, the inhibitory impact of EF on emissions is excellent. The unburned hydrocarbons are additionally encouraged by an increase in EF strength, which lowers combustion efficiency and increases ash formation. As a result, different emission criteria may be met by altering the EF's intensities.

Due to the temporal difference between simulation and experimental

timescales, EF strengths in ReaxFF MD are often several magnitudes higher than those in experiments, which is also corroborated by previous research [200-202]. Because of the expensive computational costs, ReaxFF MD frequently speeds up simulations by using higher temperatures than in experiments, which has been verified to replicate the response processes shown in experiments [94, 154, 183]. This strategy greatly speeds up particle random motion compared to experimentation. As a result, stronger EF intensities are needed to alter particle motion and product yields in MD simulations.

5.2 Pyridine Oxidation with Ozone Addition

5.2.1 Simulation Details

Seven simulated systems are constructed with the number of O_3 addition changing from 0 to 240 in order to study the effects of O_3 addition on pyridine combustion. The density of all systems is 0.3 g/cm^3. The ratio of the number of pyridine, $n(C_5H_5N)$, to the number of ozone, $n(O_3)$, is defined as β to aid in analysis. In all systems, the numbers of O_2 and C_5H_5N are 540 and 80, respectively. The setup details of each system are listed in Table 5.4. Figure 5.6 shows an initial configuration of $C_5H_5N/O_2/O_3$ system.

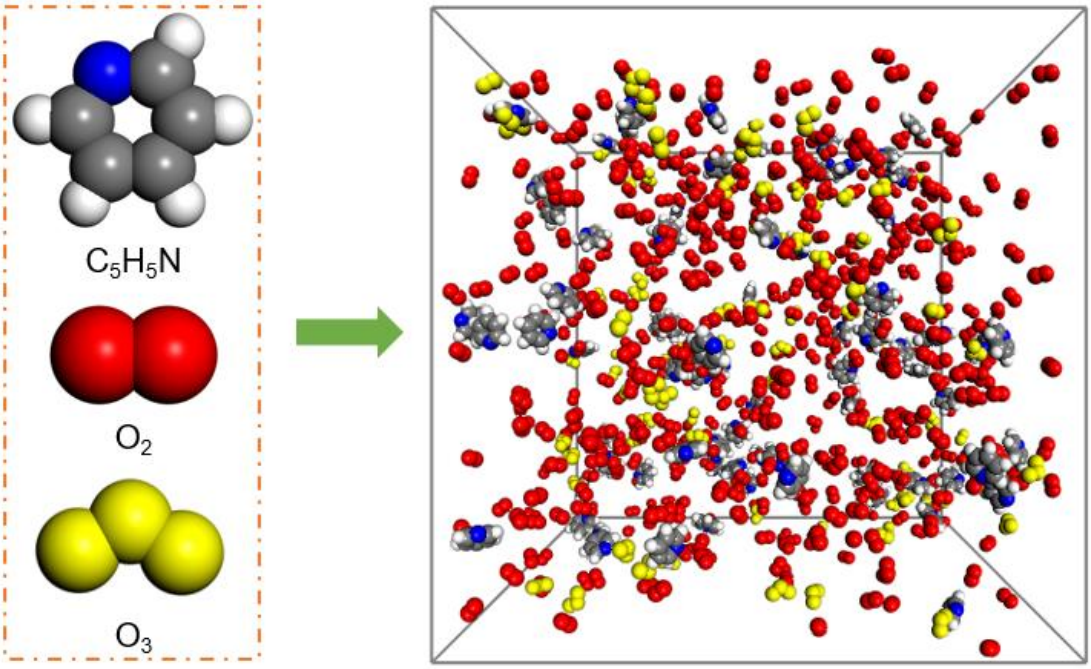

Figure 5.6 Initial configuration of $C_5H_5N/O_2/O_3$ system. Red: O_2. Yellow: O_3. Light grey: H atom. Dark grey: C atom. Blue: N atom.

Table 5.4 Information of modelling systems.

NO.	Number of molecules	β	Box length (nm)
1	$80C_5H_5N/540O_2/0O_3$	0	5.07
2	$80C_5H_5N/540O_2/40O_3$	0.5	5.21
3	$80C_5H_5N/540O_2/80O_3$	1	5.34
4	$80C_5H_5N/540O_2/120O_3$	1.5	5.46
5	$80C_5H_5N/540O_2/160O_3$	2	5.57
6	$80C_5H_5N/540O_2/200O_3$	2.5	5.69
7	$80C_5H_5N/540O_2/240O_3$	3	5.79

The bond order cutoff and timestep are 0.3 and 0.1 fs, respectively. Each system goes through equilibration and energy minimization at 500 K for 100 ps before the reactive simulations to optimise the initial configuration. The reactive temperature is then raised to 2600 K (heating rate: 100 K/ps) and maintained at that level. For each simulation, the simulated time is 1000 ps.

5.2.2 Results

5.2.2.1 Time Evolution of Reactants

Figure 5.7 presents the temporal evolution of the key reactants in β = 0-3. Figures 5.7a and 5.7b show that the consumption rates of C_5H_5N rise as the amount of O_3 addition increases, demonstrating that O_3 has the abilities to accelerate fuel combustion. As shown in Figure 5.7c, in the ozone-free condition, the number of O_2 lowers all the time; in the ozone situations, the amount of O_2 firstly reaches a maximum value and then decreases. The peak quantity of O_2 increases as values increase. Figure 5.7d indicates that the first 100 ps are totally utilised by O_3 molecules. Figures 5.7c and 5.7d imply that O_3-related processes may explain the first rise in O_2 quantity. More specifics of O_3 reaction pathways are required to substantiate such a conclusion, as presented in the next section.

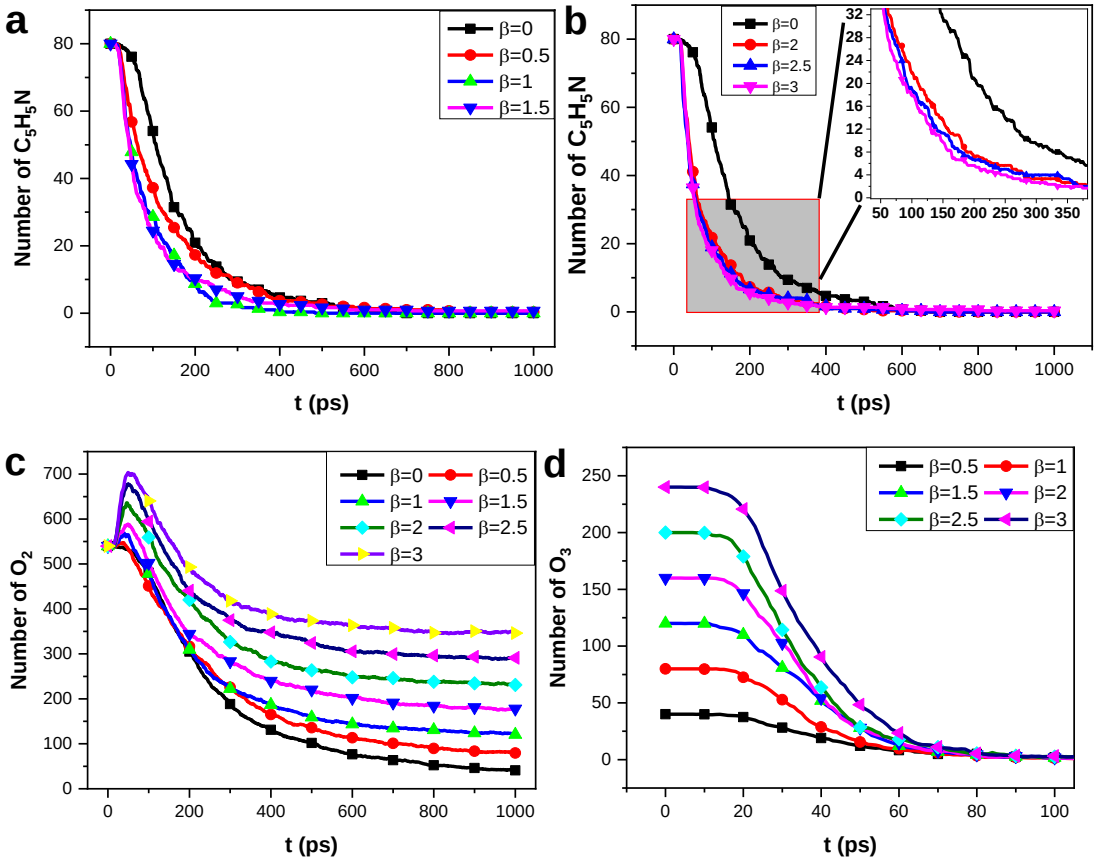

Figure 5.7 Time evolution of main reactants. (a) C_5H_5N (β = 0-1.5); (b) C_5H_5N (β = 0&2-3); (c) O_2; (d) O_3.

5.2.2.2 Reaction Mechanisms of O_2 and O_3

This section investigates the reaction processes of O_3 and O_2 to further explain the impacts of ozone on the reaction rates of the primary reactants. Through R5.28 and R5.29, O_2 reacts with species to form HO_2 and oxygen-containing intermediates.

$$C_xH_yO_zN_n + O_2 \rightarrow C_xH_yO_{z+2}N_n \quad \text{(R5.28)}$$

$$C_xH_yO_zN_n + O_2 \rightarrow C_xH_{y-1}O_zN_n + HO_2 \quad \text{(R5.29)}$$

The oxygen-containing intermediates decompose by dissociation of O and OH:

$$C_xH_yO_zN_n \rightarrow C_xH_yO_{z-1}N_n + O \quad \text{(R5.30)}$$

$$C_xH_yO_zN_n \rightarrow C_xH_{y-1}O_{z-1}N_n + OH \quad \text{(R5.31)}$$

O_2 reacts with H and OH generating HO_2 and HO_3 via R5.32 and R5.33, respectively.

$$O_2 + H \rightarrow HO_2 \quad \text{(R5.32)}$$

$$O_2 + OH \rightarrow HO_3 \quad \text{(R5.33)}$$

As indicated in R5.34 and R5.35, H_2O_2 is generated through HO_2 reacts with

H_2O and HO_2, respectively.

$HO_2 + H_2O \rightarrow H_2O_2 + OH$ (R5.34)

$HO_2 + HO_2 \rightarrow H_2O_2 + O_2$ (R5.35)

Aside from R5.36 and R5.34, the reaction of H_2O and O, as well as the breakdown of H_2O_2, both bringing active OH radicals.

$H_2O + O \rightarrow HO + HO$ (R5.36)

$H_2O_2 \rightarrow HO + HO$ (R5.37)

The active species (OH, HO_2, HO_3, and H_2O_2) formed by O_2 eventually engage in reactions that produce important products such as NO, NO_2, N_2, CO and CO_2. The O_3 related processes in pyridine combustion with ozone addition are divided into three categories: heat degradation, reactions with hydrocarbons, and reactions with other main radicals [13]. O_2 and O are released during the thermal breakdown of ozone through R5.38:

$O_3 \rightarrow O_2 + O$ [13] (R5.38)

O_2 and oxygen-containing intermediates are generated from the reactions of ozone with hydrocarbons via R5.39:

$C_xH_yO_zN_n + O_3 \rightarrow C_xH_yO_{z+1}N_n + O_2$ (R5.39)

Ozone concentrations are related to the reactions of O_3 and intermediates. The reactions between O_3 and OH to generating HO_2 are through R5.40-R5.42.

$HO_2 + O_3 \rightarrow O_2 + O_2 + OH$ [13] (R5.40)

$OH + O_3 \rightarrow O_2 + HO_2$ [13] (R5.41)

$HO_2 + O_3 \rightarrow O_2 + HO_3$ (R5.42)

In conditions where β = 1.5-3, O_3 combines with O to produce O_2 through R5.43. When β is greater than 2, O_3 molecules take part in reactions with H and O_3 via R5.44 and R5.45.

$O_3 + O \rightarrow O_2 + O_2$ [13] (R5.43)

$O_3 + H \rightarrow O_2 + HO$ [13] (R5.44)

$O_3 + O_3 \rightarrow O_2 + O_2 + O_2$ (R5.45)

To sum up, O_3 has abilities to enhance the oxidation of reactants directly. Furthermore, O_3 could aid in the generation of OH, HO_2, HO_3, O_2 and H_2O_2, which explains the growing profiles of O_2 in ozone-addition cases (Figure 5.7c) and the highest yields of OH, HO_2, HO_3, and H_2O_2 with (Figure 5.8). Furthermore, as demonstrated in Figures 5.7a and 5.7b, a rise in active radicals promotes fuel combustion, leading to quicker consumption rates of pyridine molecules.

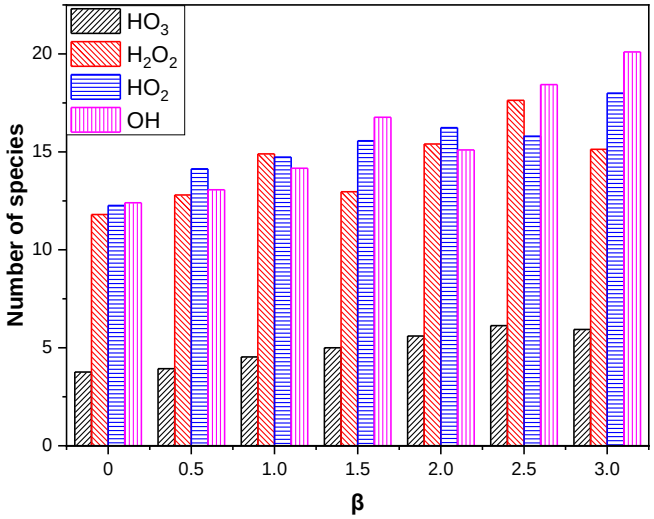

Figure 5.8 Maximum number of HO_3, H_2O_2, HO_2 and HO.

5.2.2.3 Impacts of O_3 on the Production of Main Products

Figures 5.9a and 5.9b show that the number of CO drops with rising *β*, but that increasing ozone increases CO_2 generation during pyridine combustion when *β* changes from 0 to 1.5. The variations in CO and CO_2 production with are not noticeable when *β* is larger than 1.5. Figures 5.9c and 5.9d indicate that the yields of NO and NO_2 follow the same pattern as CO and CO_2. According to Figure 5.9f, when *β* is larger than 0.5, the number of N_2 falls with the increase of O_3 molecules in system. It is clear from Figure 5.9e that NOx has the opposite tendency as N_2. The effect of ozone on NOx and CO production is consistent with earlier research [46, 47].

The impacts of ozone addition on product yields are examined subsequently. The channels of nitrogen-free and nitrogen-containing products are identified in Sections 5.2.2.4 and 5.2.2.5, respectively, further determining the impacts of ozone on the generation of main products during pyridine combustion.

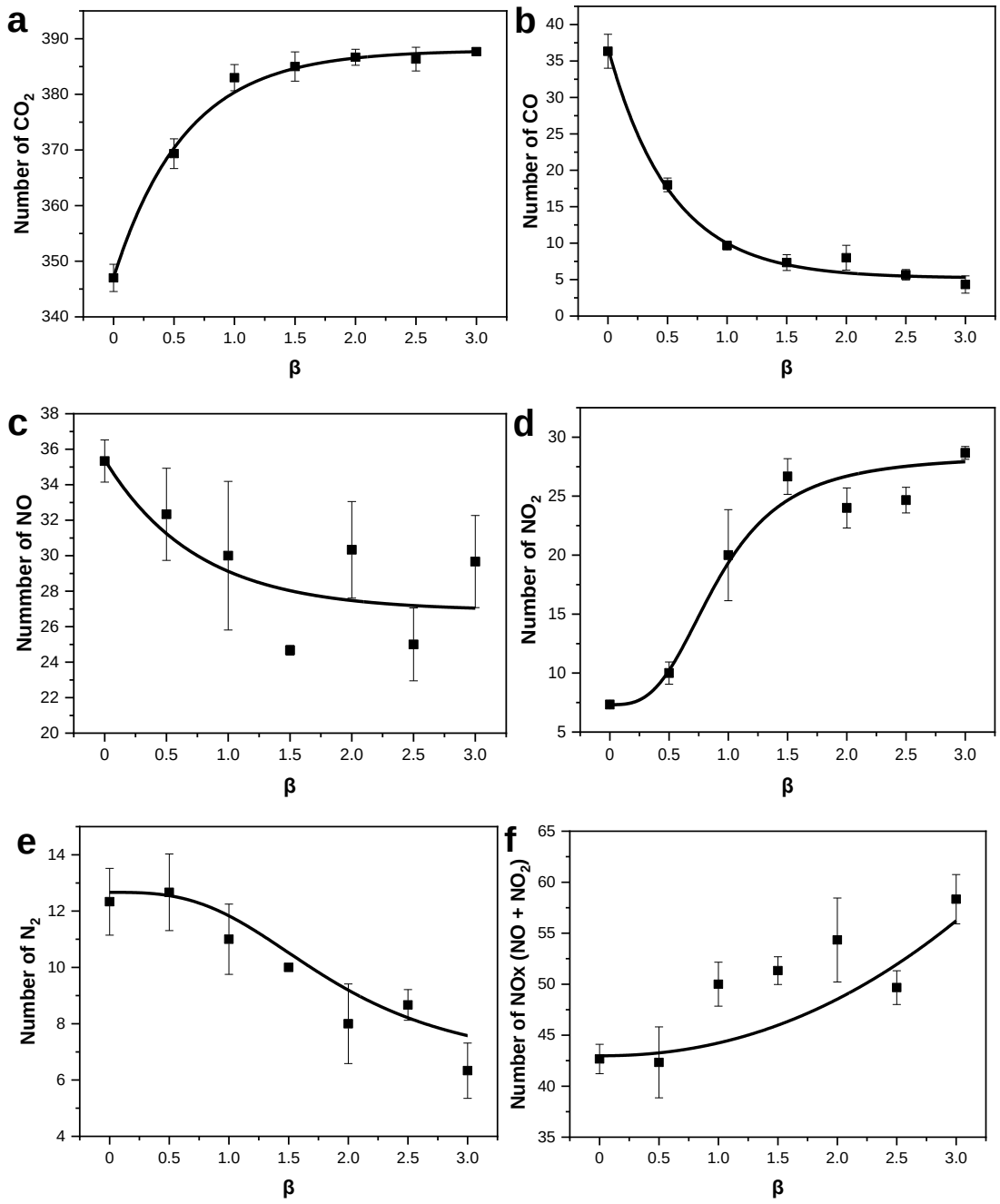

Figure 5.9 Influence of O_3 on the numbers of key products. (a) CO_2; (b) CO; (c) NO; (d) NO_2; (e) N_2; (f) NOx.

5.2.2.4 Reaction Pathways of CO and CO_2

During the pyridine oxidation process, nitrogen-containing compounds are produced in two stages. As illustrated in R5.46 and R5.47, the first generation of CO and CO_2 is due to the thermal breakdown of oxygen-containing precursors. The CO will then be transformed to CO_2 via reactions with active species (HO_2, HO_3, O_2, O_3 and H_2O_2).

$$C_xH_yO_zN_n \rightarrow C_{x-1}H_yO_{z-1}N_n + CO \quad \text{(R5.46)}$$

$C_xH_yO_zN_n \rightarrow C_{x-1}H_yO_{z-2}N_n + CO_2$ (R5.47)

It is clear from Figure 5.10 that the impacts of ozone on the ratios of R5.46 and R5.47 are insignificant, which are 63% and 37%, respectively. The results show that the rise in CO_2 generation with O_3 additives is due to the promotion influence on the conversion from CO to CO_2 during pyridine oxidation. Table 5.5 depicts the NF of the key pathways associated in CO_2 conversion. The findings indicate that ozone greatly promotes the CO consumption and CO_2 formation when β is less than 1.5, but the yields of CO and CO_2 nearly remain constant when β = 1.5-3, which agrees well with the ozone impact on CO and CO_2 yields in Figure 5.9.

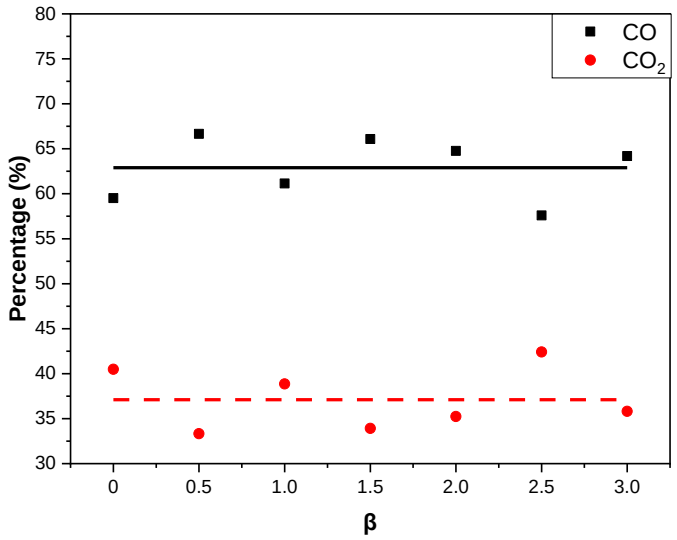

Figure 5.10 Proportion of CO and CO_2 formed from oxygen-containing species pyrolysis.

The conversion from CO to CHO_2, CHO_3, CHO_4 CO_2, CO_3 and CO_4 are the six pathways for CO consumption. It is clear from Table 1 that the NF of CO → CO_3 increases as β rises. Whereas, ozone has no effect on the conversion of CO to CHO_3. As illustrated in Table 5.6, R5.48 and R5.49 are the reactions that generate CO_3 and CHO_3 from CO, respectively.

The pathways CO → CHO_2 and CO → CO_2 present similar tendencies, peaking at β = 0.5 and 1.5, respectively, and subsequently decreasing with increasing ozone addition in the pyridine oxidation. The conversion from CO to CHO_2 is through R5.50 to R5.52. The reaction between CO and OH occupies a dominant position in the generation of CHO_2. The CO_2 generation from CO through six different pathways, as shown in R5.53 to R5.58.

CO_2 formation from reaction between CO with H_2O_2 is observed in β = 0&3 cases (R5.59). In all ozone-containing conditions, CO will combine with O_3 to produce CO_2 (R5.60).

Furthermore, ozone stimulates the reactions R5.56, R5.58, and R5.60, as well as the channel CO → CO_2 when β ranges from 0 to 1.5. R5.53, R5.54, and R5.58 are inhibited with β over 1.5, leading in a decrease in CO_2 conversion. Furthermore, at β = 3, CO molecules are transformed to CHO_4 and CO_4 via R5.61 and R5.62.

Mutual transformation channels for important intermediates formed by R5.48 to R5.62 (such as the conversions from CHO_2 to CHO_4 and CO_3 to CHO_3) are discovered. The transfer channels of CO_2 production are the primary emphasis of this section. Table 9.2 illustrates the NF of CO_2 generation pathways through CHO_2, CHO_3, CHO_4, CO, CO_3 and CO_4. Overall, ozone encourages the pathways CO → CO_2, CHO_3 → CO_2, and CHO_4 → CO_2. The NF of the conversion from CHO_2 to CO_2 peaks at β = 0.5 and gradually drops as β climbs to 3. The NF of the conversion from CO_4 to CO_2 is zero when β = 0-1.5, whereas ozone increases CO_2 production when is more than 1.5.

According to R5.63 through R5.68, CO_2 is formed via thermal breakdown of CO_3 and interactions of CO_3 with H_2O, O_2, OH, HO_2 and CO. R5.63 to R5.66 are found in all conditions. R5.67 occurs in β = 0-1.5, 2 and 2.5 conditions, while R5.53 occurs in cases with β ranging from 1 to 3. Furthermore, the rise in NF of pathway CO_3 → CO_2 with increasing β is attributed to ozone molecules enhancing R5.63. The pathway CHO_2 → CO_2 is through reactions R5.69 to R5.73.

R5.69 to R5.71 occur in all conditions. R5.72 occurs with β = 0 & 1-2. R5.73 occurs when β = 0.5, 1, 2.5, and 3. The major reaction from CHO_2 to CO_2 is R5.69. R5.74 and R5.75 are used to convert CHO_3 to CO_2, and R5.60 occurs exclusively in the β = 1, 2, and 3 situations. Increasing ozone addition enhances R5.75, which is the primary cause of the enhancement of the pathway CHO_3 → CO_2. The conversion from CHO_4 → CO_2 and CO_4 → CO_2 are depicted in R5.76 and R5.77, respectively.

Table 5.5 Net flux (NF) of key channels related to conversion from CO to CO_2.

Pathways	0	0.5	1	1.5	2	2.5	3
$CO \rightarrow CO_2$	171	164	165	181	178	151	155
$CO \rightarrow CO_3$	259	273	280	283	312	323	310
$CO \rightarrow CHO_2$	126	147	143	133	121	121	125
$CO \rightarrow CHO_3$	21	24	23	26	24	23	26
$CO \rightarrow CHO_4$	0	0	0	0	0	0	7
$CO \rightarrow CO_4$	0	0	0	0	0	0	4
Total CO consumption	577	608	611	623	635	618	627
$CO \rightarrow CO_2$	171	164	165	181	178	151	155
$CO_3 \rightarrow CO_2$	163	223	215	232	232	259	232
$CHO_2 \rightarrow CO_2$	101	155	106	138	123	118	124
$CHO_3 \rightarrow CO_2$	65	70	64	76	76	71	75
$CHO_4 \rightarrow CO_2$	10	12	28	11	19	38	27
$CO_4 \rightarrow CO_2$	0	5	2	1	9	15	30
Total CO_2 generation	510	629	580	639	637	652	643

Table 5.6 List of reactions linked with CO_2 generation.

ID	Reactions	ID	Reactions
R5.48	$CO + O_2 \rightarrow CO_3$	R5.63	$CO_3 \rightarrow CO_2 + O$
R5.49	$CO + HO_2 \rightarrow CHO_3$	R5.64	$CO_3 + H_2O \rightarrow CO_2 + HO + HO$
R5.50	$CO + OH \rightarrow CHO_2$	R5.65	$CO_3 + OH \rightarrow CO_2 + HO_2$
R5.51	$CO + H_2O_2 \rightarrow CHO_2 + HO$	R5.66	$CO_3 + O_2 \rightarrow CO_2 + O_3$
R5.52	$CO + HO_3 \rightarrow O_2 + CHO_2$	R5.67	$CO_3 + CO \rightarrow CO_2 + CO_2$
R5.53	$CO + HO_2 \rightarrow CO_2 + HO$	R5.68	$CO_3 + HO_2 \rightarrow CO_2 + O_2 + HO$
R5.54	$CO + O_2 \rightarrow CO_2 + O$	R5.69	$CHO_2 + O_2 \rightarrow CO_2 + HO_2$
R5.55	$CO + NO_2 \rightarrow CO_2 + NO$	R5.70	$CHO_2 \rightarrow CO_2 + H$
R5.56	$CO + O_2 + HO \rightarrow CO_2 + HO_2$	R5.71	$CHO_2 + HO \rightarrow H_2O + CO_2$
R5.57	$CO + O \rightarrow CO_2$	R5.72	$CHO_2 + H_2O_2 \rightarrow H_2O + CO_2 + HO$
R5.58	$CO + OH \rightarrow CO_2 + H$	R5.73	$O_2 + CHO_2 \rightarrow CO_2 + HO + O$
R5.59	$CO + H_2O_2 \rightarrow H_2O + CO_2$	R5.74	$CHO_3 \rightarrow CO_2 + HO$
R5.60	$CO + O_3 \rightarrow CO_2 + O_2$	R5.75	$CHO_3 + O_2 \rightarrow CO_2 + HO_3$
R5.61	$CO + O_2 + HO \rightarrow CHO_4$	R5.76	$CHO_4 \rightarrow CO_2 + HO_2$
R5.62	$CO + O_3 \rightarrow CO_4$	R5.77	$CO_4 \rightarrow CO_2 + O_2$

5.2.2.5 Reaction pathways of NO, NO_2 and N_2

Figure 9.6 depicts the NO and NO_2 transfer mechanisms at various concentrations. HNO, CNO, and $CHNO_3$ and CNO_2 radicals are key

intermediates for NOx production during pyridine combustion. Further information on the processes of pyridine combustion can refer to previous works [193, 203]. The channels $CNO_3 \rightarrow NO$, $CNO_2 \rightarrow NO$, $HNO \rightarrow NO$ and $CHNO_3 \rightarrow NO$ occur in all situations during NO production, and NO_3 NO is detected in the β = 0.5-2 and 3 conditions. NO is consumed forming HNO_3, NO_2, HNO_2 and CN_2O_2. The conversion from NO to CN_2O_2 exists only when β ranges from 0 to 2.5. Furthermore, HNO_2 and HNO_3 are key species in the production of NO_2. When the range of β is between 0.5 and 3, the pathways $CNO_2 \rightarrow CNO_4 \rightarrow NO_2$ and $HNO_4 \rightarrow NO_2$ are identified, and HNO_4 is mostly derived from the conversion of NO_3, HNO_2 and HNO_3. In terms of NO_2 consumption, $NO_2 \rightarrow NO_3$ and $NO_2 \rightarrow CNO_3$ occur when β = 0.5-1.5&2.5-3 and 0-1&2&3, respectively.

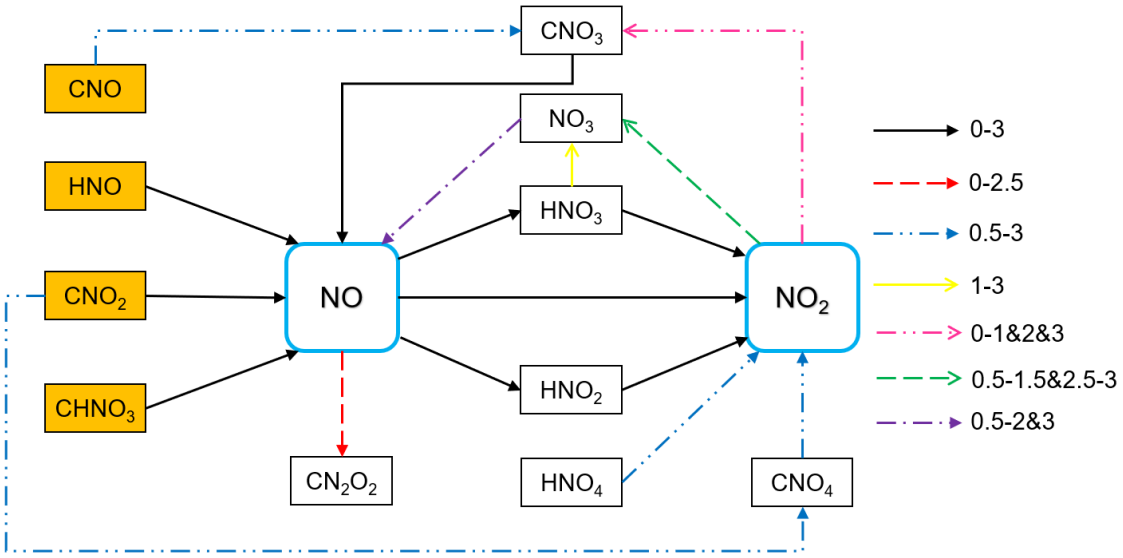

Figure 5.11 Influence of ozone on the channels of NO and NO_2. The starting species are in yellow boxes. The numerical values represent β values.

To further understand the effects of ozone on the generation of NO and NO_2, the NF values linked with NO and NO_2 were carried out, as illustrated in Table 5.7. The NF of NO net generation shows a declining trend, which is consistent with the number of NO at various O_3 additions. Furthermore, rising β promotes NO creation marginally, whereas O_3 dramatically increases NO consumption. As a result, it can be deduced that the effects of O_3 on NO consumption occupy an important position in the yield of NO in products. Furthermore, pathways $NO \rightarrow NO_2$ and $NO \rightarrow HNO_2$ rise with β values. The NF of $NO \rightarrow HNO_3$ drops firstly until it reaches its lowest value in the β = 1.5 case, then increases as β is higher than 1.5. Regarding the conversion from NO to CN_2O_2, its NF almost keeps constant

with β = 0-1, but drops when β is greater than 1.

The conversion between NO and NO_2 is presented in Table 5.8 as R5.78 to R5.85. In ozone addition situations, R5.78, R5.79, R5.81, and R5.82 are detected. R5.80 occurs in β = 0-2.5 of the instances. R5.83 occurs with β of 1 and 3. In β = 0.5-3 occurrences, R5.84 is observed. R5.85 occurs exclusively in the β = 2 case. When β varies from 0-1.5, R5.78, R5.79, and R5.81 all play vital roles in NO yield. Ozone, in particular, stimulates the pathway NO → NO_2 via R5.79 and R5.81, but inhibits the conversion from NO_2 to NO via R5.78, explaining the rise in NO consumption via NO → NO_2 with β less than 1.5. When β is greater than 1.5, O_3 presents insignificant impact on R5.78, R5.79, and R5.81, but it enhances the total production of NO_2.

Pathways NO → CN_2O_2 and NO → HNO_3 are via reactions R5.86 and R5.87, respectively. The channel from NO to HNO_2 is by R5.88 to R5.91. R5.88 and R5.89 have been observed in all conditions. R5.90 is found in β = 0.5 and 2-3 conditions. R5.91 may be found in β = 0.5&1&2-3 conditions. Furthermore, NO + HO → HNO_2 (R5.89) plays important role in the pathway NO → HNO_2.

In terms of NO_2 generation and consumption, the NF of NO_2 net generation is consistent with NO_2 yield under varied ozone circumstances. Furthermore, the NF of NO_2 consumption almost keeps constant, therefore the amount of NO_2 is governed by NO_2 formation. Furthermore, ozone increases NO_2 production from HNO_4 and NO. The NF of the conversion from HNO_3 to NO_2 is decreasing with β = 0-1, however this pathway is promoted by ozone when β is greater than 1. Regarding NO_2 formation from HNO_2 and CNO_2, the NF of them rises to a peak at β = 1.5 and subsequently falls. The results show that ozone's enhancement influence on NO_2 production from HNO_2, NO, HNO_4 and CNO_4 produce a rise in NO_2 quantity with β = 0-1.5. Furthermore, when β is increased from 1.5 to 3, the suppression of NO_2 generation from CNO_4 and HNO_2 leads to the yields of NO_2 remaining essentially constant.

The NO_2 production from CNO_4, HNO_3 and HNO_4 are through R5.92 to R5.94. The pathway HNO_2 → NO_2 are through reactions R5.95 to R5.97, the reaction between HNO_2 and O_2 (R5.96) is the primary source of NO_2 generation.

In terms of N_2 generation, $C_2N_2O_2$ is the primary precursor produced by R5.98. $C_2N_2O_2$ → N_2 (R5.99) and $C_2N_2O_2$ → CN_2O → N_2 (R5.100 to R5.101) are two channels forming N_2. The addition of ozone during pyridine burning hinders the conversion of $C_2N_2O_2$ and CN_2O to N_2, resulting in a reduction in N_2

production as the value of β increases.

Table 5.7 Net flux (NF) of key channels related to NO, NO_2 and N_2.

Pathways	0	0.5	1	1.5	2	2.5	3
$CNO_2 \rightarrow NO$	90	101	113	112	117	96	127
$HNO \rightarrow NO$	13	18	12	6	11	11	25
$CHNO_3 \rightarrow NO$	14	6	11	9	2	9	5
$CNO_3 \rightarrow NO$	12	6	12	9	6	5	6
$NO_3 \rightarrow NO$	0	5	1	1	9	0	-2
NO generation	129	136	149	137	145	121	161
$NO \rightarrow CN_2O_2$	8	7	9	2	1	4	0
$NO \rightarrow NO_2$	3	10	38	18	27	22	33
$NO \rightarrow HNO_3$	17	16	7	8	5	17	24
$NO \rightarrow HNO_2$	2	-2	32	51	24	53	32
NO consumption	30	31	86	79	57	96	89
Net NO generation	99	105	63	58	88	25	72
$HNO_3 \rightarrow NO_2$	13	10	1	14	6	11	24
$HNO_2 \rightarrow NO_2$	1	12	17	44	18	26	25
$CNO_4 \rightarrow NO_2$	0	9	13	6	10	12	8
$HNO_4 \rightarrow NO_2$	0	1	2	-5	8	2	8
NO_2 generation	17	42	71	77	69	73	98
$NO_2 \rightarrow CNO_3$	7	8	10	0	5	0	10
$NO_2 \rightarrow NO_3$	0	4	-2	-1	0	7	-1
NO_2 consumption	7	12	8	-1	5	7	9
Net NO_2 generation	10	30	63	78	64	66	89
$CN_2O \rightarrow N_2$	5	11	7	4	0	5	0
$C_2N_2O_2 \rightarrow N_2$	7	5	7	6	7	0	0
$N_2O \rightarrow N_2$	0	0	0	0	0	0	2
N_2 formation	12	16	14	10	7	5	2

Table 5.8 List of reactions linked with NO, NO_2 and N_2.

ID	Reactions	ID	Reactions
R5.78	$CO + NO_2 \rightarrow CO_2 + NO$	R5.90	$HNO_2 + HO_2 \rightarrow H_2O + O_2 + NO$
R5.79	$HO_2 + NO \rightarrow HO + NO_2$	R5.91	$O_2 + HNO_2 \rightarrow HO_3 + NO$
R5.80	$H_2O_2 + NO \rightarrow H2O + NO_2$	R5.92	$HNO_3 \rightarrow HO + NO_2$
R5.81	$NO + O \rightarrow NO_2$	R5.93	$CNO_4 \rightarrow CO_2 + NO_2$
R5.82	$H + NO_2 \rightarrow NO + HO$	R5.94	$HNO_4 \rightarrow HO_2 + NO_2$
R5.83	$CO_3 + NO \rightarrow CO_2 + NO_2$	R5.95	$HNO_2 + HO \rightarrow H_2O + NO_2$
R5.84	$HO_2 + NO_2 \rightarrow O_2 + NO + HO$	R5.96	$HNO_2 + O_2 \rightarrow HO2 + NO_2$
R5.85	$NO + O_3 \rightarrow O_2 + NO_2$	R5.97	$HNO_2 \rightarrow H + NO_2$
R5.86	$NO + CNO \rightarrow CN_2O_2$	R5.98	$CNO + CNO \rightarrow C_2N_2O_2$
R5.87	$NO + HO_2 \rightarrow HNO_3$	R5.99	$C_2N_2O_2 \rightarrow N_2 + 2CO$
R5.88	$H_2O_2 + NO \rightarrow HNO_2 + HO$	R5.100	$C_2N_2O_2 \rightarrow CN_2O + CO$
R5.89	$NO + HO \rightarrow HNO_2$	R5.101	$CN_2O \rightarrow N_2 + CO$

5.2.3 Discussion

When ozone is introduced to pyridine combustion, it alters reactant consumption rates and production yields by directly interacting with species and promoting the formation of active intermediates such as H_2O_2, OH_3, HO_2 and HO.

According to the current study, ozone performs well in decreasing CO and NO emissions with β = 0-1.5. The selective catalytic reduction (SCR) method, which uses NH_3 to convert NO molecules to N_2 with costly catalysts, can minimise exhaust gas treatment operating expenses by lowering NO emissions. In the meantime, ozone increases the proportion of NO_2 in NOx pollutants during coal combustion, which can be easily eliminated by water. Whereas ozone molecules promote the oxidation of nitrogenous species instead of N_2 formation, increasing NOx (total NO and NO_2) pollutants, agreeing well with previous research [46, 47]. Therefore, in practice, ozone concentrations should be adequately engineered during fuel combustion.

Chapter 6 Conclusions and Future Work

6.1 Conclusions

In the present thesis, the underlying mechanisms of nitrogen element migration during coal splitting and staging as well as assisted combustion were investigated by ReaxFF MD simulations. Specifically, pyridine pyrolysis process in both water and water-free environments was studied first. The influence of varied water concentrations on pyridine pyrolysis processes was thoroughly revealed. In addition, the processes of NO abatement by nitrogen-containing species in pyrolysis gas (HCN and NH_3) are investigated using ReaxFF simulations under varying temperatures, oxygen (O_2) content, nitrogen-containing species content and nitrogen-free components (CH_4, CO and H_2) addition, respectively. Finally, ReaxFF MD simulations are performed to explore the impacts of electric field (EF) and ozone (O_3) on pyridine oxidation. The main conclusions are summarized as follows:

6.1.1 Effects of Water on Pyridine Pyrolysis

In the starting stages of pyridine pyrolysis, H_2O molecules promote the formation of active OH species and speed up pyridine reduction. Water has an inhibiting effect on pyridine consumption as pyrolysis progresses because it significantly slows down the condensation process of pyridine molecules. Additionally, during pyridine pyrolysis, H_2O molecules play an important role on the overall species numbers, and intermediates are discovered and defined in varying situations. H_2O molecules also lower the polycondensation product's (C_5+) N content.

6.1.2 Mechanisms of NO Removal by HCN and NH_3

During NO abatement, HCN contributes in three different ways. The first way involves the oxidation of HCN to NO via HCN → CN → CNO_2 → NO. The second process is N_2 generation through HCN → CHNO → CNO → $C_2N_2O_2$ → N_2 and HCN → CHNO → CNO → $C_2N_2O_2$ → CN_2O → N_2, which have no contribution to NO consumption or generation. Finally, the NO combines with radicals (N, CNO and NH) from HCN to produce N_2. Besides, part of NH_3 molecules directly

produce N_2 without reacting with NO through $NH_3/NH_2 \rightarrow N_2H_4 \rightarrow N_2H_3 \rightarrow N_2H \rightarrow N_2$ and $NH_3/NH_2 \rightarrow N_2H_4 \rightarrow N_2H_3 \rightarrow N_2H_2 \rightarrow N_2$. N_2 can also be formed from interactions between NO and nitrogenous species (like NH, NH_2 and NH_3). Also, NH_3 is about 19.1% higher performance in NO removal than HCN, and it is less influenced by temperatures. The increase of temperature improves NO reduction performance under both HCN and NH_3 circumstances.

In the NO reduction with HCN cases, O_2 shows negative influence on the NO removal owing to the promotion of HCN oxidation forming NO molecules. Although the NF of NO molecules consumption almost remains the same under varying O_2 concentrations, the intermediates of NO consumption change from CN, HCN and CN_2 to CNO with λ increasing. O_2 molecules promote the generation of CNO radical significantly, which can react with NO or itself (CNO) and generate N_2 eventually. However, the number of N_2 reaches maximum when λ is 0.6 due to the inhibition on the N_2 formation from HN_2O, N_2H, CN_3O and CNO when λ is greater than 0.6. Besides, the performance of NO removal and N_2 formation is suppressed by O_2 under NO reduction by NH_3. That is because the NO consumption by NH_3 and NH_2 generating H_2N_2O or HN_2O is weakened as O_2 concentrations increase, which will be converted into N_2 eventually. Moreover, the increase of O_2 decreases the N_2 formation.

The increase of HCN/NO and NH_3/NO ratios can promote NO removal performance, but the reduction efficiency peaks at the *R* value of 1.6. Specifically, the enhancement of NO removal is mainly by the promotion of the reactions of NH radical and NO molecules, and forming N_2 eventually. In addition, high *R* values also promote N_2 formation. Moreover, the 'self-consumption' of HCN for N_2 formation is enhanced with the rising HCN/NO ratios. Regarding NO abatement with NH_3, the increase of NH_3 molecules improves the NO reduction performance mainly by promoting the reaction of NO molecules with NH_3 and NH_2 to generate H_2N_2O, which will convert to N_2 finally. Also, the 'self-consumption' effect of NH_3 is promoted by high R values via the conversion from N_2H_3 and N_2H_2 to N_2, which is produced by the reactions between NH_3, NH_2 and NH.

CH_4 benefits NO reduction in both HCN and NH_3 cases. On the other hand, the conversion from NO to N_2 formation is inhibited in the NO abatement by HCN and NH_3 with CH_4 addition. The proportion of HCN/CN, NH_i and $C_xN_yO_z$ is promoted by CH_4 molecules in both HCN and NH_3 cases. The influence of CO

addition on the number of NO in the HCN cases is insignificant, but CO slightly promotes the number of NO in the NH_3 cases. The yields of N_2 decrease with CO addition in both HCN and NH_3 cases. When NO is removed by HCN, the percentage of HCN/CN increases slightly with CO addition. The numbers of $C_xN_yO_z$ and NH_i almost remain the same. For NO removal with NH_3, CO addition promotes the formation of $C_xN_yO_z$ and HCN/CN, but has insignificant influence on NH_i production. H_2 molecules promote the NO consumption significantly and N_2 formation slightly in both HCN and NH_3 cases. In NO removal by HCN cases, the H_2 addition also increases the percentages of HCN/CN and NH_i, but the $C_xN_yO_z$ content remains the same with H_2/NO ratio changing from 0 to 1.5. The NH_i content shows an upward trend with H_2 addition during NO reduction with NH_3.

6.1.3 Pyridine Assisted Combustion

With *E* ranging from 0 to 2.5 V/nm, EF reduces C_5H_5N and O_2 consumption, while it speeds up reaction rates when *E* ranges from 2.5 to 7.5 V/nm. Additionally, when the EF intensities rise, more species can be produced during pyridine combustion. Additionally, EF lowers the yields of NO and CO, but in all circumstances has little effect on NO_2 and N_2. When the EF intensity is more than 2.5 V/nm, the number of CO_2 rises, but it almost remains constant between *E* = 0 and 2.5 V/m.

The amount of CO decreases as the O_3/C_5H_5N ratio rises, but as the ratio rises from 0 to 1.5, more CO_2 is produced during the burning of pyridine. The generation of CO and CO_2 almost remains same when the O_3/C_5H_5N ratio is more than 1.5. Similar to CO and CO_2, respectively, the numbers of NO and NO_2 exhibit a similar pattern. When the O_3/C_5H_5N ratio is larger than 0.5, the amount of N_2 falls while the amount of O_3 increases. Ozone encourages pyridine's overall NOx emissions.

In summary, the current thesis offers new insight into underlying mechanisms of pyridine pyrolysis, NO abatement by nitrogenous agents in pyrolysis gas (HCN and NH_3) and fuel-NOx emissions formation process assisted by EF and ozone at atomic-level, which are important processes related to NOx regulations. That may contribute to optimisation of operating conditions to achieve lower NOx

emissions during coal combustion and development of future high-performance NOx reduction technologies. This research also proves that ReaxFF MD is a valuable and promising approach to explore chemical mechanisms that is well consistent with previous studies.

6.2 Future Work

In the current thesis, a series of important reactions related to NOx control were revealed at atomic scales and pointed out key reaction pathways and elementary reactions through ReaxFF MD simulations. In future work, the following areas can be improved and extended:

A. It is beyond the capabilities of ReaxFF (or 'regular ReaxFF') MD to describe sub-atomic phenomena like electron transport processes, calculate potential profiles, determine transition states for elementary reactions and kinetic parameters during pyrolysis, oxidation and reduction processes. To expand the understanding of key reactions, it is anticipated that the results from current conventional ReaxFF MD simulations will be further investigated via the hybrid ReaxFF (recently developed eReaxFF [204, 205]), or QM approaches.

B. Due to the limitations of the current computational speed, the simulated times and spatial scales are limited, which is significantly smaller than those in experiments. Also, to study the complete chemical process, the strategy, artificially increasing the parameters like temperature, pressure and EF strength of the system, is adopted in ReaxFF MD simulations. Although it is a common strategy, it still remains debatable. Further work can focus on the quantitative analysis of the errors of the strategy and the improvement of the capability of ReaxFF MD at large time and temporal scales using advanced computational techniques.

C. By studying the important reactions related to NOx formation and reduction in theory, a number of new ways of regulating fuel NOx emissions were demonstrated during coal combustion in the current work. Suitable experiments ,for instance coal assisted combustion as well as coal splitting and staging process, can be carried out to put these methods into practice. The combination of experimental and theoretical methodologies leads to a more comprehensive understanding of important reaction mechanisms and the discovery of new phenomena.

D. To accelerate the study of the nitrogen mitigation process, the model was simplified by choosing the main nitrogen-containing compound, pyridine, as the representative in this thesis. However, there are other important components, like functional groups and alkali metals in coal that may affect the NOx control process. Thus, this area still needs further investigation.

E. The development of low-cost, highly efficient catalysts is another promising way to control NOx emissions. Data-driven techniques have the capability to reveal complete feature-property connections between materials based on scientific data. Therefore, data-driven methods for material design related to NOx reduction will be a promising way to develop more clean and effective methods for NOx control.

References

1. Otaka Y, Han P. Study on the strategic usage of coal in the EAS region: a technical potential map and update of the first-year study. Economic Research Institute for ASEAN and East Asia (ERIA), Jakarta https://www eria org/RPR-FY2014-36 pdf Accessed. 2020;10.

2. Nalbandian-Sugden H. Operating ratio and cost of coal power generation. London: IEA Clean Coal Centre. 2016:46-82.

3. Otaka Y, Phoumin H. Study on the Strategic Usage of Coal in the EAS Region: A Technical Potential Map and Update of the First-Year Study. Economic Research Institute for ASEAN and East Asia (ERIA). 2015.

4. Bowman CT. Control of combustion-generated nitrogen oxide emissions: technology driven by regulation. Symposium (International) on Combustion. 1992;24(1):859-78.

5. Greul U, Spliethoff H, Magel H-C, Schnell U, Rüdiger H, Hein K, et al. Impact of temperature and fuel-nitrogen content on fuel-staged combustion with coal pyrolysis gas. Symposium (International) on Combustion. 1996;26(2):2231-9.

6. IEA. Coal consumption by region, 2000 to 2021, IEA, Paris.

7. Rüdiger H, Greul U, Spliethoff H, Hein KR. Distribution of fuel nitrogen in pyrolysis products used for reburning. Fuel. 1997;76(3):201-5.

8. Imamura O, Chen B, Nishida S, Yamashita K, Tsue M, Kono M. Combustion of ethanol fuel droplet in vertical direct current electric field. Proceedings of the Combustion Institute. 2011;33(2):2005-11.

9. Bradley D, Nasser S. Electrical coronas and burner flame stability. Combustion and flame. 1984;55(1):53-8.

10. Altendorfner F, Kuhl J, Zigan L, Leipertz A. Study of the influence of electric fields on flames using planar LIF and PIV techniques. Proceedings of the Combustion Institute. 2011;33(2):3195-201.

11. Glarborg P, Jensen A, Johnsson JE. Fuel nitrogen conversion in solid fuel fired systems. Progress in energy and combustion science. 2003;29(2):89-113.

12. Mok YS, Lee H-J. Removal of sulfur dioxide and nitrogen oxides by using ozone injection and absorption–reduction technique. Fuel Processing Technology. 2006;87(7):591-7.

13. Sun W, Gao X, Wu B, Ombrello T. The effect of ozone addition on combustion: Kinetics and dynamics. Progress in Energy and Combustion Science. 2019;73:1-

25.
14. EPA E. Nitrogen Oxides (NOx), Why and How They Are Controlled. Nitrogen Oxides (NOx), Why and How They Are Controlled (accessed 2-24-2019). 1999.
15. EPA U. Integrated science assessment for oxides of nitrogen–health criteria. US Environmental Protection Agency, Washington, DC [Google Scholar]. 2016.
16. Al-jaf SJ, Al-Taai OT. Impact of nitrous oxide (N_2O) concentrations on atmospheric air temperature changes over Iraq and some neighboring regions. Journal of the University of Garmian. 2019;6(1):338-43.
17. Johnson DW, Turner J, Kelly J. The effects of acid rain on forest nutrient status. Water Resources Research. 1982;18(3):449-61.
18. DeHayes DH, Schaberg PG, Strimbeck GR. Red spruce (Picea rubens Sarg.) cold hardiness and freezing injury susceptibility. Conifer cold hardiness: Springer; 2001. p. 495-529.
19. Lazarus BE, Schaberg PG, Hawley GJ, DeHayes DH. Landscape-scale spatial patterns of winter injury to red spruce foliage in a year of heavy region-wide injury. Canadian Journal of Forest Research. 2006;36(1):142-52.
20. Rodhe H, Dentener F, Schulz M. The global distribution of acidifying wet deposition. Environmental Science & Technology. 2002;36(20):4382-8.
21. Likens GE, Driscoll CT, Buso DC. Long-term effects of acid rain: response and recovery of a forest ecosystem. Science. 1996;272(5259):244-6.
22. Larssen T, Lydersen E, Tang D, He Y, Gao J, Liu H, et al. Acid rain in China. ACS Publications; 2006.
23. Kesler SE, Simon AC, Simon AF. Mineral resources, economics and the environment: Cambridge University Press; 2015.
24. Reisener A, Stöckle B, Snethlage R. Deterioration of copper and bronze caused by acidifying air pollutants. Water, air, and soil pollution. 1995;85(4):2701-6.
25. Boden H. Approaches in modeling the impact of air pollution-induced material degradation. 1989.
26. EPA U. What is acid rain?
27. Fox W. Photochemical smog. 1996.
28. Beer J, Bowman C, Chen S, Corley T, De Soete G. Pulverized-coal combustion: Pollutant formation and control, 1970-1980. Final report. Radian Corp., Research Triangle Park, NC (USA); 1990.
29. Srivastava R, Neuffer W, Grano D, Khan S, Staudt J, Jozewicz W. Controlling

NOx emission from industrial sources. Environmental progress. 2005;24(2):181-97.
30. Srivastava RK, Hall RE, Khan S, Culligan K, Lani BW. Nitrogen oxides emission control options for coal-fired electric utility boilers. Journal of the Air & Waste Management Association. 2005;55(9):1367-88.
31. Javed MT, Irfan N, Gibbs B. Control of combustion-generated nitrogen oxides by selective non-catalytic reduction. Journal of environmental management. 2007;83(3):251-89.
32. Muzio L, Quartucy G. Implementing NOx control: research to application. Progress in Energy and Combustion Science. 1997;23(3):233-66.
33. Ma Y, Li T, Yan J, Wang X, Gao J, Sun Z. A comprehensive review of the influence of electric field on flame characteristics. 2020.
34. Zake M, Turlajs D, Purmals M. Electric field control of NOx formation in the flame channel flows. Global Nest: The Int J. 2000;2(1):99-108.
35. Barmina I, Kolmickovs A, Valdmanis R, Zake M. Control of combustion dynamics by an electric field. Chemical Engineering Transactions. 2015;43:973-8.
36. Most D, Hammer T, Lins G, Branston D, Altendorfner F, Beyrau F, et al., editors. Electric Field Effects for Combustion Control-Optimized Geometry. International Conference on Phenomena in Ionized Gases; 2007.
37. Vatazhin A, Likhter V, Sepp V, Shul'Gin V. Effect of an electric field on the nitrogen oxide emission and structure of a laminar propane diffusion flame. Fluid dynamics. 1995;30(2):166-74.
38. Krickis O, Jaundālders S, editors. Impact of electric field in the stabilized premixed flame on NOx and CO emissions. 2017 IEEE 58th International Scientific Conference on Power and Electrical Engineering of Riga Technical University (RTUCON); 2017: IEEE.
39. Barmina I, Turlajs D, Zake M. Electric Field Effects on the Swirling Combustion Dynamics. Rigas Tehniskas Universitates Zinatniskie Raksti. 2008;1:39.
40. Yamada H, Yoshii M, Tezaki A. Chemical mechanistic analysis of additive effects in homogeneous charge compression ignition of dimethyl ether. Proceedings of the Combustion Institute. 2005;30(2):2773-80.
41. Foucher F, Higelin P, Mounaïm-Rousselle C, Dagaut P. Influence of ozone on the combustion of n-heptane in a HCCI engine. Proceedings of the Combustion

Institute. 2013;34(2):3005-12.
42. Gao X, Zhang Y, Adusumilli S, Seitzman JM, Sun W, Ombrello T, et al., editors. The Effect of Ozone Addition on Flame Propagation. 53rd AIAA Aerospace Sciences Meeting; 2015.
43. Gluckstein ME, Morrison RB, Khammash TB. Combustion with ozone-modification of flame speeds C_2 hydrocarbon-air mixtures. 1955.
44. Zhang Y, Zhu M, Zhang Z, Shang R, Zhang D. Ozone effect on the flammability limit and near-limit combustion of syngas/air flames with N_2, CO_2, and H_2O dilutions. Fuel. 2016;186:414-21.
45. Weng W, Nilsson E, Ehn A, Zhu J, Zhou Y, Wang Z, et al. Investigation of formaldehyde enhancement by ozone addition in CH_4/air premixed flames. Combustion and Flame. 2015;162(4):1284-93.
46. Tachibana T, Hirata K, Nishida H, Osada H. Effect of ozone on combustion of compression ignition engines. Combustion and flame. 1991;85(3-4):515-9.
47. Nasser SH, Morris S, James S. A novel fuel efficient and emission abatement technique for internal combustion engines. SAE transactions. 1998:1410-25.
48. Gómez-García M, Pitchon V, Kiennemann A. Pollution by nitrogen oxides: an approach to NOx abatement by using sorbing catalytic materials. Environment international. 2005;31(3):445-67.
49. Staudt JE. Status report on NOx: Control technologies and cost effectiveness for utility boilers: Northeast States for Coordinated Air Use Management; 1998.
50. Park J-H, Ahn J-W, Kim K-H, Son Y-S. Historic and futuristic review of electron beam technology for the treatment of SO2 and NOx in flue gas. Chemical Engineering Journal. 2019;355:351-66.
51. Vascellari M. NO x Emission and Mitigation Technologies. Handbook of Clean Energy Systems. 2015:1-23.
52. Skalska K, Miller JS, Ledakowicz S. Trends in NOx abatement: A review. Science of the total environment. 2010;408(19):3976-89.
53. Chernetskiy M, Dekterev A, Chernetskaya N, Hanjalić K. Effects of reburning mechanically-activated micronized coal on reduction of NOx: Computational study of a real-scale tangentially-fired boiler. Fuel. 2018;214:215-29.
54. Miura K. Mild conversion of coal for producing valuable chemicals. Fuel processing technology. 2000;62(2-3):119-35.
55. Arenillas A, Rubiera F, Pis J, Cuesta M, Iglesias M, Jiménez A, et al. Thermal behaviour during the pyrolysis of low rank perhydrous coals. Journal of Analytical

and Applied Pyrolysis. 2003;68:371-85.
56. Zhao Y, Hu H, Jin L, Wu B, Zhu S. Pyrolysis behavior of weakly reductive coals from northwest China. Energy & fuels. 2009;23(2):870-5.
57. Alonso M, Alvarez D, Borrego A, Menéndez R, Marbán G. Systematic effects of coal rank and type on the kinetics of coal pyrolysis. Energy & fuels. 2001;15(2):413-28.
58. Mondragon F, Jaramillo A, Saldarriaga F, Quintero G, Fernandez J, Ruiz W, et al. The effects of morphological changes and mineral matter on H2S evolution during coal pyrolysis. Fuel. 1999;78(15):1841-6.
59. Solomon PR, Colket MB. Evolution of fuel nitrogen in coal devolatilization. Fuel. 1978;57(12):749-55.
60. Nelson PF, Kelly MD, Wornat MJ. Conversion of fuel nitrogen in coal volatiles to NOx precursors under rapid heating conditions. Fuel. 1991;70(3):403-7.
61. Zheng M, Li X, Liu J, Guo L. Initial chemical reaction simulation of coal pyrolysis via ReaxFF molecular dynamics. Energy & Fuels. 2013;27(6):2942-51.
62. Zheng M, Li X, Liu J, Wang Z, Gong X, Guo L, et al. Pyrolysis of Liulin coal simulated by GPU-based ReaxFF MD with cheminformatics analysis. Energy & fuels. 2014;28(1):522-34.
63. Castro-Marcano F, Russo Jr MF, van Duin AC, Mathews JP. Pyrolysis of a large-scale molecular model for Illinois no. 6 coal using the ReaxFF reactive force field. Journal of Analytical and Applied Pyrolysis. 2014;109:79-89.
64. Gao M, Li X, Guo L. Pyrolysis simulations of Fugu coal by large-scale ReaxFF molecular dynamics. Fuel Processing Technology. 2018;178:197-205.
65. Zheng M, Li X, Guo L. Investigation of N behavior during coal pyrolysis and oxidation using ReaxFF molecular dynamics. Fuel. 2018;233:867-76.
66. Gou X, Zhou J, Liu J, Cen K. Effects of water vapor on the pyrolysis products of pulverized coal. Procedia Environmental Sciences. 2012;12:400-7.
67. Liu J, Fan X-r, Zhao W, Hu B, Liu D-j, Lu Q, et al. Catalytic mechanism of calcium on the formation of HCN during pyrolysis of pyrrole and indole: A theoretical study. Energy & Fuels. 2019;33(11):11516-23.
68. Zhang J, Han C-L, Yan Z, Liu K, Xu Y, Sheng C-D, et al. The varying characterization of alkali metals (Na, K) from coal during the initial stage of coal combustion. Energy & fuels. 2001;15(4):786-93.
69. Chen C, Wang J, Liu W, Zhang S, Yin J, Luo G, et al. Effect of pyrolysis conditions on the char gasification with mixtures of CO2 and H2O. Proceedings

of the combustion institute. 2013;34(2):2453-60.
70. Ouyang J, Hong D, Jiang L, Li Z, Liu H, Luo G, et al. Effect of CO_2 and H_2O on char properties. Part 1: pyrolysis char structure and reactivity. Energy & Fuels. 2020;34(4):4243-50.
71. Hu E, Zeng X, Ma D, Wang F, Yi X, Li Y, et al. Effect of the moisture content in coal on the pyrolysis behavior in an indirectly heated fixed-bed reactor with internals. Energy & Fuels. 2017;31(2):1347-54.
72. Wang Ca, Du Y, Jin X, Che D. Pyridine and pyrrole oxidation under oxy-fuel conditions. Energy Sources, Part A: Recovery, Utilization, and Environmental Effects. 2016;38(7):975-81.
73. Houser TJ, McCarville ME, Biftu T. Kinetics of the thermal decomposition of pyridine in a flow system. International Journal of Chemical Kinetics. 1980;12(8):555-68.
74. Terentis A, Doughty A, Mackie JC. Kinetics of pyrolysis of a coal model compound, 2-picoline, the nitrogen heteroaromatic analog of toluene. 1. Product distributions. The Journal of Physical Chemistry. 1992;96(25):10334-9.
75. Doughty A, Mackie JC. Kinetics of pyrolysis of a coal model compound, 2-picoline, the nitrogen heteroaromatic analogue of toluene. 2. The 2-picolyl radical and kinetic modeling. The Journal of Physical Chemistry. 1992;96(25):10339-48.
76. Hämäläinen JP, Aho MJ, Tummavuori JL. Formation of nitrogen oxides from fuel-N through HCN and NH3: a model-compound study. Fuel. 1994;73(12):1894-8.
77. Laskin A, Lifshitz A. Thermal decomposition of quinoline and isoquinoline. The role of 1-indene imine radical. The Journal of Physical Chemistry A. 1998;102(6):928-46.
78. Bruinsma OS, Tromp PJ, de Sauvage Nolting HJ, Moulijn JA. Gas phase pyrolysis of coal-related aromatic compounds in a coiled tube flow reactor: 2. Heterocyclic compounds, their benzo and dibenzo derivatives. Fuel. 1988;67(3):334-40.
79. Axworthy A, editor Chemistry and kinetics of fuel nitrogen conversion to nitric oxide. AIChE Symposium Series; 1975.
80. Doughty A, Mackie JC. Kinetics of thermal decomposition of the diazines: shock-tube pyrolysis of pyrimidine. Journal of the Chemical Society, Faraday Transactions. 1994;90(4):541-8.
81. Jones J, Bacskay GB, Mackie JC, Doughty A. Ab initio studies of the thermal

decomposition of azaaromatics: free radical versus intramolecular mechanism. Journal of the Chemical Society, Faraday Transactions. 1995;91(11):1587-92.
82. Doughty A, Mackie JC, Palmer JM, editors. Kinetics of the thermal decomposition and isomerisation of pyrazine (1, 4 diazine). Symposium (International) on Combustion; 1994: Elsevier.
83. Kambara S, Takarada T, Yamamoto Y, Kato K. Relation between functional forms of coal nitrogen and formation of nitrogen oxide (NOx) precursors during rapid pyrolysis. Energy & Fuels. 1993;7(6):1013-20.
84. Zhai L, Zhou X, Liu R. A theoretical study of pyrolysis mechanisms of pyrrole. The Journal of Physical Chemistry A. 1999;103(20):3917-22.
85. Martoprawiro M, Bacskay GB, Mackie JC. Ab initio quantum chemical and kinetic modeling study of the pyrolysis kinetics of pyrrole. The Journal of Physical Chemistry A. 1999;103(20):3923-34.
86. Lifshitz A, Shweky I, Tamburu C. Thermal decomposition of N-methylpyrrole: experimental and modeling study. The Journal of Physical Chemistry. 1993;97(17):4442-9.
87. Laskin A, Lifshitz A. Isomerization and decomposition of indole. Experimental results and kinetic modeling. The Journal of Physical Chemistry A. 1997;101(42):7787-801.
88. Axworthy AE, Dayan VH, Martin GB. Reactions of fuel-nitrogen compounds under conditions of inert pyrolysis. Fuel. 1978;57(1):29-35.
89. Cox EG, Cruickshank DWJ, Smith J. The crystal structure of benzene at—3 C. Proceedings of the Royal Society of London Series A Mathematical and Physical Sciences. 1958;247(1248):1-21.
90. Ninomiya Y, Dong Z, Suzuki Y, Koketsu J. Theoretical study on the thermal decomposition of pyridine. Fuel. 2000;79(3-4):449-57.
91. Mackie JC, Colket MB, Nelson PF. Shock tube pyrolysis of pyridine. Journal of Physical Chemistry. 1990;94(10):4099-106.
92. Hore N, Russell D. Radical pathways in the thermal decomposition of pyridine and diazines: a laser pyrolysis and semi-empirical study. Journal of the Chemical Society, Perkin Transactions 2. 1998(2):269-76.
93. Memon H, Bartle K, Taylor J, Williams A. The shock tube pyrolysis of pyridine. International journal of energy research. 2000;24(13):1141-59.
94. Liu J, Guo X. ReaxFF molecular dynamics simulation of pyrolysis and combustion of pyridine. Fuel Processing Technology. 2017;161:107-15.

95. Liu J, Lu Q, Jiang X-y, Hu B, Zhang X-l, Dong C-q, et al. Theoretical investigation of the formation mechanism of NH_3 and HCN during pyrrole pyrolysis: the effect of H_2O. Molecules. 2018;23(4):711.
96. Wang Z, Zhou J, Zhu Y, Wen Z, Liu J, Cen K. Simultaneous removal of NOx, SO_2 and Hg in nitrogen flow in a narrow reactor by ozone injection: Experimental results. Fuel Processing Technology. 2007;88(8):817-23.
97. WC Jr G. Gas-phase combustion chemistry: Springer Science & Business Media; 2012.
98. Zeldvich YB. The oxidation of nitrogen in combustion and explosions. J Acta Physicochimica. 1946;21:577.
99. Lavoie GA, Heywood JB, Keck JC. Experimental and theoretical study of nitric oxide formation in internal combustion engines. Combustion science and technology. 1970;1(4):313-26.
100. Hebbar GS. NOx from diesel engine emission and control strategies-a review. International Journal of Mechanical Engineering and Robotics Research. 2014;3(4):471.
101. Fenimore CP, editor Formation of nitric oxide in premixed hydrocarbon flames. Symposium (International) on Combustion; 1971: Elsevier.
102. Ashman PJ, Haynes BS, Nicholls PM, Nelson PF. Interactions of gaseous NO with char during the low-temperature oxidation of coal chars. Proceedings of the Combustion Institute. 2000;28(2):2171-9.
103. Aihara T, Matsuoka K, Kyotani T, Tomita A. Mechanism of N2 formation during coal char oxidation. Proceedings of the combustion Institute. 2000;28(2):2189-95.
104. Pevida C, Arenillas A, Rubiera F, Pis J. Synthetic coal chars for the elucidation of NO heterogeneous reduction mechanisms. Fuel. 2007;86(1-2):41-9.
105. Coda B, Kluger F, Förtsch D, Spliethoff H, Hein K, Tognotti L. Coal-nitrogen release and NO x evolution in air-staged combustion. Energy & fuels. 1998;12(6):1322-7.
106. Ninomiya Y. Characteristics of emission of char NO during the combustion of a single particle of coal char. International Chemical Engineering;(USA). 1989;29(3).
107. Yue G, Pereira F, Sarofim A, Beer J. Char nitrogen conversion to NOx in a fluidized bed. Combustion science and technology. 1992;83(4-6):245-56.

108. Richard J-R, Al Majthoub M, Aho MJ, Pirkonen PM. The effect of pressure on the formation of nitrogen oxides from coal char combustion in a small fixed-bed reactor. Fuel. 1994;73(7):1034-8.
109. Brodén H. Dynamic single particle char combustion and its influence on the fate of fuel bound nitrogen. Numerical modelling and experiments. 1994.
110. Wang W, Brown SD, Hindmarsh CJ, Thomas KM. NOx release and reactivity of chars from a wide range of coals during combustion. Fuel. 1994;73(9):1381-8.
111. Cahill P, Smith M, Vallender S, editors. Characterisation of British coals for low NOx combustion. 1991 International Conference on Coal Science Proceedings; 1991: Elsevier.
112. de Andrés AIG, Thomas KM. The influence of mineral matter and carbonization conditions on nitrogen release during coal combustion. Fuel. 1994;73(5):635-41.
113. Wang W, Brown SD, Thomas KM, Crelling JC. Nitrogen release from a rank series of coals during temperature programmed combustion. Fuel. 1994;73(3):341-7.
114. Hindmarsh CJ, Wang W, Thomas KM, Crelling JC. The release of nitrogen during the combustion of macerals, microlithotypes and their chars. Fuel. 1994;73(7):1229-34.
115. Tullin CJ, Goel S, Morihara A, Sarofim AF, Beer JM. Nitrogen oxide (NO and N2O) formation for coal combustion in a fluidized bed: effect of carbon conversion and bed temperature. Energy & Fuels. 1993;7(6):796-802.
116. Furusawa T, Shimizu T, Kawaguchi H, Kojima T, Chihara Y. Conversion ratio of fuel bond nitrogen of a single coal particle to nitric oxide during fluidized bed combustion, experimental and theoretical investigations. Coal science and technology. 1987;11:853-6.
117. Bai Z, Jiang XZ, Luo KH. Effects of water on pyridine pyrolysis: A reactive force field molecular dynamics study. Energy. 2022;238:121798.
118. Klippenstein SJ, Harding LB, Glarborg P, Miller JA. The role of NNH in NO formation and control. Combustion and Flame. 2011;158(4):774-89.
119. Cao Q, Liu H, Wu S-H, Zhao L-P, Huang X. Kinetic study of promoted SNCR process by different gas additives. 2008 2nd International Conference on Bioinformatics and Biomedical Engineering. 2008:4034-8.
120. Arand J, Muzio L, Sotter J. Urea reduction of NO/sub x/in combustion effluents. 1980.

121. Lyon R. Method for the reduction of the concentration of NO in combustion effluents using NH_3. US Patent 3900554. 1975.
122. Wenli D, Dam-Johansen K, Østergaard K, editors. Widening the temperature range of the thermal DeNOx process. An experimental investigation. Symposium (International) on Combustion; 1991: Elsevier.
123. Lyon RK, Hardy JE. Discovery and development of the thermal DeNOx process. Industrial & engineering chemistry fundamentals. 1986;25(1):19-24.
124. Alzueta MU, Røjel H, Kristensen PG, Glarborg P, Dam-Johansen K. Laboratory study of the CO/NH3/NO/O2 system: Implications for hybrid reburn/SNCR strategies. Energy & Fuels. 1997;11(3):716-23.
125. Wang Z-H, Zhou J-h, Zhang Y-w, Lu Z-m, Fan J-r, Cen K-f. Experiment and mechanism investigation on advanced reburning for NOx reduction: influence of CO and temperature. Journal of Zhejiang University Science B. 2005;6(3):187.
126. Hemberger R, Muris S, Pleban K-U, Wolfrum J. An experimental and modeling study of the selective noncatalytic reduction of NO by ammonia in the presence of hydrocarbons. Combustion and Flame. 1994;99(3-4):660-8.
127. Zamansky VM, Lissianski VV, Maly PM, Ho L, Rusli D, Gardiner Jr WC. Reactions of sodium species in the promoted SNCR process. Combustion and Flame. 1999;117(4):821-31.
128. Kuihua H, Chunmei L. Kinetic model and simulation of promoted selective non-catalytic reduction by sodium carbonate. Chinese Journal of Chemical Engineering. 2007;15(4):512-9.
129. Zhou Z, Guo L, Chen L, Shan S, Wang Z. Study of pyrolysis of brown coal and gasification of coal-water slurry using the ReaxFF reactive force field. International Journal of Energy Research. 2018;42(7):2465-80.
130. Bae SW, Roh SA, Kim SD. NO removal by reducing agents and additives in the selective non-catalytic reduction (SNCR) process. Chemosphere. 2006;65(1):170-5.
131. Yao T, Duan Y, Yang Z, Li Y, Wang L, Zhu C, et al. Experimental characterization of enhanced SNCR process with carbonaceous gas additives. Chemosphere. 2017;177:149-56.
132. ur Rahman Z, Wang X, Zhang J, Baleta J, Vujanović M, Tan H. Kinetic study and optimization on SNCR process in pressurized oxy-combustion. Journal of the Energy Institute. 2021;94:263-71.
133. Seo DK, Park SS, Kim YT, Hwang J, Yu T-U. Study of coal pyrolysis by

thermo-gravimetric analysis (TGA) and concentration measurements of the evolved species. Journal of Analytical and Applied Pyrolysis. 2011;92(1):209-16.
134. Cypres R, Furfari S. Fixed-bed pyrolysis of coal under hydrogen pressure at low heating rates. Fuel. 1981;60(9):768-78.
135. Jamil K, Hayashi J-i, Li C-Z. Pyrolysis of a Victorian brown coal and gasification of nascent char in CO_2 atmosphere in a wire-mesh reactor. Fuel. 2004;83(7-8):833-43.
136. Matsuoka K, Ma Z-x, Akiho H, Zhang Z-g, Tomita A, Fletcher TH, et al. High-pressure coal pyrolysis in a drop tube furnace. Energy & fuels. 2003;17(4):984-90.
137. Zeng X, Wang Y, Yu J, Wu S, Zhong M, Xu S, et al. Coal pyrolysis in a fluidized bed for adapting to a two-stage gasification process. Energy & fuels. 2011;25(3):1092-8.
138. Rath J. Low temperature polycrystalline silicon: a review on deposition, physical properties and solar cell applications. Solar Energy Materials and Solar Cells. 2003;76(4):431-87.
139. Sprecher RF, Retcofsky HL. Observation of transient free radicals during coal pyrolysis. Fuel. 1983;62(4):473-6.
140. Jia L, Weng J, Wang Y, Sun S, Zhou Z, Qi F. Online analysis of volatile products from bituminous coal pyrolysis with synchrotron vacuum ultraviolet photoionization mass spectrometry. Energy & fuels. 2013;27(2):694-701.
141. Wendt JO, Linak WP, Groff PW, Srivastava RK. Hybrid SNCR-SCR technologies for NOx control: Modeling and experiment. AIChE Journal. 2001;47(11):2603-17.
142. Friesner RA. Ab initio quantum chemistry: Methodology and applications. Proceedings of the National Academy of Sciences. 2005;102(19):6648-53.
143. Parr RG, Craig DP, Ross IG. Molecular orbital calculations of the lower excited electronic levels of benzene, configuration interaction included. The Journal of Chemical Physics. 1950;18(12):1561-3.
144. Schlick T. Molecular modeling and simulation: an interdisciplinary guide: an interdisciplinary guide: Springer Science & Business Media; 2010.
145. Feng M, Jiang XZ, Luo KH. A reactive molecular dynamics simulation study of methane oxidation assisted by platinum/graphene-based catalysts. Proceedings of the Combustion Institute. 2019;37(4):5473-80.
146. Frenkel D, Smit B. Understanding molecular simulation: from algorithms to

applications: Elsevier; 2001.
147. Feng M. Reactive Molecular Dynamics of Fuel Oxidation and Catalytic Reactions: UCL (University College London); 2019.
148. Weiner SJ, Kollman PA, Case DA, Singh UC, Ghio C, Alagona G, et al. A new force field for molecular mechanical simulation of nucleic acids and proteins. Journal of the American Chemical Society. 1984;106(3):765-84.
149. Momany FA, Rone R. Validation of the general purpose QUANTA® 3.2/CHARMm® force field. Journal of Computational Chemistry. 1992;13(7):888-900.
150. Dauber-Osguthorpe P, Roberts VA, Osguthorpe DJ, Wolff J, Genest M, Hagler AT. Structure and energetics of ligand binding to proteins: Escherichia coli dihydrofolate reductase-trimethoprim, a drug-receptor system. Proteins: Structure, Function, and Bioinformatics. 1988;4(1):31-47.
151. Rasmussen K, Engelsen S, Fabricius J, Rasmussen B. The Consistent Force Field: Development of potential energy functions for conformational analysis. Recent experimental and computational advances in molecular spectroscopy: Springer; 1993. p. 381-419.
152. Halgren TA. Merck molecular force field. I. Basis, form, scope, parameterization, and performance of MMFF94. Journal of computational chemistry. 1996;17(5-6):490-519.
153. Jiang XZ, Luo KH. Reactive and electron force field molecular dynamics simulations of electric field assisted ethanol oxidation reactions. Proceedings of the Combustion Institute. 2021;38(4):6605-13.
154. Feng M, Jiang XZ, Zeng W, Luo KH, Hellier P. Ethanol oxidation with high water content: A reactive molecular dynamics simulation study. Fuel. 2019;235:515-21.
155. Van Duin AC, Dasgupta S, Lorant F, Goddard WA. ReaxFF: a reactive force field for hydrocarbons. The Journal of Physical Chemistry A. 2001;105(41):9396-409.
156. Bhoi S, Banerjee T, Mohanty K. Molecular dynamic simulation of spontaneous combustion and pyrolysis of brown coal using ReaxFF. Fuel. 2014;136:326-33.
157. ACT vD. ReaxFF User Manual. 2002.
158. Senftle TP, Hong S, Islam MM, Kylasa SB, Zheng Y, Shin YK, et al. The ReaxFF reactive force-field: development, applications and future directions. npj

Computational Materials. 2016;2(1):1-14.
159. Rappe AK, Goddard III WA. Charge equilibration for molecular dynamics simulations. The Journal of Physical Chemistry. 1991;95(8):3358-63.
160. Ongari D, Boyd PG, Kadioglu O, Mace AK, Keskin S, Smit B. Evaluating charge equilibration methods to generate electrostatic fields in nanoporous materials. Journal of chemical theory and computation. 2018;15(1):382-401.
161. Aktulga HM, Fogarty JC, Pandit SA, Grama AY. Parallel reactive molecular dynamics: Numerical methods and algorithmic techniques. Parallel Computing. 2012;38(4-5):245-59.
162. Nakano A. Parallel multilevel preconditioned conjugate-gradient approach to variable-charge molecular dynamics. Computer Physics Communications. 1997;104(1-3):59-69.
163. Parr RG, Pearson RG. Absolute hardness: companion parameter to absolute electronegativity. Journal of the American chemical society. 1983;105(26):7512-6.
164. Verlet L. Computer" experiments" on classical fluids. I. Thermodynamical properties of Lennard-Jones molecules. Physical review. 1967;159(1):98.
165. Swope WC, Andersen HC, Berens PH, Wilson KR. A computer simulation method for the calculation of equilibrium constants for the formation of physical clusters of molecules: Application to small water clusters. The Journal of chemical physics. 1982;76(1):637-49.
166. Zhang Z, Liu C-J, Walsh MR, Guo G-J. Effects of ensembles on methane hydrate nucleation kinetics. Physical Chemistry Chemical Physics. 2016;18(23):15602-8.
167. Berendsen H, Postma J, van Gunsteren W, DiNola A, Haak J. Size and Chirality Dependent Elastic Properties of Graphene Nanoribbons under Uniaxial Tension. J Chem Phys. 1984;81:3684-90.
168. Hünenberger PH. Thermostat algorithms for molecular dynamics simulations. Advanced computer simulation: Springer; 2005. p. 105-49.
169. Pratt LR, Haan SW. Effects of periodic boundary conditions on equilibrium properties of computer simulated fluids. I. Theory. The Journal of Chemical Physics. 1981;74(3):1864-72.
170. Pratt LR, Haan SW. Effects of periodic boundary conditions on equilibrium properties of computer simulated fluids. II. Application to simple liquids. The Journal of Chemical Physics. 1981;74(3):1873-6.

171. Hanwell MD, Curtis DE, Lonie DC, Vandermeersch T, Zurek E, Hutchison GR. Avogadro: an advanced semantic chemical editor, visualization, and analysis platform. Journal of cheminformatics. 2012;4(1):17.
172. Martínez L, Andrade R, Birgin EG, Martínez JM. PACKMOL: a package for building initial configurations for molecular dynamics simulations. Journal of computational chemistry. 2009;30(13):2157-64.
173. Humphrey W, Dalke A, Schulten K. VMD: visual molecular dynamics. Journal of molecular graphics. 1996;14(1):33-8.
174. Thompson AP, Aktulga HM, Berger R, Bolintineanu DS, Brown WM, Crozier PS, et al. LAMMPS-a flexible simulation tool for particle-based materials modeling at the atomic, meso, and continuum scales. Computer Physics Communications. 2022;271:108171.
175. Döntgen M, Przybylski-Freund M-D, Kröger LC, Kopp WA, Ismail AE, Leonhard K. Automated discovery of reaction pathways, rate constants, and transition states using reactive molecular dynamics simulations. Journal of chemical theory and computation. 2015;11(6):2517-24.
176. Arvelos S, Hori CE. ReaxFF study of ethanol oxidation in O_2/N_2 and O_2/CO_2 Environments at high temperatures. Journal of chemical information and modeling. 2020;60(2):700-13.
177. Zhang L, Duin ACv, Zybin SV, Goddard Iii WA. Thermal decomposition of hydrazines from reactive dynamics using the ReaxFF reactive force field. The Journal of Physical Chemistry B. 2009;113(31):10770-8.
178. Zhang L, Zybin SV, Van Duin AC, Dasgupta S, Goddard III WA, Kober EM. Carbon cluster formation during thermal decomposition of octahydro-1, 3, 5, 7-tetranitro-1, 3, 5, 7-tetrazocine and 1, 3, 5-triamino-2, 4, 6-trinitrobenzene high explosives from ReaxFF reactive molecular dynamics simulations. The Journal of Physical Chemistry A. 2009;113(40):10619-40.
179. Strachan A, van Duin AC, Chakraborty D, Dasgupta S, Goddard III WA. Shock waves in high-energy materials: The initial chemical events in nitramine RDX. Physical Review Letters. 2003;91(9):098301.
180. Strachan A, Kober EM, Van Duin AC, Oxgaard J, Goddard III WA. Thermal decomposition of RDX from reactive molecular dynamics. The Journal of chemical physics. 2005;122(5):054502.
181. Van Duin AC, Zeiri Y, Dubnikova F, Kosloff R, Goddard WA. Atomistic-scale simulations of the initial chemical events in the thermal initiation of

triacetonetriperoxide. Journal of the American Chemical Society. 2005;127(31):11053-62.
182. Zeng J, Cao L, Xu M, Zhu T, Zhang JZ. Complex reaction processes in combustion unraveled by neural network-based molecular dynamics simulation. Nature communications. 2020;11(1):1-9.
183. Hong D, Li P, Si T, Guo X. ReaxFF simulations of the synergistic effect mechanisms during co-pyrolysis of coal and polyethylene/polystyrene. Energy. 2021;218:119553.
184. Sadiq SK, Wright DW, Kenway OA, Coveney PV. Accurate ensemble molecular dynamics binding free energy ranking of multidrug-resistant HIV-1 proteases. Journal of chemical information and modeling. 2010;50(5):890-905.
185. Wan S, Coveney PV. Rapid and accurate ranking of binding affinities of epidermal growth factor receptor sequences with selected lung cancer drugs. Journal of the Royal Society Interface. 2011;8(61):1114-27.
186. Wan S, Knapp B, Wright DW, Deane CM, Coveney PV. Rapid, precise, and reproducible prediction of peptide–MHC binding affinities from molecular dynamics that correlate well with experiment. Journal of chemical theory and computation. 2015;11(7):3346-56.
187. Wright DW, Hall BA, Kenway OA, Jha S, Coveney PV. Computing clinically relevant binding free energies of HIV-1 protease inhibitors. Journal of chemical theory and computation. 2014;10(3):1228-41.
188. Wan S, Sinclair RC, Coveney PV. Uncertainty quantification in classical molecular dynamics. Philosophical Transactions of the Royal Society A. 2021;379(2197):20200082.
189. Bhati AP, Wan S, Coveney PV. Ensemble-based replica exchange alchemical free energy methods: the effect of protein mutations on inhibitor binding. Journal of chemical theory and computation. 2018;15(2):1265-77.
190. Potterton A, Husseini FS, Southey MW, Bodkin MJ, Heifetz A, Coveney PV, et al. Ensemble-based steered molecular dynamics predicts relative residence time of A2A receptor binders. Journal of Chemical Theory and Computation. 2019;15(5):3316-30.
191. Amaro RE, Baudry J, Chodera J, Demir Ö, McCammon JA, Miao Y, et al. Ensemble docking in drug discovery. Biophysical journal. 2018;114(10):2271-8.
192. Hong D, Liu L, Huang Y, Zheng C, Guo X. Chemical effect of H_2O on CH_4 oxidation during combustion in O_2/H_2O environments. Energy & Fuels.

2016;30(10):8491-8.
193. Luo J, Zou C, He Y, Jing H, Cheng S. The characteristics and mechanism of NO formation during pyridine oxidation in O_2/N_2 and O_2/CO_2 atmospheres. Energy. 2019;187:115954.
194. Greul U, Spliethoff H, Magel H-C, Schnell U, Rüdiger H, Hein K, et al., editors. Impact of temperature and fuel-nitrogen content on fuel-staged combustion with coal pyrolysis gas. Symposium (International) on Combustion; 1996: Elsevier.
195. Rüdiger H, Kicherer A, Greul U, Spliethoff H, Hein K. Pyrolysis gas from biomass and pulverized biomass as reburn fuels in staged coal combustion. Developments in Thermochemical Biomass Conversion: Springer; 1997. p. 1387-98.
196. Dagaut P, Lecomte F. Experiments and kinetic modeling study of NO-reburning by gases from biomass pyrolysis in a JSR. Energy & fuels. 2003;17(3):608-13.
197. Glarborg P, Kristensen PG, Dam-Johansen K, Alzueta M, Millera A, Bilbao R. Nitric oxide reduction by non-hydrocarbon fuels. Implications for reburning with gasification gases. Energy & Fuels. 2000;14(4):828-38.
198. Locci C, Vervisch L, Farcy B, Domingo P, Perret N. Selective non-catalytic reduction (SNCR) of nitrogen oxide emissions: a perspective from numerical modeling. Flow, Turbulence and Combustion. 2018;100(2):301-40.
199. Jiang XZ, Feng M, Zeng W, Luo KH. Study of mechanisms for electric field effects on ethanol oxidation via reactive force field molecular dynamics. Proceedings of the Combustion Institute. 2019;37(4):5525-35.
200. English NJ, Waldron CJ. Perspectives on external electric fields in molecular simulation: progress, prospects and challenges. Physical Chemistry Chemical Physics. 2015;17(19):12407-40.
201. English NJ, MacElroy J. Hydrogen bonding and molecular mobility in liquid water in external electromagnetic fields. The Journal of chemical physics. 2003;119(22):11806-13.
202. Saitta AM, Saija F, Giaquinta PV. Ab initio molecular dynamics study of dissociation of water under an electric field. Physical review letters. 2012;108(20):207801.
203. Ikeda E, Nicholls P, Mackie JC. A kinetic study of the oxidation of pyridine. Proceedings of the Combustion Institute. 2000;28(2):1709-16.
204. Islam MM, Kolesov G, Verstraelen T, Kaxiras E, van Duin ACT. eReaxFF: A

Pseudoclassical Treatment of Explicit Electrons within Reactive Force Field Simulations. Journal of Chemical Theory and Computation. 2016;12(8):3463-72.
205. Islam MM, van Duin ACT. Reductive Decomposition Reactions of Ethylene Carbonate by Explicit Electron Transfer from Lithium: An eReaxFF Molecular Dynamics Study. The Journal of Physical Chemistry C. 2016;120(48):27128-34.

Publications and Conferences

Journal papers

1. **Zhongze Bai**, Xi Zhuo Jiang, Kai H. Luo. Effects of water on pyridine pyrolysis: A reactive force field molecular dynamics study. Energy, 238 (2022),121798. (Chapter 3)
2. **Zhongze Bai**, Xi Zhuo Jiang, Kai H. Luo. A reactive molecular dynamics study of NO removal by nitrogen-containing species in coal pyrolysis gas. Proceedings of the Combustion Institute, https://doi.org/10.1016/j.proci.2022.07.154. (Chapter 4.1)
3. **Zhongze Bai**, Xi Zhuo Jiang, Kai H. Luo. Impact of oxygen and nitrogen-containing species content on the performance of NO removal by coal pyrolysis gas: A reactive molecular dynamics simulation study. Process Safety and Environmental Protection, 173(2023), 229–236. (Chapter 4.2)
4. **Zhongze Bai**, Xi Zhuo Jiang, Kai H. Luo. Effects of nitrogen-free species on NO removal performance by coal pyrolysis gas via reactive molecular dynamics simulations. Journal of the Energy Institute, 107(2023), 101172. (Chapter 4.3)
5. **Zhongze Bai**, Xi Zhuo Jiang, Kai H. Luo. Reactive force field molecular dynamics simulation of pyridine combustion assisted by electric field. Fuel, 333(2022), 126455. (Chapter 5.1)
6. **Zhongze Bai**, Xi Zhuo Jiang, Kai H. Luo. Understanding mechanisms of pyridine oxidation with ozone addition via reactive force field molecular dynamics simulations. Chemical Engineering Science, 266(2023), 118290. (Chapter 5.2)

Conferences

Zhongze Bai, Xi Zhuo Jiang, Kai H. Luo. A reactive molecular dynamics study of NO removal by nitrogen-containing species in coal pyrolysis gas. 39th International Symposium on Combustion. July 24 – 29, 2022, Vancouver, Canada.

Zhongze Bai, Xi Zhuo Jiang, Kai H. Luo. The effects of oxygen on the performance of NO reduction by HCN. 14th International Conference on Applied Energy. August 8 – 11, 2022, Ruhr University Bochum, Germany.